

DESIGN AND DEVELOPMENT OF EFFICIENT CATALYSTS AND  
DETERMINATION OF REACTION MECHANISM FOR CARBON DIOXIDE  
REFORMING OF METHANE (CDRM)

by

Aysun İpek Paksoy

B.S., Chemical Engineering, Istanbul Technical University, 2008

M.S., Chemical Engineering, Boğaziçi University, 2010

Submitted to the Institute for Graduate Studies in  
Science and Engineering in partial fulfillment of  
the requirements for the degree of  
Doctor of Philosophy

Graduate Program in Chemical Engineering

Boğaziçi University

2016

*to my family*

## ACKNOWLEDGEMENTS

In this PhD journey of many challenges, I am grateful for the people supporting me in different ways. To start with, I would like to express my truthful gratitude to my thesis supervisor Prof. Ahmet Erhan Aksoylu for his guidance, encouragement and trust in me. He devoted his time to guide me and share his expertise and experiences in catalysis and reaction engineering. It was a privilege for me to work with him during this study.

I would like to express my sincere appreciations for Dr. Burcu Selen Çağlayan for her considerable time and effort in XPS, Raman and TPO studies. Her guidance throughout my study was very valuable.

I would also like to thank the members of the thesis committee, Prof. Ayşe Nilgün Akın, Prof. Hüsnü Atakül, Assoc. Prof. Hasan Bedir and Prof. Ramazan Yıldırım for reading and commenting on my thesis.

I should also thank Bilge Gedik Uluocak for her effort in SEM analyses conducted at Boğaziçi University Advanced Technologies Research and Development Center.

Heartfelt thanks are for my dear friends: Ali Uzun, Aybüke Leba, B. Merve Eropak, Elif Can, Elif Erdiñ, Elif Gençtürk and Melek Selcen Başar. Their friendships are one of the biggest assets that I have gained in my life. I was also very lucky to work with the CATREL team, Barış Burnak, Burcu Acar, Cihat Öztepe, Çağla Odabaşı, Çağla Uzunoğlu, Çoşar Doğa Demirhan, Hatice Eyvaz, S. Emre Demirel, Serhat Erşahin and Sezin Sezen. Their endless support was very valuable for me and our interaction helped me learn a lot.

Cordial thanks are kindly for Bilgi Dedeoğlu. His technical assistance and friendship during my thesis was highly noticeable. I would also like to thank Melike Gürbüz, Başak Ünen and Yakup Bal for their friendly attitude.

Finally, I would like to express my dearest appreciations to all my family members for their patience, encouragement and moral support throughout my whole education.

Their endless love and trust in me was what made me motivated all the time. It was marvelous to see my father as a rock, my mother as a shelter and my brother as an organizer whenever I needed their help. This is why I dedicate this work to them.

Financial support provided by TUBITAK through the project 111M144, Boğaziçi University through the project BAP M6755, and State Planning Organization through the project DPT 07K120630 is gratefully acknowledged.

The graduate scholarship provided by TÜBİTAK through the program 2211 for my PhD studies deserves thankful recognition.

## ABSTRACT

### **DESIGN AND DEVELOPMENT OF EFFICIENT CATALYSTS AND DETERMINATION OF REACTION MECHANISM FOR CARBON DIOXIDE REFORMING OF METHANE (CDRM)**

The aim of the current work is to design and develop effective non-PGM based CDRM catalysts, to confirm the roles of each catalyst component, to determine optimum reaction conditions for the highest performance, and to reveal the details of CDRM reaction mechanism. In activity and selectivity tests, the reaction temperature, feed ratio and space velocity were used as the parameters. The properties of both the catalysts and the type of carbon deposited on them during CDRM were analyzed via SEM-EDX, TPO, XPS, HRTEM-EDX and Raman Spectroscopy. The kinetic behaviors of the catalysts were parametrically analyzed by varying temperature and partial pressures of both reactants and products. FTIR-DRIFT studies were also performed to obtain information on both catalyst surface and CDRM mechanism. It was indicated that Co particles partially cover evenly distributed Ce particles. The lowest degree of ceria reduction, and the highest asymmetry of the O1s XP spectrum, due to lattice oxygen vacancies and adsorbed oxygen, were obtained for the catalyst with the highest Co/Ce ratio. It was also verified that Co species in the catalyst samples with higher Co loading are more oxidized. The roles of each species in the catalyst design were confirmed: Co is responsible for CH<sub>4</sub> dehydrogenation, ceria has a pronounced effect on surface oxygen transfer, and ZrO<sub>2</sub> serves for surface oxygen production via CO<sub>2</sub> dissociation stages of CDRM. The fraction of different carbon types formed on the catalyst surface were dependent both on catalyst composition and reaction conditions. The kinetic studies have shown that CH<sub>4</sub> utilization is a key factor in CDRM, even affecting CO<sub>2</sub> utilization, and H<sub>2</sub> introduction has an inhibitory effect on the mechanism. The effect of Co/Ce ratio on C balance of CDRM was also highlighted with the combined evaluation of performance, kinetic and FTIR-DRIFT studies.

## ÖZET

### **KARBON DİOKSİTİN KURU REFORMLAMASI İÇİN ETKİN KATALİZÖRLERİN TASARIMI, GELİŞTİRİLMESİ VE REAKSİYON MEKANİZMASININ BULUNMASI**

Bu çalışmanın amacı, platin grup metal içermeyen kuru reformlama katalizörleri tasarlamak ve geliştirmek, her bir katalizör bileşeninin rolünü teyit etmek, en yüksek performans için optimum reaksiyon koşullarını belirlemek ve kuru reformlama reaksiyon mekanizmasını ortaya çıkarmaktır. Aktivite ve seçicilik testlerinde sıcaklık, besleme gazlarının oranı ve kalma süresi deneysel parametreler olarak kullanılmıştır. Hem katalizörlerin hem de kuru reformlama sırasında katalizörler üzerinde biriken karbon türlerinin özellikleri SEM-EDX, TPO, XPS, HRTEM-EDX ve Raman Spektrometresi ile analiz edilmiştir. Katalizörlerin kinetik davranışları sıcaklık, besleme ve ürün kısmi basınçları parametrik olarak değiştirilerek analiz edilmiştir. Gerek katalizörlerin yüzeyi gerekse de kuru reformlama mekanizması hakkında bilgi edinmek amacıyla FTIR-DRIFT çalışmaları yürütülmüştür. Co parçacıklarının homojen dağılmış Ce parçacıklarını kısmen kapattığı belirlenmiştir. En yüksek Co/Ce oranına sahip olan katalizör için, en düşük serya indirgenme derecesi ve en yüksek O1s XP spektrumu asimetrisi, ki bu veri latis oksijen boşlukları ile adsorplanan oksijene bağlı olmaktadır, elde edilmiştir. Ayrıca, Co yüklemesi daha fazla olan katalizör örneklerindeki Co türlerinin daha çok oksitlenmiş olduğu teyit edilmiştir. Kuru reformlamada katalizör sisteminin tüm bileşenlerine ait roller doğrulanmıştır. Co'nun CH<sub>4</sub> parçalanmasında, seryanın yüzey oksijeni taşınımında, ZrO<sub>2</sub>'nin ise kuru reformlamanın CO<sub>2</sub> parçalanması basamakları aracılığıyla yüzey oksijeni üretiminde rol oynadığı anlaşılmıştır. Katalizör yüzeyinde oluşan farklı karbon tiplerinin dağılımı hem katalizör bileşimine hem de reaksiyon koşullarına bağlıdır. Kinetik çalışmalar, CH<sub>4</sub> kullanımının CO<sub>2</sub> kullanımını dahi etkileyerek kuru reformlamada anahtar rol oynadığını ve H<sub>2</sub>'in mekanizmada olumsuz etkisi olduğunu ortaya koymuştur. Kuru reformlamanın C dengesinde Co/Ce oranının etkisi de performans, kinetik ve FTIR-DRIFT çalışmalarının birlikte değerlendirilmesi sonucunda anlaşılmıştır.

## TABLE OF CONTENTS

ACKNOWLEDGEMENTS .....	iv
ABSTRACT .....	vi
ÖZET .....	vii
LIST OF FIGURES .....	xi
LIST OF TABLES .....	xvii
LIST OF SYMBOLS .....	xix
LIST OF ACRONYMS/ABBREVIATIONS .....	xx
1. INTRODUCTION .....	1
2. LITERATURE SURVEY .....	5
2.1. Carbon Dioxide Reforming of Methane .....	5
2.2. Catalytic Activity Inhibition .....	8
2.3. Catalysts for Carbon Dioxide Reforming of Methane .....	10
2.3.1. Noble Metal Catalysts .....	10
2.3.2. Ni-based Catalysts .....	12
2.3.3. Co-based Catalysts .....	16
2.4. Catalyst Supports and Promoters .....	19
2.4.1. Supports .....	19
2.4.2. Promoters .....	24
2.5. Kinetics of Carbon Dioxide Reforming of Methane .....	27
3. EXPERIMENTAL WORK .....	33
3.1. Materials .....	33
3.1.1. Chemicals .....	33
3.1.2. Gases and Liquids .....	33
3.2. Experimental Systems .....	34
3.2.1. Catalyst Preparation Systems .....	35
3.2.2. Catalyst Characterization Systems .....	35
3.2.2.1. Scanning Electron Microscopy (SEM) .....	35
3.2.2.2. High Resolution Transmission Electron Microscopy (HR- TEM) .....	36

3.2.2.3. Intelligent Gravimetric Analyzer (IGA) .....	36
3.2.2.4. Raman Spectroscopy .....	36
3.2.2.5. X-Ray Photoelectron Spectroscopy (XPS) .....	36
3.2.2.6. Fourier Transform Infrared Spectroscopy .....	36
3.2.3. Catalytic Reaction System .....	38
3.2.4. Product Analysis System .....	41
3.3. Catalyst Preparation and Pretreatment .....	41
3.3.1. Support Preparation .....	42
3.3.2. Preparation of Co-Ce/ZrO <sub>2</sub> catalyst .....	42
3.3.3. Pretreatment .....	43
3.4. Catalyst Characterization .....	44
3.4.1. Temperature Programmed Oxidation (TPO) .....	44
3.4.2. Raman Spectroscopy .....	44
3.4.3. X-Ray Photoelectron Spectroscopy (XPS) .....	45
3.4.4. FTIR Spectroscopy .....	45
3.5. Reaction Tests .....	45
3.5.1. Blank Tests .....	45
3.5.2. CDRM Performance and Kinetic Tests .....	46
4. RESULTS AND DISCUSSIONS .....	51
4.1. Characterization and CDRM Performance of Co-Ce/ZrO <sub>2</sub> Catalyst .....	51
4.1.1. Characterization of Co-Ce/ZrO <sub>2</sub> Catalyst .....	51
4.1.2. Performance Tests .....	62
4.1.2.1. The Effect of Reaction Temperature .....	64
4.1.2.2. The Effect of CH <sub>4</sub> /CO <sub>2</sub> Feed Ratio .....	67
4.1.2.3. The Effect of Space Velocity .....	68
4.1.3. Stability Test .....	70
4.2. The Effects of Co/Ce Loading Ratio and Reaction Conditions on CDRM Performance of Co-Ce/ZrO <sub>2</sub> Catalysts .....	70
4.2.1. Characterization of Co-Ce/ZrO <sub>2</sub> System .....	71
4.2.2. CDRM Performance of Co-Ce/ZrO <sub>2</sub> System .....	77
4.3. Kinetic and Mechanistic Features of CDRM over Co-Ce/ZrO <sub>2</sub> Catalysts ....	85
4.3.2. The Product Influence on CDRM Rate .....	89
4.3.3. Surface Reaction Models .....	91

4.4. FTIR-DRIFT Studies over Co-Ce/ZrO <sub>2</sub> Catalysts .....	95
4.4.1. The Effect of Pretreatment on Catalyst Surface Characterization .....	96
4.4.2. Surface Interaction of Each Species at Co-Ce/ZrO <sub>2</sub> System .....	98
4.4.3. CO Adsorption on Co-Ce/ZrO <sub>2</sub> Catalyst System .....	100
4.4.4. ZrO <sub>2</sub> -CO <sub>2</sub> Interaction .....	102
4.4.5. CO <sub>2</sub> -Co-Ce/ZrO <sub>2</sub> System Interaction .....	106
4.4.6. CH <sub>4</sub> -Co-Ce/ZrO <sub>2</sub> System Interaction .....	107
4.4.7. CDRM over Co-Ce/ZrO <sub>2</sub> System .....	108
5. CONCLUSION .....	114
5.1. Conclusions .....	114
5.2. Recommendations .....	116
REFERENCES .....	118

## LIST OF FIGURES

Figure 3.1.	Schematic diagram of the impregnation system. ....	35
Figure 3.2.	Schematic representation of FTIR-DRIFTS system. ....	37
Figure 3.3.	Schematic diagram of the microreactor system. ....	40
Figure 4.1.	Co-Ce-Zr mapping of freshly reduced 5%Co-2%Ce/ZrO <sub>2</sub> catalyst. ...	52
Figure 4.2.	HRTEM images of selected regions on freshly reduced catalyst sample. ....	52
Figure 4.3.	XP spectrum of Ce3d region of 5%Co-2%Ce/ZrO <sub>2</sub> catalyst (a) tested at 973 K and CH <sub>4</sub> /CO <sub>2</sub> feed ratio of 2/1, (b) tested at 873 K and CH <sub>4</sub> /CO <sub>2</sub> feed ratio of 1/1, and (c) freshly calcined and reduced.	53
Figure 4.4.	XP spectrum of Co2p region of 5%Co-2%Ce/ZrO <sub>2</sub> catalyst (a) tested at 973 K and CH <sub>4</sub> /CO <sub>2</sub> feed ratio of 2/1, (b) tested at 873 K and CH <sub>4</sub> /CO <sub>2</sub> feed ratio of 1/1, and (c) freshly calcined and reduced.	55
Figure 4.5.	Co mapping of (a) freshly reduced catalyst, (b) spent sample used during the reaction performed at 873 K and CH <sub>4</sub> /CO <sub>2</sub> =1/1, Ce mapping of (c) freshly reduced catalyst, (d) spent sample used during the reaction performed at 873 K and CH <sub>4</sub> /CO <sub>2</sub> =1/1. ....	57
Figure 4.6.	SEM images of catalyst samples used during the reactions performed at (a) 973 K and CH <sub>4</sub> /CO <sub>2</sub> =1/1, (b) 973 K and CH <sub>4</sub> /CO <sub>2</sub> =2/1, (c) 873 K and CH <sub>4</sub> /CO <sub>2</sub> =1/1, (d) 873 K and CH <sub>4</sub> /CO <sub>2</sub> =2/1. ....	58

Figure 4.7.	SEM images of the catalyst samples used during the reaction at space velocity of 20000 mL/h g-catalyst and at (a) 973 K, CH <sub>4</sub> /CO <sub>2</sub> =1/1, (b) 973 K, CH <sub>4</sub> /CO <sub>2</sub> =2/1, (c) 873 K, CH <sub>4</sub> /CO <sub>2</sub> =1/1, and (d) 873 K, CH <sub>4</sub> /CO <sub>2</sub> =2/1. ....	60
Figure 4.8.	Raman spectra of the catalyst samples used during the reaction with space velocity of 20000 mL/h.g-catalyst at 973 K, CH <sub>4</sub> /CO <sub>2</sub> =2/1, and 873 K, CH <sub>4</sub> /CO <sub>2</sub> =1/1. ....	61
Figure 4.9.	TPO of the catalyst samples used during the reaction at space velocity of 20000 mL/h.g-catalyst and at 973 K, CH <sub>4</sub> /CO <sub>2</sub> =2/1; 873 K, CH <sub>4</sub> /CO <sub>2</sub> =1/1. ....	62
Figure 4.10.	Time-on-stream activity profiles of the catalyst in terms of CH <sub>4</sub> conversion for CH <sub>4</sub> /CO <sub>2</sub> feed ratio of 2/1. ....	63
Figure 4.11.	Time-on-stream activity and selectivity profiles of the catalyst in terms of CH <sub>4</sub> conversion and H <sub>2</sub> /CO product ratio, respectively, for CH <sub>4</sub> /CO <sub>2</sub> feed ratio of 1/1. ....	64
Figure 4.12.	The effect of reaction temperature and CH <sub>4</sub> /CO <sub>2</sub> feed ratio on (a) CH <sub>4</sub> conversion, (b) CO <sub>2</sub> conversion, (c) CH <sub>4</sub> activity/CO <sub>2</sub> activity ratio, and (d) H <sub>2</sub> /CO product ratio at the end of 6 h TOS. ....	65
Figure 4.13.	Time-on-stream profile of H <sub>2</sub> yield (H <sub>2</sub> produced/CH <sub>4</sub> consumed) obtained at CH <sub>4</sub> /CO <sub>2</sub> feed ratio of 1/1 and 20000 mL/h.g-catalyst. ...	66
Figure 4.14.	CH <sub>4</sub> and CO <sub>2</sub> activities at 973 K for 20000 mL/h.g-catalyst. ....	68
Figure 4.15.	Activity and selectivity trends at 973 K as a function of CH <sub>4</sub> /CO <sub>2</sub> feed ratios and space velocities (a) CH <sub>4</sub> conversions, (b) CO <sub>2</sub> conversions, and (c) H <sub>2</sub> /CO product ratio. ....	69

Figure 4.16.	Stability test over 5%Co-2%Ce/ZrO <sub>2</sub> . .....	70
Figure 4.17.	HRTEM area images and EDX results for (a) 5%Co-2%Ce/ZrO <sub>2</sub> , and (b) 10%Co-3%Ce/ZrO <sub>2</sub> catalysts. ....	71
Figure 4.18.	HRTEM images of 5%Co-2%Ce/ZrO <sub>2</sub> catalyst. ....	72
Figure 4.19.	HRTEM area images for (a) 5%Co-2%Ce/ZrO <sub>2</sub> , (b) 10%Co- 2%Ce/ZrO <sub>2</sub> , and (c) 10%Co-3%Ce/ZrO <sub>2</sub> catalysts. ....	72
Figure 4.20.	(a) HRTEM image of 5%Co-2%Ce/ZrO <sub>2</sub> catalyst, (b) Co, Ce, Zr and O mapping of the region. ....	73
Figure 4.21.	(a) HRTEM image of 5%Co-2%Ce/ZrO <sub>2</sub> catalyst, (b) Co EDX-Line and mapping analysis, and (c) Ce EDX-Line and mapping analysis of the selected region, indicated by a line in (a). ....	73
Figure 4.22.	XP spectra of Ce3d region for freshly calcined and reduced (a) 5%Co-2%Ce/ZrO <sub>2</sub> , (b) 5%Co-3%Ce/ZrO <sub>2</sub> , (c) 10%Co-2%Ce/ZrO <sub>2</sub> , and (d) 10%Co-3%Ce/ZrO <sub>2</sub> . ....	74
Figure 4.23.	XP spectra of O1s region for freshly calcined and reduced (a) 5%Co-2%Ce/ZrO <sub>2</sub> , (b) 5%Co-3%Ce/ZrO <sub>2</sub> , (c) 10%Co-2%Ce/ZrO <sub>2</sub> , and (d) 10%Co-3%Ce/ZrO <sub>2</sub> . ....	76
Figure 4.24.	XP spectra of Co2p region for freshly calcined and reduced (a) 5%Co-2%Ce/ZrO <sub>2</sub> , (b) 5%Co-3%Ce/ZrO <sub>2</sub> , (c) 10%Co-2%Ce/ZrO <sub>2</sub> , and (d) 10%Co-3%Ce/ZrO <sub>2</sub> . ....	77
Figure 4.25.	Activity profiles of tested catalysts at 973 K with 1/1 CH <sub>4</sub> /CO <sub>2</sub> feed ratio (a) CH <sub>4</sub> activity, and (b) CO <sub>2</sub> activity. ....	79

Figure 4.26.	Selectivity profiles of tested catalysts at 973 K with 1/1 CH <sub>4</sub> /CO <sub>2</sub> feed ratio. ....	80
Figure 4.27.	Activity and selectivity profiles of tested catalysts at 923 K with 1/1 CH <sub>4</sub> /CO <sub>2</sub> feed ratio (a) CH <sub>4</sub> activity, (b) CO <sub>2</sub> activity, and (c) H <sub>2</sub> /CO product ratio. ....	81
Figure 4.28.	Activity and selectivity profiles of tested catalysts at 873 K with 1/1 CH <sub>4</sub> /CO <sub>2</sub> feed ratio (a) CH <sub>4</sub> activity, (b) CO <sub>2</sub> activity, and (c) H <sub>2</sub> /CO product ratio. ....	82
Figure 4.29.	Activity profiles in terms of CH <sub>4</sub> conversion for tested catalysts at 973 K (a) with the feed ratio of 2/1 (b) with the feed ratio of 1/2, and (c) for all tested feed ratios. ....	84
Figure 4.30.	Selectivity profiles of tested catalysts with the feed ratio of 2/1 at (a) 873 K, (b) 923 K and (c) 973 K. ....	85
Figure 4.31.	Variation of reaction rates according to feed ratio. ....	89
Figure 4.32.	Variation of intrinsic rate according to (a) CO, and (b) H <sub>2</sub> content in the feed. ....	90
Figure 4.33.	FTIR-DRIFT spectra upon He flush for 1% CO adsorption at room temperature for 5%Co-2%Ce/ZrO <sub>2</sub> catalyst with (a) pretreatment 1, (b) pretreatment 2, (c) pretreatment 3, and (d) pretreatment 4. ....	97
Figure 4.34.	FTIR-DRIFT spectra obtained from 1% CO adsorption at room temperature for (a) ZrO <sub>2</sub> , (b) 2%Ce/ZrO <sub>2</sub> , (c) 5%Co/ZrO <sub>2</sub> and (d) 5%Co-2%Ce/ZrO <sub>2</sub> just after CO adsorption (grey spectra), and upon after He flush (black spectra). ....	99

Figure 4.35.	FTIR-DRIFT spectra from 1% CO adsorption at room temperature for (a) 5%Co-2%Ce/ZrO <sub>2</sub> , (b) 5%Co-3%Ce/ZrO <sub>2</sub> , (c) 10%Co-2%Ce/ZrO <sub>2</sub> , and (d) 10%Co-3%Ce/ZrO <sub>2</sub> just after CO adsorption (grey spectra), and upon He flush (black spectra). .....	101
Figure 4.36.	FTIR-DRIFT spectra after He flush of 10% CO <sub>2</sub> adsorption at (a) room temperature, (b) 373 K, and (c) 573 K. ....	103
Figure 4.37.	FTIR-DRIFT spectra obtained from just after 10% CO <sub>2</sub> adsorption at (a) room temperature, (b) 373 K, and (c) 573 K. ....	104
Figure 4.38.	FTIR-DRIFT spectra obtained from CO <sub>2</sub> adsorption at 573 K over ZrO <sub>2</sub> just after CO <sub>2</sub> adsorption (grey spectra), and upon He flush (black spectra) under (a) 10% CO <sub>2</sub> flow, and (b) 40% CO <sub>2</sub> flow. ....	105
Figure 4.39.	FTIR-DRIFT spectra obtained from 40% CO <sub>2</sub> adsorption at 573 K over 5%Co-2%Ce/ZrO <sub>2</sub> just after CO <sub>2</sub> adsorption of 1 hour (grey spectra), and upon He flush for 30 minutes (black spectra). ....	106
Figure 4.40.	FTIR-DRIFT spectra obtained from 40% CH <sub>4</sub> adsorption at 573 K over 5%Co-2%Ce/ZrO <sub>2</sub> just after CH <sub>4</sub> adsorption for 1 hour (grey spectra), and upon He flush of 30 minutes (black spectra). ....	107
Figure 4.41.	FTIR-DRIFT spectra obtained from CDRM at 573 K over (a) 5%Co-2%Ce/ZrO <sub>2</sub> , (b) 5%Co-3%Ce/ZrO <sub>2</sub> , (c) 10%Co-2%Ce/ZrO <sub>2</sub> , and (d) 10%Co-3%Ce/ZrO <sub>2</sub> just after CDRM with 1/1 feed ratio (grey spectra), and upon He flush (black spectra). ....	109
Figure 4.42.	FTIR-DRIFT spectra obtained just after CDRM at 573 K over (a) 5%Co-2%Ce/ZrO <sub>2</sub> , (b) 5%Co-3%Ce/ZrO <sub>2</sub> , (c) 10%Co-2%Ce/ZrO <sub>2</sub> , and (d) 10%Co-3%Ce/ZrO <sub>2</sub> with 2/1 feed ratio (grey spectra), and 1/2 feed ratio (black spectra). ....	111

Figure 4.43. FTIR-DRIFT spectra obtained from CDRM at 573 K over 5%Co-2%Ce/ZrO <sub>2</sub> catalyst for (a) CH <sub>4</sub> /CO <sub>2</sub> =2/1, (b) CH <sub>4</sub> /CO <sub>2</sub> =1/1, and (c) CH <sub>4</sub> /CO <sub>2</sub> =1/2 at different wavelength intervals. ....	112
--	-----

## LIST OF TABLES

Table 3.1.	Chemicals used for catalyst preparation. ....	33
Table 3.2.	Specifications and applications of the liquids used. ....	34
Table 3.3.	Specifications and applications of the gases used. ....	34
Table 3.4.	Gas analysis conditions for the system. ....	41
Table 3.5.	FTIR-DRIFTS pretreatment procedures. ....	44
Table 3.6.	List of FTIR-DRIFTS experiments for characterization. ....	45
Table 3.7.	Parameters for performance experiments over Co-Ce/ZrO <sub>2</sub> catalyst system. ....	47
Table 3.8.	List of FTIR-DRIFTS experiments for performance and kinetics. ....	48
Table 3.9.	List of kinetic parameters for determining power law type rate equation. ....	49
Table 3.10.	List of kinetic parameters to determine the effect of H <sub>2</sub> and CO partial pressures. ....	50
Table 4.1.	HRTEM-EDX analysis results for the areas in Figure 4.2a and b. ....	52
Table 4.2.	The Ce valance-binding energy (eV) relation for different reaction conditions. ....	54
Table 4.3.	Ce and Co surface atomic percentages of the spent catalysts obtained by SEM-EDX analysis. ....	59

Table 4.4.	The Ce valance-binding energy (eV) relation for different catalyst samples. ....	75
Table 4.5.	Apparent activation energies (kJ/mol) for Co-Ce/ZrO <sub>2</sub> catalysts. ....	86
Table 4.6.	Initial CDRM rates for Co-Ce/ZrO <sub>2</sub> catalysts. ....	88
Table 4.7.	Estimated reaction rate parameters. ....	89
Table 4.8.	Rate expressions tested in this study. ....	92
Table 4.9.	Model parameters obtained for 5%Co-2%Ce/ZrO <sub>2</sub> catalyst. ....	93
Table 4.10.	Model parameters obtained for 10%Co-2%Ce/ZrO <sub>2</sub> catalyst. ....	94

**LIST OF SYMBOLS**

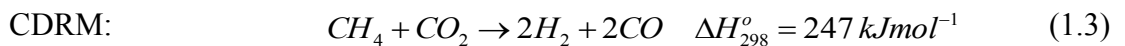
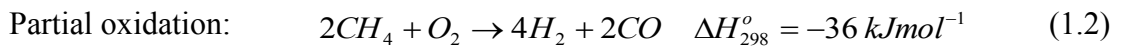
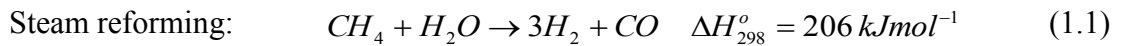
C	Concentration
$E_A$	Activation energy
F	Flow rate
$k_0$	Pre-exponential factor
K	Adsorption coefficient
P	Partial pressure
r	Reaction rate
R	Universal gas constant
T	Temperature
W	Catalyst weight
X	Conversion
A	Reaction order of methane
B	Reaction order of carbon dioxide

## LIST OF ACRONYMS/ABBREVIATIONS

BOS	Birleşik Oksijen Sanayi
CDRM	Carbon Dioxide Reforming of Methane
CRZS	Cobalt Catalysts Promoted by Ruthenium and Zirconium
DI	Deionized
DRIFTS	Diffuse Reflectance Infrared Fourier Transform Spectroscopy
EDX	Energy Dispersive X-Ray
FTIR	Fourier Transform Infrared
GC	Gas Chromatograph
HC	Hydrocarbon
HPLC	High Performance Liquid Chromatography
HRTEM	High Resolution Transmission Electron Microscopy
ID	Inner Diameter
IGA	Intelligent Gravimetric Analyzer
MCT	Mercury Cadmium Telluride
OD	Outer Diameter
OSR	Oxidative Steam Reforming
POX	Partial Oxidation
RWGS	Reverse Water-Gas Shift
SEM	Scanning Electron Microscopy
SR	Steam Reforming
SS	Stainless Steel
SV	Space Velocity
TCD	Thermal Conductivity Detector
TOS	Time-on-Stream
TPR	Temperature Programmed Reduction
TPO	Temperature Programmed Oxidation
WGS	Water-Gas Shift
XRD	X-Ray Diffraction
XPS	X-Ray Photoelectron Spectroscopy

## 1. INTRODUCTION

Owing to recent advances in its recovery and the associated drop in its prices, natural gas, which on the average consists of 80% methane and besides heavier hydrocarbons, CO<sub>2</sub> and a complex mixture of pollutant gases, have been considered as both an energy source and potential raw material for chemical and petrochemical industry (Boukha *et al.*, 2007; Reddy *et al.*, 2010; Gould *et al.*, 2015). Most of natural gas reserves, however, are situated in areas remote from the centers of highest energy consumption, leading to high costs of transportation, compression and storage (Mattos *et al.*, 2003). In order to make natural gas economically more viable, research on the conversion of methane to liquids or higher hydrocarbons has been carried out. Currently, this is industrially performed by initial conversion of natural gas to carbon monoxide and hydrogen, which together is called as synthesis gas (syngas), through steam reforming (Equation 1.1), partial oxidation, (Equation 1.2), or carbon dioxide reforming of methane, CDRM, (Equation 1.3) (Boukha *et al.*, 2007; Damyanova *et al.*, 2009).



As it can be used as a clean energy carrier in fuel cells, hydrogen is expected to be one of the main energy sources in foreseeable future. Syngas, on the other hand, is the reactant mixture of Fischer-Tropsch reaction through which a wide range of valuable hydrocarbons can be produced (Xu *et al.*, 2009).

Compared to other methods, CDRM, which is also called dry reforming, has the advantage of consuming carbon dioxide, which is a highly oxidized and thermodynamically stable greenhouse gas whose concentration rise in the atmosphere has been widely accepted as the most plausible reason for the abrupt climatic changes (Cheng *et al.*, 2006; Omae, 2006). On site syngas production through CDRM is possible for many

natural gas reserves, for which significantly high amount of CO<sub>2</sub> proper for CDRM is found mixed with CH<sub>4</sub> (Ocsachoque *et al.*, 2011; Tankov *et al.*, 2014). Therefore, utilization of two greenhouse gases and thereby contributing to limitation of global warming can be achieved without any pre-separation (Cheng *et al.*, 2006; Reddy *et al.*, 2010). Another advantage of this process is that it can be employed in areas where water is not available (Cheng and Huang, 2010). It is also beneficial with its H<sub>2</sub>/CO product ratio less than or equal to 1/1 (Moradi *et al.*, 2010). Such ratio is more suitable for producing sulfur free synthetic liquid fuels and valuable oxygenated chemicals via further reactions, like Fischer-Tropsch, than the feed(s) having high H<sub>2</sub>/CO ratio that would be produced by other traditional processes, like steam reforming (Reddy *et al.*, 2010). Since the reaction is highly endothermic, the dry reforming process can be also used in different areas, like a system for converting renewable energy to chemical energy, energy storage in the form of CO and H<sub>2</sub>, and in chemical energy transmission systems (CETS) (Gallego *et al.*, 2008a). Moreover, the process is suitable to be used as a method of recovering excess heat from gas turbine exhaust, and as a source of CO and H<sub>2</sub> for flame stabilization in low temperature methane fired gas turbines (Arkatova, 2010).

However, dry reforming also has some drawbacks compared to other industrial reactions, including low kinetics, catalyst sintering led by elevated temperatures, sometimes above 800 °C, which is required to reach high conversion levels due to the highly endothermic nature of the process in CDRM, and catalyst deactivation due to carbon deposition, preventing its practice at commercial scale (Ozkara-Aydinoglu *et al.*, 2009; Sutthiumporn and Kawi, 2011). The latter, coke formation, mainly occurs as a result of methane decomposition and carbon monoxide disproportionation (Boudouard reaction). Methane decomposition is favored at high temperatures and low pressures, whereas Boudouard reaction is favored at low temperatures and high pressures (Gallego *et al.*, 2008b).

Thermodynamic evaluation of graphitic carbon deposition in terms of reaction conditions reveals that carbon deposition is possible at CH<sub>4</sub>/CO<sub>2</sub> feed ratio of unity at temperatures up to 870 °C at atmospheric pressure. At a given pressure, the temperature limit increases as the CH<sub>4</sub>/CO<sub>2</sub> feed ratio increases. Therefore, carbon formation can be avoided thermodynamically at high temperatures like 1000 °C and also by the presence of

excess of CO<sub>2</sub>, H<sub>2</sub>O or O<sub>2</sub>. However, from industrial point of view, it is preferred to have a process running at a relatively lower temperature with a CH<sub>4</sub>/CO<sub>2</sub> feed ratio close to unity. Consequently, developing CDRM catalysts that are resistant to coking and minimize energy supply requirement, and finding optimum conditions yielding high activity towards synthesis gas formation are of great interest in recent years. Numerous supported metal catalysts have been developed and tested for their performance in CDRM (Bobrova *et al.*, 2016; Gallego *et al.*, 2008b; Pompeo *et al.*, 2009).

Moreover, a reliable kinetic equation is required to model, simulate, and optimize the CDRM reactor (Moradi *et al.*, 2010). Therefore, the work on finding appropriate mechanisms for CDRM specific to the designed and developed novel, high performance catalysts has started to get attention in the related literature. All the above mentioned endeavor aims to accelerate the transition from research and development stage to the development stage for CDRM technology.

The aim of the current work is to design and develop effective non-PGM based CDRM catalysts, to confirm the roles of each component, to determine optimum reaction conditions for the highest performance, and to reveal the details of CDRM reaction mechanism. Accordingly, non-PGM based catalysts, having Co as the non-precious metal, were designed, prepared and tested. In catalyst design, metal and promoter levels were used as parameters. The prepared catalysts were characterized by X-Ray Photoelectron Spectroscopy (XPS) for analyzing the oxidation states, Raman Spectroscopy for structural characterization and abundance of coke formation, Scanning Electron Microscopy/Electron dispersive X-Ray (SEM-EDX) for studying microstructural formations, metal mapping and local metallic formations, High Resolution Transmitting Electron Microscopy (HRTEM) and HRTEM-EDX for detailed characterization of metallic phases and their dispersion, metallic formations at interfacial boundaries of metals, and -if any- for finding evidence of surface alloy formations. The characterization procedure also involved a detailed Fourier Transformed/Diffuse Reflectance Infrared (FTIR-DRIFT) analysis by using probe molecules, like CO, in order to define the planes of the active phases present on the catalysts through frequency analysis. The performance tests of the catalysts were obtained through following an experimental procedure having reaction temperature, CH<sub>4</sub>/CO<sub>2</sub> feed ratio and space velocity as the parameters. The extent and the reasons of stability loss

(coke formation, metal sintering, etc.) were determined through TPOxidation-TPO, XPS, SEM and Raman studies. Additionally, the kinetic tests were performed to elucidate power-law type rate expressions and mechanistic kinetic expression for selected catalysts. FTIR-DRIFT system was also scrutinized for clarification of the kinetic mechanism.

Chapter 2 contains a detailed literature survey on theoretical background of CDRM, catalyst deactivation mechanism as well as kinetics of CDRM. Chapter 3 presents the experimental work carried out. The results obtained are presented and discussed in Chapter 4. Chapter 5 consists of the conclusions drawn from the present study and recommendations for future work.

## 2. LITERATURE SURVEY

### 2.1. Carbon Dioxide Reforming of Methane

Carbon dioxide reforming of methane (CDRM), Equation 2.1, which is a catalytic process to produce valuable synthesis gas by utilizing methane and carbon dioxide, occurs simultaneously with the following side reactions (Gallego *et al.*, 2008a; Nandini *et al.*, 2006; Takahabe *et al.*, 2005):

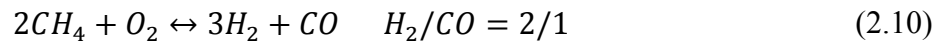
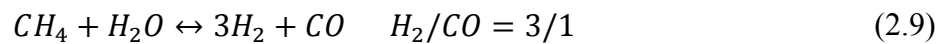


Among these reactions, RWGS, methane decomposition and Boudouard reactions seem to be the most significant ones and strongly affect the selectivity of the global process (Barroso-Quiroga and Castro-Luna, 2010).

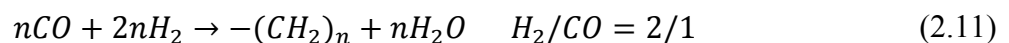
The CDRM product, synthesis gas, which is a mixture of hydrogen and carbon monoxide, make the reaction popular among the catalyst researchers. Hydrogen, itself, is important as a non-polluting fuel for fuel cells or combustion engines; it is efficiently and

benignly converted to power for mobile and small-scale stationary applications. Additionally, hydrogen is essential for oxygen removal to produce biofuels from oxygenated hydrocarbons in biomass conversion. Another area of hydrogen use is the hydro-processing of liquid fossil fuels and ammonia production. Hydrogen is needed in the chemical industry, too. Consequently, an ever increasing demand for the production of hydrogen should be anticipated. (Lin *et al.*, 2009) Synthesis gas, on the other hand, serves as a feedstock for production of valuable hydrocarbons via Fischer-Tropsch synthesis (Cheng and Huang, 2010).

CDRM provides a potential advantage over steam reforming (SR), Equation 2.9, or partial oxidation (POX), Equation 2.10, owing to its ideal H<sub>2</sub>/CO production ratio as unity, which would have an impact on the industrial sector. Both SR and POX have low H<sub>2</sub>/CO product ratio since the practical operating conditions of those reactions are strongly influenced by the co-occurrence of RWGS, and therefore, causes a decrease in H<sub>2</sub> yield, this ratio might become lower than unity. (Gallego *et al.*, 2008a; Djinovic *et al.*, 2012a)



H<sub>2</sub>/CO ratio around unity is suitable for further Fischer-Tropsch synthesis producing long-chain hydrocarbons, given in Equation 2.11, dimethyl ether synthesis, and methanol production, in Equation 2.12. It also results in a possibility of combining steam reforming and/or partial oxidation with dry reforming reactions to get the desired H<sub>2</sub>/CO ratio for different applications (Rezaei *et al.*, 2007).



Another advantage of CDRM among other reforming processes is its reactants. Since many natural gas reservoirs having both CH<sub>4</sub> and CO<sub>2</sub> are located in remote areas, the capability to convert the natural gas on site to higher value products in an efficient manner

becomes an important subject. Applying CDRM can therefore increase the cost effectiveness of remotely located reservoirs. (Corthals *et al.*, 2008; Mattos *et al.*, 2003) It should be mentioned that the increased emissions of greenhouse gases in the atmosphere have become major environmental problems leading to global climate change; this situation has heightened the interest for the control, conversion and utilization of greenhouse gases worldwide (Liu *et al.*, 2010). Since both methane and carbon dioxide are main greenhouse gases, and two of the most stable and abundant carbon-containing materials; the reformation between them is of extreme importance both for reducing the emission of greenhouse gases and for providing a renewable way of hydrogen supply as well (Xu *et al.*, 2009; Rezaei *et al.*, 2009). In addition, fossil resources can be conserved when secondary CO<sub>2</sub> is used as raw material surrogate (Djinovic *et al.*, 2012b).

The high endothermicity of CDRM allows the use of the process in energy transformation from solar to chemical energy, in energy storage in the form of CO and H<sub>2</sub> and in chemical energy transmission systems (CETS). A power source drives the endothermic reforming reaction and the product gases are transported to consumers at remote areas, where the reverse exothermic methanation reaction can be performed. (Gallego *et al.*, 2008a)

Furthermore, a comparative cost study about the production of acetic acid using three reforming processes showed that the operative cost of dry reforming of methane is lower than those of the other two processes. Hence, this process seems to be a promising route from an economic point of view and also appears to be an adequate tool for the environmental protection. (Ballarini *et al.*, 2005)

On the other hand, in addition to its low reaction rates, the major obstacle that prevents commercialization of CDRM is the high operating temperature requirement due to the highly endothermic nature of the process. Sintering, metal oxidation and significant coke formation occur at high operating temperatures causing catalyst deactivation, catalyst destruction and reactor blockage. (Al-Fatesh and Fakeeha, 2012; Daza *et al.*, 2010) Mainly two reactions, which are Boudouard and methane decomposition reactions, are responsible for coke formation. Nevertheless, it has been shown that a high dispersion of the metal species over the support can limit the coke formation (Daza *et al.*, 2010). In order to find

solutions to the problems curbing industrial use of CDRM, first the catalytic activity inhibition, with its possible causes and mechanisms, needs to be scrutinized in a detailed fashion.

## 2.2. Catalytic Activity Inhibition

Catalyst deactivation, the loss of catalytic activity and/or selectivity over time, is a continuing concern in the practice of industrial catalytic processes since the resultant catalyst replacement and process shutdown significantly affect the profitability of these chemical processes. Even though catalyst deactivation is inevitable, the fact that some of its immediate and drastic consequences may be avoided makes the research and development on deactivation issues a serious area of interest. (Bartholomew, 2001)

Deactivation can basically occur because of chemical, mechanical or thermal causes. The six intrinsic mechanisms that yield deactivation are poisoning, fouling, thermal degradation, vapor compound formation accompanied by transport, vapor-solid and/or solid-solid reactions, and attrition/crushing. Poisoning is defined as the strong chemisorption of species on catalytic sites, whereas fouling is the mechanical deposition of species from the fluid phase onto the catalyst surface, which results in activity loss due to blockage of sites and/or pores. Mechanical deposits of carbon and coke in porous catalysts can be considered as important examples of fouling. Thermal degradation and/or sintering, on the other hand, are the thermally induced loss of catalytic surface area and support area. Vapor formation is the reaction of gas with catalyst phase to produce volatile compound. Vapor-solid and solid-solid reactions are reactions producing inactive phases. Attrition/crushing is the loss of catalytic material or internal surface, which is due to abrasion or mechanical-induced crushing of the catalyst particle, respectively. (Bartholomew, 2001)

For the case of CDRM, the main causes of deactivation are fouling by carbon and sintering. The Boudouard reaction and  $\text{CH}_4$  decomposition are the side reactions that are responsible for carbon generation during CDRM (Jose-Alonso *et al.*, 2011). The Boudouard reaction given in Equation 2.6 is exothermic and favored at lower temperatures; whereas methane decomposition in Equation 2.7 is favored at higher

temperatures and lower pressures (Juan-Juan *et al.*, 2009). In the case of fouling by carbon (or coke), carbon deposits may block access of reactants to metal surface sites, or totally encapsulate a metal particle and thereby completely deactivate that particle, or plug micro- and mesopores such that access of reactants is hindered to many crystallites inside these pores (Miguel *et al.*, 2012). Finally, in extreme cases, strong carbon filaments may cause disintegration of catalyst pellets and lead to plugging of reactor voids. Deposition in pores may extend to the level that carbon generates stress and leads to fracture of the support material. (Bartholomew, 2001)

Many mechanistic studies have suggested that during CDRM, methane is decomposed to reactive carbon species on the metallic sites and these carbon species are oxidized to CO by the oxygen-containing species that originate from CO<sub>2</sub>. Thus, the rate of carbon accumulation on the catalyst surface is determined by the relative rates of the generation of carbon species and their oxidative removal. When the former is faster than the latter, carbon deposition occurs. Therefore, maintaining a dynamic balance between carbon formation and its oxidation by possible CDRM conditions, including temperature, CH<sub>4</sub>/CO<sub>2</sub> ratio, catalyst type and structure is crucial to obtain catalysts with high activity and stability. (Ruckenstein and Wang, 2002)

Another mechanism involving carbon deposition over metal surface, which occurs through the steps of migration of carbon containing species to the bulk phase of metal, saturation of these species and condensation of carbon, leads no direct catalyst deactivation. Instead, this mechanism forms filamentous carbon which accumulates continuously and leads blocking of the bed or breaking pellets. (Alberston *et al.*, 2007)

Sintering, on the other hand, mainly increases with increasing temperature and it is generally affected by the presence of water vapor (Bartholomew, 2001). As a result, the high temperature window necessary for dry reforming and the formation of H<sub>2</sub>O by the reverse water gas shift reaction make the catalysts in CDRM sensitive to metal sintering. Sintering accelerates the carbon deposition as the critical size of the metal ensembles for catalyzing CH<sub>4</sub> reforming is smaller than that for carbon formation (Corthals *et al.*, 2008).

Under the light of challenges mentioned in the related literature, the development of new CDRM catalysts with high activity and selectivity and good stability characteristics, which can be obtained through incorporating kinetic inhibition of carbon formation under conditions where carbon deposition is thermodynamically favorable, is a desired research area (Chen *et al.*, 2001).

### **2.3. Catalysts for Carbon Dioxide Reforming of Methane**

Carbon dioxide reforming of methane has been extensively studied over catalysts composed of transition metal carbides and sulfides, perovskite-type mixed oxides, unsupported metals, and supported group VIII metals, with the exception of Os. Research on the catalysts for this reaction has mainly focused on the intrinsic activity of the metal phase, developing stability of catalyst with low carbon formation, searching for the most suitable type of the support for improving the efficiency of the catalyst, and scrutinizing the reaction mechanism. Reported order of activity of the tested metals is as follows: Rh, Ru > Ir > Ni, Pt, Pd > Co > Fe, Cu. Generally, low carbon formation is observed for noble metal catalysts. However, from an industrial standpoint, non-noble catalysts are preferred due to the abundance and low price of their active phase. (Rezaei *et al.*, 2006; Xu *et al.*, 2009; Moradi *et al.*, 2010)

#### **2.3.1. Noble Metal Catalysts**

Noble metal catalysts are mostly preferred in methane reforming reactions due to their superior catalytic activity, which is attributed to reduced mobility and/or solubility of carbon in noble metals, and the fact that they suffer less from carbon deposition as compared to non-noble metal catalysts (Bartholomew, 2001; Hou *et al.*, 2006). There are many studies related to the CO<sub>2</sub> reforming reaction of methane over noble metals in order to develop a successful catalyst, and to gain an enhanced understanding of the mechanisms of reaction and deactivation. The findings in the literature has suggested that the behavior of supported noble metallic catalysts in CDRM depends on several interrelated factors such as the nature of the metal, the support type, the metallic particle size and the characteristics of metal-support interface (Damyanova *et al.*, 2009).

The activity and stability series of noble metals differs primarily depending on their coke resistance. Series of noble metal catalysts (Ru, Rh, Ir, Pt, and Pd) supported on alumina-stabilized magnesia (spinel) were analyzed in dry reforming reaction to observe this effect. The activity results expressed high activity and stability for the Ru, Rh and Pt catalysts. The TPO and TPH analyses indicated that the lower activity and stability of the Pd catalyst was due to the formation of the less reactive deposited carbon and sintering of the catalyst. (Rezaei *et al.*, 2006)

Chen and coworkers studied the effect of Ru content on the properties of the  $\text{Ce}_{0.75}\text{Zr}_{0.25}\text{O}_2$  solid solution supported catalysts (2010). The work confirmed that the highly dispersed Ru species favored the interaction between Ru and  $\text{Ce}_{0.75}\text{Zr}_{0.25}\text{O}_2$ . The reduced  $\text{Ce}_{0.75}\text{Zr}_{0.25}\text{O}_2$  was able to store hydrogen, while Ru promoted the reduction of  $\text{Ce}_{0.75}\text{Zr}_{0.25}\text{O}_2$ . Although the  $\text{CH}_4$  and  $\text{CO}_2$  conversions of the catalysts increased with the increase of Ru content, the turnover frequencies of  $\text{CH}_4$  and  $\text{CO}_2$  were higher for the catalysts with lower Ru contents, which may be resulted from the strong interaction between Ru and  $\text{Ce}_{0.75}\text{Zr}_{0.25}\text{O}_2$ .

The  $\text{CO}_2$  reforming of methane was also studied on Pt/ $\text{Al}_2\text{O}_3$ , Pt/ $\text{ZrO}_2$ , and Pt/Ce- $\text{ZrO}_2$  catalysts and the highest stability of Pt/Ce- $\text{ZrO}_2$  catalyst was explained by its higher oxygen storage/release capacity and reducibility, which allowed a continuous removal of carbonaceous deposits from the active sites. For Pt/ $\text{Al}_2\text{O}_3$  and Pt/ $\text{ZrO}_2$  catalysts, on the other hand, it was reported that the increase of carbon deposits around or near the metal particle inhibited the  $\text{CO}_2$  dissociation. (Mattos *et al.*, 2003)

Rhodium has been widely investigated as the active metal for CDRM. In their study, Djinovic and co-workers prepared 2%Rh- $\text{CeO}_2$  catalyst by using the hard template method and found out that the prepared powdered catalyst retained high thermal stability and high surface area with negligible sintering during 24 hours exposure to 973 K in an inert atmosphere (2012b). Besides  $\text{H}_2$  and  $\text{CO}$ ,  $\text{H}_2\text{O}$  was identified as a reaction product, originating from the simultaneously occurring reverse water-gas shift reaction.

The effects of operating and preparation variables, like reforming temperature,  $\text{CO}_2$  concentration, and pre-reduction, were investigated over 0.5%Pt/ $\gamma\text{-Al}_2\text{O}_3$  catalysts. It was

found that reforming at 900 °C with pre-reduction gave the highest H<sub>2</sub> production for reactant gas concentrations similar to biogas. However, a significant weight gain due to carbon deposition on the catalyst surface was measured at this high temperature. Yet, this weight gain did not cause a decrease in catalyst activity as was the case for the lower temperature tests. The suppression of the Boudouard reaction at high temperatures was proposed as a possible explanation for stability. Additionally, increasing CO<sub>2</sub> concentrations maintained the activity of the catalyst at high temperatures despite significant carbon deposition. (Barrai *et al.*, 2007)

Despite their resistance to carbon deposition and high activity, noble metal catalysts have the drawbacks of high cost and limited raw material availability, which restrict their use in industry, and form an incentive for the studies on developing non-noble catalysts appropriate for CDRM (Liu *et al.*, 2010; Ruckenstein and Wang, 2002).

### **2.3.2. Ni-based Catalysts**

Ni catalysts are of special interest in industrial applications due to their low cost, redox properties, higher availability, activity and selectivity (Gallego *et al.*, 2008a; Juan-Juan *et al.*, 2006). However, they are more prone to carbon deposition and metal sintering (Moradi *et al.*, 2010). The nickel metal can dissolve unreactive carbon residues and generate carbon filaments (whiskers) with the Ni particle on the filament top. During this process, metallic sites remain uncovered. This process results in much lower deactivation rate than that caused by graphitic carbon covering the metals surface. However, as whisker formation causes a significant expansion of the catalyst bed leading severe operational problems, it must be absolutely avoided, and since Ni is placed on the filament top, it is challenging to regenerate the catalytic system because the contact between metal and support is lost (Pompeo *et al.*, 2007). Therefore, in order to achieve long-term operation, Ni catalysts have been developed via using different types of supports, preparation method, or the addition of activity modifiers, such as noble or alkaline metals (Barroso-Quiroga and Castro-Luna, 2010).

Modified supports were studied to improve the stability and carbon resistance of nickel catalysts. Recently, Bellido and Assaf (2009) prepared 5 wt.% nickel catalysts

supported on pure  $ZrO_2$  and  $ZrO_2$  stabilized with 4 mol%, 8 mol% and 12 mol% of  $Y_2O_3$  by using the polymerization method. The XRD patterns exhibited presence of the oxide precursor (NiO) and the tetragonal phase of  $Y_2O_3$ - $ZrO_2$  solid solution. The TPR- $H_2$  analysis, on the other hand, confirmed that the reduction of various NiO species was influenced by the composition of the support. A direct relation was observed between the variations in the support, the nickel species supported on it and the performance observed in the catalytic tests.

In another study, Ni/ $La_2O_3$  catalyst was observed to be more stable than Ni/ $\gamma$ - $Al_2O_3$  and Ni/CaO. In Ni/ $La_2O_3$  catalyst,  $La_2O_3$  phase interacted with  $CO_2$  leading to formation of  $La_2O_2CO_3$  phase. It was concluded that the presence of a high concentration of oxidized carbon, presumably  $La_2O_2CO_3$  and formate-type species on the support in the Ni/ $La_2O_3$  catalyst, played an important role in enhancing the reaction rate. (Moradi *et al.*, 2010)

Nanostructured Ni-containing spinel oxide catalysts were analyzed for their CDRM performance; the higher activity exhibited by the Ni-based catalyst was found related to the higher activity of nickel metal in  $CO_2$  decomposition, while its remarkable stability seemed to be due to the presence of well dispersed  $Ni^\circ$  nano particles involved in long-term conversion. Raman analyses suggested that graphitic carbon produced by both  $Ni^\circ$  and  $Co^\circ$  species deactivated carbon deposits. It was shown that  $Ni^\circ$  and/or  $Co^\circ$  entities with high accessibility to  $CH_4$  and  $CO_2$  were responsible for high catalytic performance in CDRM. (Sousa *et al.*, 2012)

The performance of the Ni-based catalysts prepared with different nickel loading ranges over calcium-hydroxyapatite and calcium-fluoroapatite were investigated. Three types of nickel species were detected in the two series of catalysts prepared based on Ni loading. One of them was  $Ni^{2+}$  ions exchanged with  $Ca^{2+}$  ions of the apatite framework. This  $Ni^{2+}/Ca^{2+}$  exchange seemed to be restricted to nickel loadings inferior to 1 wt.% Ni. The other one was small particles of NiO exhibiting strong interactions with the carriers for nickel loadings greater than 1 wt.% Ni. The last one was large particles of NiO appearing at high loadings. The nature of the apatite changed the distribution of the nickel between these three hosting sites. It was seen that both methane conversion at 600 °C and carbon deposition on the catalysts increased with the nickel loading where  $H_2/CO$  product ratio

was close to 1. However, a significant decay of the activity after 4 hours-on-stream was not provoked. This was concluded to be the result of synergy between the basic properties of the apatites, their aptitude to chemisorb CO<sub>2</sub> and the catalytic features of the supported nickel (Boukha *et al.*, 2007).

Likewise, Garcia and co-workers studied the effect of the amount of nickel loading on Ni/Nd<sub>4</sub>Ga<sub>2</sub>O<sub>9</sub> samples containing 5, 10 and 15 wt.% of Ni (2008). The best catalytic activity was observed at 800 °C for the catalyst with 10% Ni loading reduced at 700 °C. After 12 hours-on-steam, no carbonaceous deposits were observed. High reduction temperatures observed in the TPR study indicated a strong and complex interaction between nickel and the cuspidine-like phase Nd<sub>4</sub>Ga<sub>2</sub>O<sub>9</sub> support. This feature coupled with the moderate basicity of the cuspidine-type could prevent the tendency to Ni coarsening in the catalyst and increase the resistance to coking.

In the preparation of most of the heterogeneous catalysts, the calcination step was needed to decompose the metal precursor (Juan-Juan *et al.*, 2009). Wang and co-workers studied the effect of calcination temperature as well as the Ni loading on CDRM performance (2009). Two series of Ni/MgO catalysts were prepared either by reducing NiO/MgO samples of fixed Ni loading and treated them under different calcination temperatures, or by treating the samples having varying Ni loadings under fixed calcination temperature. A complete incorporation of NiO into the MgO “support” to form NiO-MgO solid solution during the calcination stage of the catalyst preparation was identified as the essential step for the formation of stable Ni/MgO catalysts. The catalytic activity in terms of CH<sub>4</sub> turnover frequency (TOF) decreased with increasing Ni particle size. The support of the stable catalysts was actually a kind of Ni<sub>x</sub>Mg<sub>1-x</sub>O (x=0.02-0.15) solid solution, and the stable catalytic sites were proposed associated with nano-sized Ni particles (3-20 nm) which were in strong interaction with the solid solution support.

Another experimental work about the effect of calcination temperature on dry reforming was conducted by using catalysts supported on high surface area alumina. Aiming to produce CO-rich synthesis gas with a more suitable H<sub>2</sub>/CO ratio, the effect of operating temperature was also investigated. The Ni/γ-Al<sub>2</sub>O<sub>3</sub> (SA-6175) catalyst was tested in a micro tubular reactor by using a temperature range of 500-800 °C and 500-900 °C for

operation and calcination, respectively. It was observed that catalyst activity increased as calcination and reaction temperatures were both increased. Additionally, the catalysts needed be activated once before they were used for the first time. The highest conversion was obtained at 800 °C reaction temperature by using the catalyst calcined at 900 °C and activated at 700 °C. (Al-Fatesh and Fakeeha, 2012)

Like calcination, reduction is another important pretreatment step in the catalyst preparation as it is one of the primary factors influencing the final properties of the catalytically active sites. In order to study the effect of pretreatment on CDRM performance, different pretreatment procedures were used in preparation of Ni/Al<sub>2</sub>O<sub>3</sub> catalysts prior to CDRM tests (Juan-Juan *et al.*, 2009). The performed pretreatments were calcination with hydrogen reduction, direct hydrogen reduction and heat treatment up to the reaction temperature under inert atmosphere. Although the activity was not affected by the pretreatments applied, a noticeable effect on the amount of deposited coke was observed. The pretreatments affected the size and structure of nickel particles significantly. In general terms, the results revealed that the higher the mean particle size the higher the amount of deposited carbon. The reduction at 973 K without calcination yielded an active catalyst with the lowest carbon deposition suggesting that the calcination pretreatment could be avoided.

Gallego and co-workers (2008b) also worked on the effect of reduction on Ni based CDRM catalysts supported on La<sub>2</sub>NiO<sub>4</sub>-type perovskites prepared by the “self-combustion” method. The CDRM performance tests were conducted at 700 °C over the reduced and non-reduced forms of the catalyst. High CH<sub>4</sub> and CO<sub>2</sub> conversions were obtained with a H<sub>2</sub>/CO ratio lower than 1. This result was explained by the occurrence of the RWGS reaction. The use of the reduced perovskite La<sub>2</sub>NiO<sub>4</sub> as catalyst precursor led to the highest CDRM activity without carbon deposition after 160 h TOS. The reduction of the perovskite La<sub>2</sub>NiO<sub>4</sub> led to the formation of small nickel particles with average diameter of 7 nm, resulting in the catalytic activity higher than that obtained with 5% Ni/La<sub>2</sub>O<sub>3</sub>, which had an average diameter of 11 nm. As the unreduced form of the catalyst was composed of a mixture of Ni, La<sub>2</sub>O<sub>2</sub>CO<sub>3</sub> and La<sub>2</sub>NiO<sub>4</sub> during the first hours of the reaction, the catalytic activity was lower than that was obtained over the reduced perovskite.

The structure-sensitivity of carbon formation over Ni-containing catalysts allowed the possibility for inhibition of the carbon deposition by the modification of the catalyst surface. Considering this fact, Ni/Al<sub>2</sub>O<sub>3</sub> catalyst was treated by argon glow discharge plasma followed by calcination in air. The catalyst prepared by following this procedure showed an improved low-temperature activity for CDRM, compared to that of the catalyst prepared without plasma treatment. The method yielded thermally-induced generation of specific nickel species on the support, which could also improve the stability of the catalyst via enhancing the carbon resistance. (Cheng *et al.*, 2006)

### 2.3.3. Co-based Catalysts

As an alternative to nickel-based catalysts, which always have the drawback of possible methanation in the downstream gas tailed with the extracted catalyst fines, cobalt-based catalysts have been shown to have high performance in CDRM led by their good activity for soot oxidation, which may help to promote the carbon resistance of the catalyst in reforming reactions (Sousa *et al.*, 2012). However, in the case of Co catalysts, it was observed that deactivation may occur because of the metal oxidation under reaction conditions as well as the coke deposition. In this sense, it was observed that for high Co loadings (between 12 and 20 wt.%) deactivation occurred by coke deposition, while for low loadings (about 2 wt.%) deactivation occurred by oxidation of cobalt. Different approaches, like optimizing Co content, using different supports, promoters and reaction temperatures, were tested in order to avoid cobalt oxidation. (San-Jose'-Alonso *et al.*, 2009)

Catalytic performance of Co-MgO catalyst prepared by oxalate co-precipitation method was studied for dry reforming of methane at 1 MPa and 1023 K. It was seen that Co-MgO (7 mol% Co) showed a stable activity at high space velocity of 400000 cm<sup>3</sup>h<sup>-1</sup>g<sup>-1</sup>. However, the reactor was plugged during the reforming reaction with 10 mol% Co-MgO, and the activity of Co-MgO having Co contents less than 6 mol% was found to gradually decrease by the oxidation of cobalt species. (Omata *et al.*, 2004)

In the study of Budiman and co-workers, the novel silica supported cobalt catalysts promoted by ruthenium and zirconium (CRZS) were prepared in powder form via

coprecipitation method. The results revealed that the catalysts with low cobalt loadings (0-9 wt.%) had poor catalytic activities because the silica was known to have no role on activating CO<sub>2</sub> or CH<sub>4</sub>. The CRZS catalyst prepared at pH of 1 having 14.68 wt.% of cobalt, 0.14 wt.% of ruthenium, 5 wt.% of zirconium reached a comparably high catalytic activity and coke resistance. It was found out that the increase of cobalt loading results in enlargement of Co<sub>3</sub>O<sub>4</sub> clusters. The inhibition of strong Co-SiO<sub>2</sub> interaction in the proper zirconium loadings were also clearly confirmed by the tests results obtained over the catalysts having various metal loadings. (Budiman *et al.*, 2016)

In another study, the CDRM performance and carbon deposition behavior of the  $\gamma$ -Al<sub>2</sub>O<sub>3</sub> supported Co catalysts were investigated as a function of Co loading (between 2 and 20 wt.%) and calcination temperature ( $T_c=500$  or  $1000$  °C). The strong dependency of the stability of Co/ $\gamma$ -Al<sub>2</sub>O<sub>3</sub> catalysts on the Co loading and calcination temperature was confirmed. Over the catalysts with high Co loadings (higher than 12 wt.%), notable amounts of carbon were accumulated and deactivation was observed. (Ruckenstein and Wang, 2002)

A series of MgO modified Co/SiO<sub>2</sub> (5-35 wt.%) catalysts prepared by successive incipient wetness impregnation were tested in CDRM at the reaction temperature range of 500-800 °C. It was noted that at high MgO content (30-35 wt.%), a silicate adlayer Mg<sub>2</sub>SiO<sub>4</sub> was formed leading to a much improved catalytic stability. This phase favored the development of small metallic cobalt particles by preventing their coalescence under reaction conditions. A bi-functional mechanism that combines the accumulation of oxidizing agents, like carbonates and hydrogeno-carbonate adspecies, on the catalyst support led by a medium basicity of the layer and the reactivity of small metal particles in methane activation was proposed yielding stability (Bourab *et al.*, 2004)

Omata and colleagues (2004), on the other hand, worked on the catalytic performance of Co-SrO catalyst for CDRM at 1 MPa and 1023 K. Both oxalate coprecipitation method and citric acid method resulted in catalysts with a steady activity under pressure. The importance and stability of cobalt metal with strontium carbonate were suggested for the Co-SrO catalyst, and thus, it was denoted as Co-SrCO<sub>3</sub>. Moreover, it was seen that cobalt supported on strontium carbonate prepared by impregnation method

(Co/SrCO<sub>3</sub>) showed a comparable activity with high tolerance to oxidative atmosphere under reaction conditions.

Another research on CDRM performance included cobalt-based catalysts prepared by conventional impregnation of Co precursor on commercial  $\gamma$ -Al<sub>2</sub>O<sub>3</sub> support and sol-gel-made  $\gamma$ -Al<sub>2</sub>O<sub>3</sub>, and by direct sol-gel processing from organometallic compounds. All tested catalysts had the same cobalt content of 10 wt.%, and their catalytic activity was similar at 750 °C. However, at low reaction temperatures (550-650 °C) and high space velocity, relatively low catalytic activity was observed for the sample prepared by direct sol-gel due to the formation of CoAl<sub>2</sub>O<sub>4</sub>. It also possessed properties that could inhibit coke formation; like smaller metallic Co particles, richer surface OH species and stronger metal-support interaction. (Ji *et al.*, 2001)

CDRM was also conducted over cobalt based catalysts at 2 MPa prepared by adding trace amounts of platinum (Pt/Co=0.005-0.05 in atomic ratio) and ruthenium (Ru/Co=0.01-0.05) on Co/TiO<sub>2</sub>, and by replacing cobalt by nickel (Ni:Co=1:99-100:0). Co/TiO<sub>2</sub> reduced at 1123 K was noted to show slow deactivation due to oxidation of Co. The addition of noble metals enhanced the catalytic stability of Co/TiO<sub>2</sub> and the reducibility of cobalt oxide. Even though the replacement of Co by a small amount of Ni also improved the catalytic stability of Co/TiO<sub>2</sub>, it resulted in a decrease of catalytic stability due to coking. CoNi/TiO<sub>2</sub> with an optimum Co:Ni ratio of 90:10 was presented as a catalyst with high stability and insignificant coke deposition. (Nagaoka *et al.*, 2004)

San-Jose'-Alonso and coworkers tested CDRM performance of alumina supported Ni, Co and bimetallic Ni-Co catalysts at 973 K with the feed ratio of CH<sub>4</sub>/CO<sub>2</sub>=1/1 (2009). Among the catalysts studied, the monometallic catalysts with the highest cobalt content and bimetallic NiCo exhibited the highest activity and stability, but they also produced a large amount of carbon. The higher activity shown by cobalt rich catalysts was explained by higher activity of Co in methane decomposition, while their remarkable stability seemed to be due to the presence of large particles involved in long-term conversion since they produced non-deactivating carbon deposits.

Another Co-Ni bimetallic catalyst system was studied in the work of Luisetto and co-workers by using Co/CeO<sub>2</sub> (Co 7.5 wt.%), Ni/CeO<sub>2</sub> (Ni 7.5 wt.%) and Co-Ni/CeO<sub>2</sub> (Co 3.75 wt.%, Ni 3.75 wt.%) catalysts which were prepared by surfactant assisted coprecipitation method (2012). In the whole temperature range, which was between 600 °C and 800 °C, it was confirmed that the bimetallic Co-Ni/CeO<sub>2</sub> catalyst showed higher methane conversion and H<sub>2</sub>/CO selectivity than those of monometallic catalysts. The TG-DTA analysis performed on cobalt-containing spent samples used in the reaction for 20 h TOS at 750 °C indicated the catalysts has stable activity in the presence of a 6 wt.% deposited amorphous carbon, whereas Ni/CeO<sub>2</sub> showed 8% decrease in catalytic activity due to a massive, 25 wt.%, accumulation of amorphous and graphitic carbon.

## 2.4. Catalyst Supports and Promoters

### 2.4.1. Supports

Many industrial solid catalysts employ appropriate supports to disperse active metal or metal compounds. Since supports may also have a role contributing to catalytic activity and stability of the catalysts via chemical effects and/or via interaction between the active and the support phases, understanding the effect of support in the reaction network is of utmost importance for rational catalyst development. (Tao *et al.*, 2010; Wang *et al.*, 2011; Kouva *et al.*, 2014) It is well known that the structure and surface properties of the support exert a significant influence on the catalytic performance of supported catalysts. Therefore, the search of new catalysts supported on suitable carrier is still a research priority. (Damyanova *et al.*, 2009; Roh *et al.*, 2004)

Carbon formation in CDRM can be controlled by using a support that favors the dissociation reaction of CO<sub>2</sub> into CO and O, where the latter being responsible for the cleaning of the metallic surface (Ballarini *et al.*, 2005). Moreover, exploiting the metal-support synergistic interaction is a very plausible way in achieving coke deposition resistant catalysts which can exhibit stable activity in CDRM (Damyanova *et al.*, 2009). Strong metal-support interaction can also generate species that decorate metal surface, and produce oxygen to activate the reactants. Additionally, hydrogen spillover, a phenomenon involving hydrogen atoms adsorbed or generated on the metal migrate to the acceptor of

the support -when the metal interacts with the support and a direct contact forms- can promote the overall reaction. (Qian *et al.*, 2015) However, strong metal-support interaction might also become an obstacle since it may affect the reducibility of the catalysts (Ayodele *et al.*, 2016).

Although a support with large surface area (such as silica or alumina) allows active phase dispersed well throughout the porous system, it usually consists of small pores, which is not beneficial for the internal diffusion of reactants or products. A support with large pores, however, will facilitate the intrapellet diffusion, but the dispersion becomes limited due to its small surface area. (Tao *et al.*, 2010)

With its chemical and physical stability, mechanical strength and wide range of surface areas and pore volumes, the most commonly used support for CO<sub>2</sub> reforming of methane is Al<sub>2</sub>O<sub>3</sub>. Among alumina supports, the high surface area of  $\gamma$ -Al<sub>2</sub>O<sub>3</sub> provides higher metal dispersion, while  $\alpha$ -Al<sub>2</sub>O<sub>3</sub> presents better mechanical resistance (Alberton *et al.*, 2007). However, alumina presents the disadvantage of a weak metal-support interaction led by its low reactivity. (Pompeo *et al.*, 2009) Additionally,  $\gamma$ -Al<sub>2</sub>O<sub>3</sub> starts to lose its high surface area at temperatures greater than 873 K.

With distinct advantages such as nanometer-sized pore structures, high surface area and adjustable metal composition and types, mesoporous molecular sieve, as a novel support material, provides good opportunities to develop catalysts having improved catalytic performance in contrast to microporous zeolites and conventional macroporous materials (Liu *et al.*, 2010).

On the other hand, the use of supports with low concentration of Lewis acid sites and/or have basic sites, such as ZrO<sub>2</sub>, MgO, and La<sub>2</sub>O<sub>3</sub>, results in enhanced catalyst activity, lower coke deposition rate and therefore more stable CDRM performance (Rezaei *et al.*, 2009).

Among these, ZrO<sub>2</sub>, itself, shows a high thermal stability as a catalyst support. Many methods have been explored recently for catalytic applications in order to get nanocrystalline ZrO<sub>2</sub> powders with high surface area, since nanoscale supports usually

possess more edges and corners, which can result in higher performance of the catalyst. (Rezaei *et al.*, 2009) Moreover, zirconia provides an appreciable ionic conductivity due to its readiness to form defects and surface oxygen vacancies (Bellido *et al.*, 2008). ZrO<sub>2</sub> is also known to enhance CO<sub>2</sub> adsorption on the catalytic surface which ultimately leads to limited coke formation through facilitating reversed Boudouard reaction (Corthals *et al.*, 2008).

In addition to zirconia, other recently explored oxides such as ceria have attracted attention as carriers or catalysts for important industrial or environmentally friendly reactions. It is known that these oxides can enhance catalytic performances by imparting metal-support interactions either through the oxygen-storage/transport characteristics of the support or through the generation of active centers at the interface between metal and support. (Damyanova *et al.*, 2009)

The large oxygen storage capacity via a facile reaction, given in Equation 2.13, makes CeO<sub>2</sub> and Ce-containing mixed oxides promising catalyst supports for CDRM (Wang *et al.*, 2011).



Besides, the research on the interaction between hydrogen and ceria has indicated that ceria is able to store hydrogen (Chen *et al.*, 2010).

However, CeO<sub>2</sub> is easily susceptible to sintering at high temperatures, reducing both its specific surface area and oxygen storage capacity. It has been found that the thermal stability, oxygen storage capacity and redox property of CeO<sub>2</sub> can be improved by doping Zr<sup>4+</sup> ions. Such addition also promotes metal dispersion. (Wang *et al.*, 2011; Corthals *et al.*, 2008)

Considering the combined effect of CeO<sub>2</sub> and ZrO<sub>2</sub>, Roh and co-workers employed a co-precipitation/digestion method in a single step to prepare Ni-Ce-ZrO<sub>2</sub> catalysts useful for CDRM (2004). The loading amount of Ni and the ratio of CeO<sub>2</sub> to ZrO<sub>2</sub> were systematically varied to optimize the co-precipitated Ni-Ce-ZrO<sub>2</sub> catalysts. The methane

conversion was found to be higher than 97% at 800 °C over 15% Ni incorporated in cubic-phase structured  $\text{Ce}_{0.8}\text{Zr}_{0.2}\text{O}_2$ , and such activity was maintained without significant loss during the reaction for 100 hours TOS. However, due to carbon formation, Ni-Ce-ZrO<sub>2</sub> having tetragonal phase ( $\text{Ce}_{0.2}\text{Zr}_{0.8}\text{O}_2$ ) or mixed phase ( $\text{Ce}_{0.5}\text{Zr}_{0.5}\text{O}_2$ ) deactivated during the reaction. The enhanced catalytic activity and stability of the co-precipitated Ni- $\text{Ce}_{0.8}\text{Zr}_{0.2}\text{O}_2$  catalyst were attributed to a combination of the nano-crystalline nature of cubic  $\text{Ce}_{0.8}\text{Zr}_{0.2}\text{O}_2$  support and the finely dispersed nano-sized NiO<sub>x</sub> crystallites leading intimate contact between Ni and  $\text{Ce}_{0.8}\text{Zr}_{0.2}\text{O}_2$  particles.

In order to optimize the CDRM performance, the Co-incorporated  $\text{Ce}_{1-x}\text{Zr}_x\text{O}_2$  catalysts were prepared by co-precipitation method with the varying ratio of Ce to Zr. It was observed that the Co- $\text{Ce}_{0.8}\text{Zr}_{0.2}\text{O}_2$  sample containing 16% CoO exhibited a higher catalytic activity among the tested catalysts, and it maintained its activity without significant loss during the reaction for 60 h TOS. CO<sub>2</sub> conversion over this catalyst was found as 75% while the CH<sub>4</sub> conversion was 67% at 750 °C and 0.1 MPa for 36000 ml/h.g-catalyst and CO<sub>2</sub>/CH<sub>4</sub> molar feed ratio of 1/1. The cubic  $\text{Ce}_{0.8}\text{Zr}_{0.2}\text{O}_2$  facilitated a higher dispersion and a higher reducibility of the cobalt component. (Wang *et al.*, 2010)

Cerium promoted mixed oxides also appear to be a good choice of catalyst to be used in CDRM. In the study of Guzzi and co-workers, the amorphous and filamentous carbon formation on Ni-K/CeO<sub>2</sub>/Al<sub>2</sub>O<sub>3</sub> was observed at moderated temperatures (2010). The carbon filament growth and its kinetics were found linked to methane cracking and carbon dioxide disproportionation properties of the catalyst surface.

Pompeo and co-workers used Ni catalysts supported on commercial  $\alpha\text{-Al}_2\text{O}_3$  modified by addition of CeO<sub>2</sub> and/or ZrO<sub>2</sub> to evaluate the effect of support on performance and stability (2009). Their results exhibited that catalysts supported on Ce-Zr- $\alpha\text{-Al}_2\text{O}_3$  composites had better reforming activity and stability noticeably higher than those obtained in the case of the reference  $\alpha\text{-Al}_2\text{O}_3$  support. The presence of  $\text{Ce}_x\text{Zr}_{1-x}\text{O}_2$  type mixed oxides facilitated the formation of active phases with higher interaction through improving the Ni dispersion and the reducibility of metal particles. This interaction limited deactivation by sintering via conferring a higher contribution of adsorbed oxygen species to the system, favoring elimination of deposited carbon. These improvements were directly

dependent on the Ce/Zr ratio of the composite and it was indicated that catalysts with 4/1 ratios have higher stability.

Other mixed oxide catalyst systems have also gained attention with their superior properties in CDRM. In the study of Reddy and co-workers, ZrO<sub>2</sub>/SiO<sub>2</sub> mixed oxides with different ratios (2/1 to 4/1) were prepared by deposition-precipitation method and used as supports for platinum nano-particles (2010). A better thermal stability of the prepared ZrO<sub>2</sub>/SiO<sub>2</sub> supports compared to that of ZrO<sub>2</sub> was evidenced after ageing at 1073 K for 16 h in particular for the ZrO<sub>2</sub>/SiO<sub>2</sub> ratio of 4/1. Additionally, very high reforming activity was observed for the Pt/ZrO<sub>2</sub>/SiO<sub>2</sub> (4/1) sample among all the prepared catalysts. The better catalytic properties of this sample were explained by higher Pt dispersion owing to the absence of remaining free silica and the presence of amorphous ZrSiO<sub>4</sub> in higher amount, which were determined by X-ray diffraction patterns, BET and H<sub>2</sub> chemisorption measurements, X-ray photoelectron and FTIR spectra.

#### 2.4.2. Promoters

Introducing a second metal component to form a bimetallic system is widely used in improving the anti-coking property of the CDRM catalysts (Xu *et al.*, 2009). The addition of metallic promoters, such as Sn, leads catalysts to have a very high resistance to carbon deposition, which may be explained by high structure sensitivity of carbon formation reactions compared to that of syngas formation reactions (Pompeo *et al.*, 2007). The promoters are also known to decrease the carbon adsorption energy preventing carbon nucleation on the catalyst (Gould *et al.*, 2015).

It has been reported that incorporation of alkali, alkaline-earth and lanthanide oxides, and the use of highly dispersed metal particles on a substrate contribute to the reduction of carbon deposition and, therefore, to catalytic stability (Barroso-Quiroga and Castro-Luna, 2010).

Sutthiumporn and Kawi (2011) were investigated Mg, Ca and Sr, which are alkaline earth elements, as the promoters for Ni-La<sub>2</sub>O<sub>3</sub> CDRM catalyst. The performance results obtained at 600 °C exhibited that the Sr-doped Ni-La<sub>2</sub>O<sub>3</sub> catalyst had the lowest carbon

deposition over the catalyst surface with the highest CH<sub>4</sub> and CO<sub>2</sub> conversions and H<sub>2</sub> production. The presence of a high amount of surface lattice oxygen species, which promoted C-H activation in CDRM, resulting in high H<sub>2</sub> production observed, and it was suggested as the reason for the enhanced performance. Moreover, these surface oxygen species on the catalyst could adsorb CO<sub>2</sub> molecules to form bidentate carbonate species, which could then react with the surface carbon species formed during CDRM, yielding to higher CO<sub>2</sub> conversion and lower carbon formation.

In another study, Juan-Juan and colleagues investigated the influence of potassium content on the activity and selectivity of the NiK/Al<sub>2</sub>O<sub>3</sub> catalysts in CDRM (2006). Catalytic tests at 973 K were carried out for 6 and 24 h TOS. Even though the presence of potassium in Ni/Al<sub>2</sub>O<sub>3</sub> catalysts hindered the accumulation of coke on the catalyst surface during CDRM, it caused a decrease in the catalytic activity. It was also suggested that an optimum amount of potassium (0.2 wt.% K<sub>2</sub>O) led to a catalyst with a very low coke formation tendency and an acceptably high catalytic activity. With this amount, the coke deposition decreased more than 90% with only less than 10% loss in the catalytic activity. The study also revealed that the catalytic activity remained almost constant during at least 24 hours, independent of the potassium amount. This was an indication that the deactivation of the catalysts was not due to the coke deposition since Ni particles were formed on the top of carbon filaments during reaction.

The effect of potassium, tin, manganese and calcium on the behavior of a Ni-Al<sub>2</sub>O<sub>3</sub> catalyst prepared by sol-gel method was also observed. The preparation method yielded a massive catalyst with a small and homogeneous nickel particle size having high resistance to sintering. A dramatic decrease in catalytic activity and significantly high carbon deposition were observed in the case of Ca, Mn and Sn. However, it was confirmed that the introduction of 0.5 wt.% K hindered the accumulation of carbon on the catalyst surface, increased the reducibility, probably through modifying the metal-support interaction, while modified neither the size nor the structure of the nickel particles. (Luna and Iriarte, 2008)

The modification of non-noble metal catalysts by addition of low concentrations of noble metals was suggested to result in catalytic systems of accessible cost with good catalytic properties and low sensitivity to carbon formation (Ocsachoque *et al.*, 2011).

Moreover, it was reported that the addition of noble metals to Ni catalysts could promote the reducibility of Ni, and stabilize its degree of reduction during the catalytic process (Miguel *et al.*, 2012).

Regarding the enhanced properties of noble metal promoted catalysts, the surface characteristics of silica-supported monometallic Ni, Rh and bimetallic Ni-Rh catalysts, and their CDRM performance were studied. Effective process of Ni-Rh alloy formation was seen to take place in the case of SiO<sub>2</sub> supported bimetallic Ni-Rh catalysts unless high temperature calcination in oxygen stream is carried out. Additionally, segregation of metals led to the formation of Ni-rich surface alloy. (Jozwiak *et al.*, 2005)

Likewise, two bimetallic PtNi catalysts supported on a nanostructured  $\gamma$ -Al<sub>2</sub>O<sub>3</sub> together with the corresponding monometallic materials were analyzed in the study of Garcia-Dieguez and co-workers (2010). IR spectra of adsorbed CO indicated that the surface of the PtNi catalysts was dominated by Pt centers, whose electron-withdrawing character was increased by Ni. The alloy formation was associated with higher activity and lower production of carbonaceous materials during dry reforming of methane.

Due to its oxygen exchange capacity, ceria was reported to be another effective promoter for CDRM catalysts. It has two stable oxidation states, +4 and +3, and the relatively easy switching between these two states (i.e. red-ox cycle) allow it to uptake and release oxygen (Melchionna and Fornasiero, 2014; Du *et al.*, 2012). The oxygen species could therefore react with surface hydrocarbon species, which were formed upon CH<sub>4</sub> disproportionation, resulting in reduced coke formation (Corthals *et al.*, 2008). The role of ceria in improving the catalytic performance was also recognized to lie in the ability of increasing metal dispersion (Damyanova *et al.*, 2009).

Ni/Mo/SBA-15 catalyst modified with CeO<sub>2</sub> was studied and the results were compared with those obtained over unmodified catalyst aiming to observe the effect of CeO<sub>2</sub> promotion. Although both the Ni/Mo/SBA-15 and CeO<sub>2</sub>/Ni/Mo/SBA-15 catalysts expressed good catalytic activities at atmospheric pressure, adding CeO<sub>2</sub> to a Ni/Mo/SBA-15 catalyst was found beneficial since catalysts with low CeO<sub>2</sub> amounts (up to 2 wt.%) exhibited excellent stability at 800 °C for 100 h TOS, and no carbon deposits were

observed on the spent sample. FTIR spectra of fresh and used catalysts showed characteristic peaks of the mesoporous molecular sieve SBA-15, and this was attributed as a reason for prevention of carbon deposition and sintering of the nickel species in the CeO<sub>2</sub>/Ni/Mo/SBA-15 catalyst. (Jian *et al.*, 2012)

## 2.5. Kinetics of Carbon Dioxide Reforming of Methane

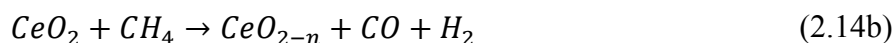
CDRM reaction mechanism over the catalysts plays an important role in designing and defining the optimal operation parameters of the CDRM reactor. However, the works on the kinetics of CDRM are limited, as the reaction has only recently attained attention.

It is known that the speed of CDRM is less than that of steam reforming, and this stays as a crucial obstacle in the commercialization of CDRM process. In the study of Avetisov and co-workers, a critical analysis of kinetic models of both steam and dry methane reforming over Ni-catalysts was performed and the reason for the difference in the rates of these two reforming reactions was explained by the significant surface coverage of carbon monoxide during CDRM (2010).

Kinetics of coke formation and removal stand as a significant issue in CDRM since carbon laydown, which is an inevitable result of CDRM, is often considered as the main cause of catalyst deactivation led by blockage of active sites. Even though many characterization techniques along with temperature programmed ones have been used to characterize carbon deposits, there is still a lack of information and agreement on the mechanism of carbon utilization in CDRM. By considering that, Foo and co-workers modelled the kinetics of carbon deposition on lanthanide-promoted Co-Ni/Al<sub>2</sub>O<sub>3</sub> catalyst by a power-law expression, with negative activation energy estimates for the examined temperature 923-1023 K range (2012). The presence of a reactive and a relatively non-reactive carbon species on the used catalyst were calculated based on the results of regeneration studies. While the oxidation-reduction (TPO-TPR) scheme was able to completely and more quickly remove carbon, marginal catalyst sintering was observed compared with the reduction-oxidation-reduction (TPR-TPO-TPR) scheme. Additionally, it was seen that lanthanide promotion resulted in lower coke formation due to interaction of the rare-earth oxide with the more reactive surface carbonaceous matter in redox reactions.

For the CDRM mechanism over Ru-based catalysts, it was stated that methane and carbon dioxide were adsorbed and dissociated on the transition metal surface. The adsorbed oxygen species and CO came from the dissociation of CO<sub>2</sub>, whereas the adsorbed CH<sub>x</sub> (0<x<3) species and H<sub>2</sub> derived from the dissociation of CH<sub>4</sub>. The support was also involved in production of CO and H<sub>2</sub> through the reaction between oxygen species and CH<sub>x</sub> species. According to these findings, the following mechanism of CDRM over Ru/Ce<sub>0.75</sub>Zr<sub>0.25</sub>O<sub>2</sub> was suggested: (Chen *et al.*, 2010)

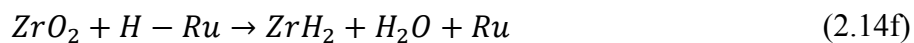
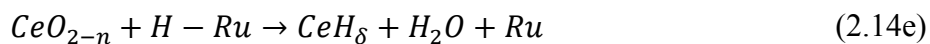
Dissociation of CH<sub>4</sub>;



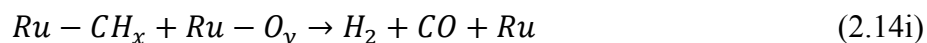
Dissociation of CO<sub>2</sub>;

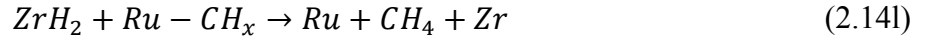
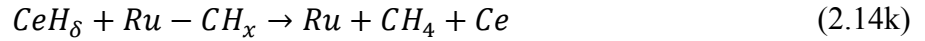
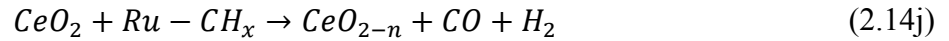


Formation of CeH<sub>8</sub> and ZrH<sub>2</sub>;

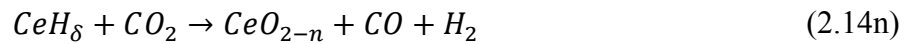


Elimination of CH<sub>x</sub>;





Other possible surface reactions were;



In this mechanism, the hydrides, existing in the reduced  $Ce_{0.75}Zr_{0.25}O_2$ , catalyze hydrogenation through providing hydrogen to promote the elimination of  $CH_x$  species. Only limited amount of carbon deposit on the spent catalyst was attributed to the resistance of metallic Ru to carbon deposition, the redox property of the  $Ce_{0.75}Zr_{0.25}O_2$  and the hydrogen storage ability of the reduced  $Ce_{0.75}Zr_{0.25}O_2$ . (Chen *et al.*, 2010)

In another study, the kinetics of CDRM over a ceria-promoted  $Mo_2C/\gamma-Al_2O_3$  (3 wt.% Ce, 30 wt.% Mo) catalyst were determined in the absence of mass-transfer limitations. Although the activation energy of the promoted  $Mo_2C$  catalyst, 45.5 kcal/mol, was similar to that of the bulk  $Mo_2C$  catalyst, the activity of the ceria-promoted catalyst was found higher. This was probably due to the higher dispersion of the promoted catalyst. Ceria promotion also appeared to affect the reaction by enhancing relatively strong  $CO_2$  adsorption, thereby lowering the reaction order of  $CO_2$  to zero. Accordingly, the following mechanism, which involved both the  $CO_2$  and  $CO$  redox reaction on the ceria particles, and  $CH_4$  and  $CO_2$  activation on the  $Mo_2C$  particles, was discussed (Darujati and Thomson,

2006), where (■) and (\*) represented an adsorption site on the ceria and a vacancy near the surface of the Mo<sub>2</sub>C, respectively:



Thus, the reaction given in Equation 2.15c was not a simple dual site reaction with adsorbed carbon and adsorbed oxygen, but it also involved a solid state reaction. This mechanism was seen to be consistent with the high activation energy of the supported catalyst. (Darujati and Thomson, 2006)

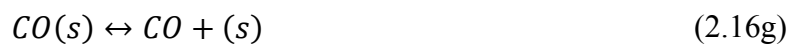
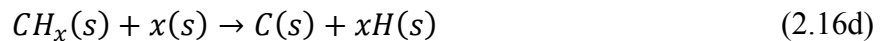
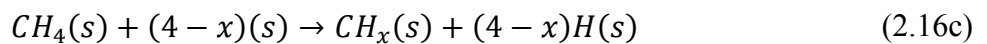
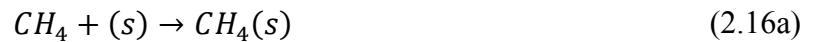
Schulz and coworkers (2015) studied with isotope-labeled reactants over Ni and Pt-based catalysts in order to both explain and improve the carbon reforming-oxidation balance. It was shown that <sup>13</sup>CO<sub>2</sub> is converted faster than CH<sub>4</sub> leading to a higher concentration of <sup>13</sup>CO compared with <sup>12</sup>CO in the product stream. The reversibility of the C-H and C-O bond formation and cleavage was also expressed by the presence of <sup>13</sup>CH<sub>4</sub> formed from <sup>13</sup>CO<sub>2</sub>, and <sup>12</sup>CO formed from <sup>12</sup>CH<sub>4</sub>.

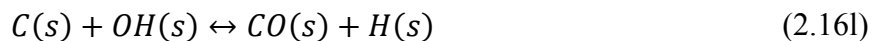
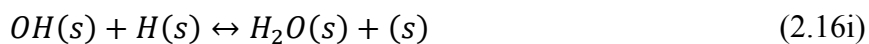
Fourier transform infrared spectroscopy, FTIR, is an important tool in examining CDRM with its ability to present information on reaction kinetics by either through the characterization of catalysts employed or the *in-situ* observation of the reaction. As a result, some studies have included FTIR results as well to conclude about the reaction mechanism of CDRM.

In the work of Verykios, for example, FTIR results were used in confirming the plausible mechanism from the proposed CDRM mechanisms based on kinetic studies over Ni-La<sub>2</sub>O<sub>3</sub> catalyst, (2003a). It was shown that Ni-La<sub>2</sub>O<sub>3</sub> catalyst exhibited a remarkably stable performance in contrast to other Ni-based catalysts, which suffered from continuous deactivation during TOS tests. XPS and FTIR studies provided evidence that catalytic activity occurred at the Ni-La<sub>2</sub>O<sub>2</sub>CO<sub>3</sub> interface, while the oxycarbonate species

participated directly by reacting with deposited carbon, allowing the activity of the Ni sites at the interface to be restored. Additionally, the rate determining steps in the reaction sequence were determined to be the methane cracking on Ni sites and the surface reaction between deposited carbon and oxycarbonate species. A kinetic model was developed based on this mechanistic scheme and it was confirmed that the model predicted the kinetic measurements satisfactorily.

Verykios also studied CDRM kinetics over Rh/Al<sub>2</sub>O<sub>3</sub> catalyst by applying *in-situ* FTIR spectroscopy as well as other steady-state tracing and transient techniques (2003b). The surface coverage of active carbon-containing species, which were involved in the reaction pathway forming CO, was found to be of the order of 0.2. On the other hand, the surface coverage of active oxygen-containing species, which led to the formation of CO, was very small. From TPH and TPO results, accumulation of three kinds of carbonaceous species was determined on the catalyst surface during reaction. It was also seen that this carbon mostly originates from the CO<sub>2</sub> molecule, while the contribution of CH<sub>4</sub> was small. Based on the results of the applied techniques, the following elementary reaction steps seemed appropriate to describe the CDRM mechanism over Rh/Al<sub>2</sub>O<sub>3</sub> catalyst:





Here, (s) was a site on the rhodium surface. It was discussed that the reaction steps (2.16a), (2.16c), (2.16d), the backward step (2.16f), and the forward step (2.16l) had to be relatively fast in the case of production of CO via the CH<sub>4</sub> molecular pathway, as compared to the corresponding steps of CO formation via the CO<sub>2</sub> molecular pathway. This important result suggested that sites, which accommodated carbon-containing species derived from CH<sub>4</sub> and CO<sub>2</sub>, are of different natures. (Verykios, 2003b)

CDRM reaction mechanism was also studied for Rh/Al<sub>2</sub>O<sub>3</sub> catalysts promoted with TiO<sub>2</sub> and V<sub>2</sub>O<sub>5</sub> by applying *in-situ* FTIR-DRIFT. The dissociation of carbon dioxide and methane was also examined. The results revealed that there were no significant differences in the CH<sub>4</sub> decomposition on different catalysts but the dissociation of carbon dioxide occurred most easily on vanadia promoted catalyst. Adsorbed CO and in some cases formate species were detected during the catalytic run on the catalysts far above their desorption temperature; the formation rates of CO and formate species were higher than their desorption, decomposition or further reaction rate. TPR and XPS results revealed that during the pre-treatment of the catalysts reduction of Rh as well as TiO<sub>2</sub> and V<sub>2</sub>O<sub>5</sub> occurred below 600 K. The dissociation of carbon dioxide occurred most easily on vanadia promoted catalyst. Vanadia and titania promoted Rh/Al<sub>2</sub>O<sub>3</sub> was determined to be more active than the unpromoted catalyst. The reason for this could be the oxygen vacancies, which were formed on the additives during the pretreatment and the reaction. (Sarusi *et al.*, 2011)

Aiming to understand the stable performance of Rh/La<sub>2</sub>O<sub>3</sub> catalysts in CDRM, the system was characterized by XRD, LRS, DRIFTS, and XPS, and the kinetic measurements were made. The combined results of the applied characterization techniques revealed that calcined Rh/La<sub>2</sub>O<sub>3</sub> after reduction was made up of a mixture of La<sub>2</sub>O<sub>3</sub> and oxycarbonates

on which reduced dispersed rhodium clusters were formed. The XPS data of the used catalyst showed that the only visible surface species were lanthanum oxycarbonate and mainly Rh<sup>0</sup>. Additionally, the DRIFTS data obtained during reaction indicated the presence of both Ia- and II-La<sub>2</sub>O<sub>2</sub>CO<sub>3</sub>, as well as both linear and bridge-bonded CO adsorbed on metallic rhodium. These results supported a reaction mechanism in which the slow steps were proposed as the methane decomposition and the surface reaction of the lanthanum oxycarbonate with the carbon residues left on the surface upon methane decomposition. (Munera *et al.*, 2007)

The CDRM kinetics over LaNiO<sub>3</sub>, Ni/La<sub>2</sub>O<sub>3</sub>, Rh/La<sub>2</sub>O<sub>3</sub> catalysts were investigated as a function of temperature and partial pressures of CH<sub>4</sub> and CO<sub>2</sub>. FTIR and XRD studies determined that there was a strong interaction between CO<sub>2</sub> and the La<sub>2</sub>O<sub>3</sub> support leading to the formation of stable La<sub>2</sub>O<sub>2</sub>CO<sub>3</sub> species. The proposed mechanistic scheme stated that perovskite structure was destroyed and La<sub>2</sub>O<sub>3</sub> and Ni<sup>0</sup> were formed at reaction temperatures higher or equal to 700 °C. CH<sub>4</sub> was reversibly adsorbed on the metallic clusters, liberating H<sub>2</sub> slowly. CO<sub>2</sub>, on the other hand, rapidly reacted with La<sub>2</sub>O<sub>3</sub> to generate oxycarbonate which in turn reacted with the carbon that was adsorbed on Ni<sup>0</sup> site to produce CO. It was noted that RWGS occurred simultaneously all of the time and was always equilibrated. The study also concluded that at higher range of reaction temperatures, Rh/La<sub>2</sub>O<sub>3</sub> and LaNiO<sub>3</sub> possessed more activity than Ni/La<sub>2</sub>O<sub>3</sub> although the three catalysts displayed the same mechanism with the rate expression reported in Equation 2.17. (Moradi *et al.*, 2010)

$$r_{CH_4} = \frac{K_1 k_2 K_3 k_4 [CH_4][CO_2]}{K_1 K_3 k_4 [CH_4][CO_2] + K_1 k_2 [CH_4] + K_3 k_4 [CO_2]} \quad (2.17)$$

The rate expressions proposed according to the kinetic studies on CDRM might differ due to the difference in the supports, promoters and operating conditions, and especially temperature range employed in the CDRM.

### 3. EXPERIMENTAL WORK

#### 3.1. Materials

##### 3.1.1. Chemicals

The chemicals used for catalyst preparation are presented in Table 3.1. All the chemicals used are research grade with high purity.

Table 3.1. Chemicals used for catalyst preparation.

Chemicals	Formula	Specification (%)	Source	Molecular Weight (g/mol)
Cerium (III) nitrate hexahydrate	$\text{Ce}(\text{NO}_3)_3 \cdot 6\text{H}_2\text{O}$	98.5	Merck	434.23
Cobalt (II) nitrate hexahydrate	$\text{Co}(\text{NO}_3)_2 \cdot 6\text{H}_2\text{O}$	97	BDH	290.93
Zirconium oxide	$\text{ZrO}_2$	99.99	Alfa Aesar	123.22

##### 3.1.2. Gases and Liquids

All of the gases used in this study were bought from Birleşik Oksijen Sanayi (BOS) A.Ş. and Linde Group, Istanbul. Liquid nitrogen was supplied by HABAŞ and Advanced Technologies Research and Development Center. Table 3.2 and Table 3.3 show the specifications and applications of the liquids and gases employed in this research.

Table 3.2. Specifications and applications of the liquids used.

<b>Liquid</b>	<b>Specification</b>	<b>Application</b>
Nitrogen	HABAŞ Advanced Technologies R&D Center	MCT Detector
Water	Deionized	Aqueous solutions

Table 3.3. Specifications and applications of the gases used.

<b>Gas</b>	<b>Specification (%)</b>	<b>Application</b>
Argon	99.995	GC Carrier Gas, Inert
Carbon dioxide	99.995	Reactant
Carbon monoxide	99.999	Product
Dry Air	99.998	Calcination, GC 6-way Pneumatic Valve
Helium	99.999	Inert
Hydrogen	99.99	Reduction
Methane	99.5	Reactant

### 3.2. Experimental Systems

The experimental systems used in this study can be described in four groups:

- **Catalyst Preparation Systems:** This group of experimental systems involved the set-up used for preparing catalysts by incipient-to-wetness impregnation technique.
- **Catalyst Characterization Systems:** Different analytical and spectroscopic techniques that were used to characterize the physical, microstructural and electronic properties of the catalyst samples prepared and to examine any carbonaceous deposits deposited on catalyst surface during the reactions were involved in this group of systems.
- **Catalytic Reaction System:** A continuous flow microreactor system including gas and liquid flow control, temperature controlled feed, transfer and product lines, temperature controlled gas/liquid mixing, and reaction chamber, and feed and

product sampling sections was used for assessing catalytic activity, selectivity and stability, and for analyzing reaction kinetics.

- Product Analysis System: The quantitative determination of the composition of the species both in the reactor effluent and feed stream was conducted by a gas chromatograph connected on-line to the microreactor flow system.

### 3.2.1. Catalyst Preparation Systems

The system used for preparing catalysts by incipient-to-wetness impregnation technique (Figure 3.1) included a Retsch UR1 ultrasonic mixer, a vacuum pump, a Buchner flask and a MasterFlex computerized-drive peristaltic pump.

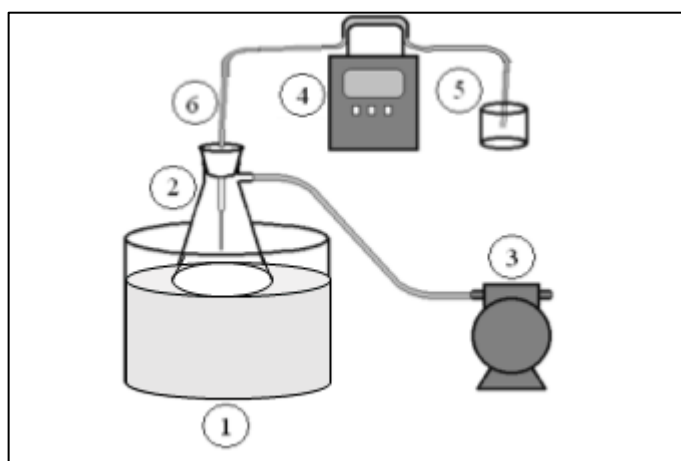


Figure 3.1. Schematic diagram of the impregnation system (1. Ultrasonic mixer, 2. Buchner flask, 3. Vacuum pump, 4. Peristaltic pump, 5. Precursor solution, 6. Silicone tubing).

### 3.2.2. Catalyst Characterization Systems

3.2.2.1. Scanning Electron Microscopy (SEM). SEM and Energy Dispersive X-Ray (EDX) analyses were conducted on freshly reduced Co-Ce/ZrO<sub>2</sub> catalyst samples in order to elucidate their micro-structural properties. The SEM micrographs of the spent samples were also used to observe the morphology of the deposited carbon. The tests were conducted in a Philips XL 30 ESEM-FEG system, having a maximum resolution of 2 nm.

The experiments were performed at the Advanced Technologies Research and Development Center of Boğaziçi University.

3.2.2.2. High Resolution Transmission Electron Microscopy (HR-TEM). To obtain information on the surface morphology variation of the freshly reduced catalyst samples, HR-TEM analyses were carried out using JEOL 2100 LaB6 HRTEM operating at 200 kV. The analyses were performed at the Institute of Materials at TUBITAK-MAM.

3.2.2.3. Intelligent Gravimetric Analyzer (IGA). Temperature Programmed Oxidation (TPO) experiments were performed on the coke deposited spent catalyst samples via an Intelligent Gravimetric Analyzer (Hiden Isochema) connected online to a dynamic sampling mass spectrometer (Hiden Analytical) for monitoring the combustion ( $\text{CO}_2 + \text{CO}$ ) products.

3.2.2.4. Raman Spectroscopy. Raman spectra of the spent catalysts were obtained by using a Renishaw inVia Raman microscope at Advanced Technologies Research and Development Center of Boğaziçi University.

3.2.2.5. X-Ray Photoelectron Spectroscopy (XPS). The amounts and oxidation states of the metallic species present on the fresh and used samples and, based on these results, the extent of electronic interaction between metal components of the freshly reduced samples the was investigated by X-ray photoelectron spectroscopy (XPS). The tests were conducted in Thermo Scientific K-Alpha X-ray Photoelectron Spectrometer at Advanced Technologies Research and Development Center of Boğaziçi University.

3.2.2.6. Fourier Transform Infrared Spectroscopy. The FTIR absorbance spectra have been collected on a Bruker Vertex v70V equipped with a MCT detector. The incorporated PIKE Technologies DRIFTS cell with ZnSe window with PIKE Technologies temperature controller and feed section involving Brooks mass flow controllers for preparation of predetermined feed streams allowed thermal treatments under controlled atmospheres, and spectrum scanning under controlled atmosphere at controlled temperatures (293-593 K).

Figure 3.2 shows the schematic representation of the FTIR-DRIFTS system. The feed section was composed of mass flow control systems, 1/4", 1/8" and 1/16" stainless steel tubing and fittings for feeding gaseous mixtures with controlled compositions, i.e. carbon monoxide, carbon dioxide, methane, helium, argon and hydrogen. The high purity gases were supplied by pressurized cylinders and were passed through the gas flow regulators. The flow rates of the gasses were controlled by Brooks Instrument mass flow controllers and the set values of were adjusted by two Brooks Instrument 0154 series control boxes. On-off valves were placed in front of the mass flow controllers to protect them from possible back-pressure fluctuations. In order to meter the flow of individual species and adjust desired feed ratios, each gas was fed from an independent line.

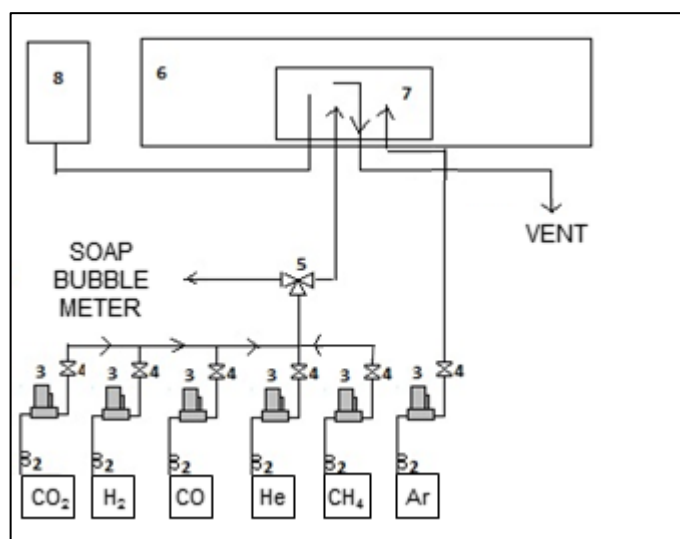


Figure 3.2. Schematic representation of FTIR-DRIFTS system (1. Gas cylinders, 2. Gas regulator, 3. Mass flow controller, 4. On-off valve, 5. Three-way valve, 6. FTIR, 7. DRIFTS cell, 8. Heating chamber).

### 3.2.3. Catalytic Reaction System

The catalytic reaction system was designed and constructed at the Chemical Engineering Department of Boğaziçi University involving three characteristic sections:

- Feed section,
- Reaction section, and

- Product analysis section.

The feed section included mass flow control systems, 1/4", 1/8" and 1/16" stainless steel tubes and fittings for feeding water (vapor) and gaseous species, i.e. methane, carbon dioxide, dry air, oxygen, argon and hydrogen (see Table 3.3 for specifications) at desired flow and compositions accurately. The gases supplied by pressurized tubes were passed through the gas flow regulators (items 1 in Figure 3.3) and the calibrated Brooks Instrument mass flow controllers (items 2 in Figure 3.3), the set values of which were adjusted by the main control unit, according to the targeted flow rate and composition. On-off valves (items 3 in Figure 3.3) were placed in front of the mass flow controllers to protect them from possible back-pressure formation. Each gas was fed is supplied through its independent line, so that it was possible to meter the flow of individual species and adjust desired feed ratios. The gases were then passed through a primary mixing zone (zone 6a in Figure 3.3) to ensure the flow of a homogeneous reactant gas mixture into the reactor.

The system was constructed providing an opportunity for combined steam reforming and dry reforming experiments. In this case, the liquid water was introduced into the reaction system at constant flow rates by using an Autoclave Engineers HPLC pump. The 1/16" tube, through which water was allowed to flow and the line going to the reactor after the primary mixing zone, was kept at  $393 \pm 3$  K by using a 1.4 m heating tape and Love Controls temperature controller to feed water in the form of steam (line 5 in Figure 3.3). 16-gauge wire K type sheathed thermocouple was placed at the middle point of heated zone to measure and control the temperatures. The heating tape was covered with ceramic wool insulation to prevent heat losses. Steam and homogeneous gas mixture were mixed in a secondary mixing zone (zone 6b in Figure 3.3) to introduce a homogeneous mixture of all the reactants into the reactor. However, this feature of the system was not used in this specific work, since the main concern was to see the performance of the catalyst in dry reforming only.

By using a three way valve 4a, it was possible to divert the flow direction of feed gases before entering the reactor through the direction of bypass line, so that the feed composition could be obtained by using the gas chromatograph.

The reactants, measured and mixed in the feed section, were allowed to flow through the reaction section. This section was composed of a 40 cm × 2.4 cm ID tube furnace controlled by  $\pm 0.1\text{K}$  by a Shimaden FP-21 programmable temperature controller and a 12 mm ID, 70 cm long quartz microreactor. Since the reactor was longer than the furnace by 15 cm out of furnace at each end, the temperature distribution could well be adjusted.

For connecting the quartz reactor with the rest of the system through both ends of the reactor, stainless steel quartz-steel connectors welded to 1/4" stainless steel tubes were designed and constructed. Both fittings were identical with an inner diameter of 12 mm, an outer diameter of 24 mm and a height of 50 mm. They held the reactor tight and still, preventing any gas leak or any damages from outside.

The reaction temperature was measured by a K-type sheathed thermocouple which was placed at the center of the furnace adjacent to the reactor. The position of the catalyst bed was adjusted to remain within the constant-temperature zone (10 cm) of tube furnace.

Sintered quartz disc, which was welded to the center of the quartz microreactor, was used to hold the catalyst bed in fixed position. Ceramic glass wool insulations were placed in top and bottom ends of the reactor furnace to prevent heat loss from the furnace and to provide a good temperature profile.

To remove the steam that might have been involved in the product stream leaving the reactor, ice cold traps were placed in flasks at 273 K before GC inlet.

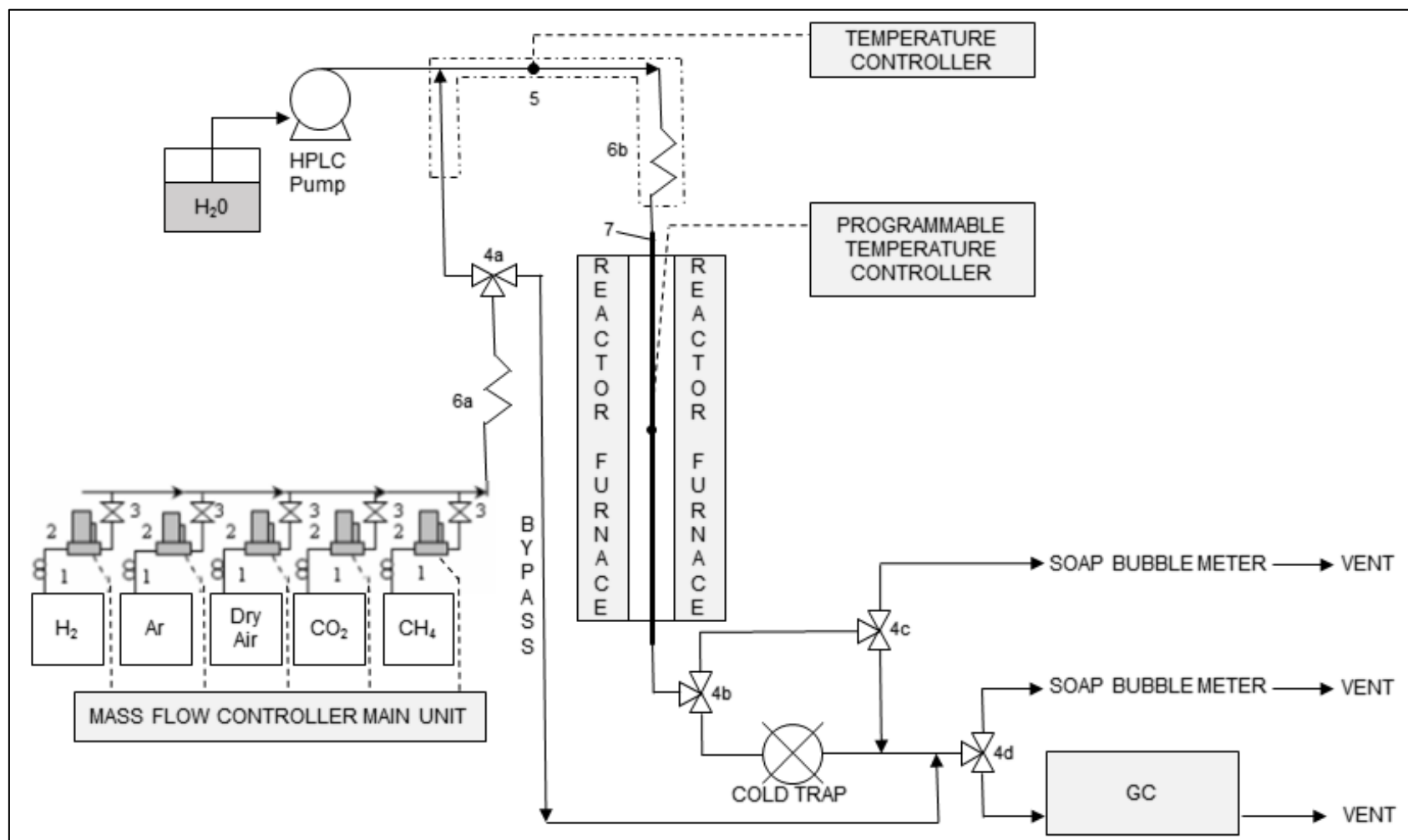


Figure 3.3. Schematic diagram of the microreactor system (1. Gas regulator, 2. Mass flow controller, 3. On-off valve, 4. Three-way valve, 5. Heated zone, 6. Mixing zone, 7. Differential reactor).

### 3.2.4. Product Analysis System

A temperature-controlled and programmable gas chromatograph, Hewlett Packard HP5890, equipped with a Thermal Conductivity Detector (TCD) and a HayeSep D column was used for feed and product gas analysis. Analysis conditions are given in Table 3.4.

Table 3.4. Gas analysis conditions for the system.

GC Parameters	GC-Hewlett Packard HP5890
Carrier gas	Argon
Carrier gas flow rate, mL/min	25
Column length and inner diameter	3 m × 3 mm
Column packing material	HayeSep D
Column temperature, K	323
Column tubing material	Stainless steel
Detector temperature, K	373
Injector temperature, K	343
TCD temperature, K	373

Before proceeding with the experiments, the gas chromatograph was calibrated by injecting known concentrations of the species to be analyzed from the injection ports to the column under the conditions given in Table 3.4 and by reading the area under the peak calculated by the integrator. Using this procedure, volume versus peak area curves were constructed for each gas and the corresponding calibration factors were determined by linear regression.

### 3.3. Catalyst Preparation and Pretreatment

5%Co/ZrO<sub>2</sub>, 2%Ce/ZrO<sub>2</sub>, 5%Co-2%Ce/ZrO<sub>2</sub>, 5%Co-3%Ce/ZrO<sub>2</sub>, 10%Co-2%Ce/ZrO<sub>2</sub> and 10%Co-3Ce%/ZrO<sub>2</sub> catalysts were prepared for the experiments in this study.

### 3.3.1. Support Preparation

Since the reforming of methane with carbon dioxide is known to be a highly endothermic reaction conducted at high temperatures, the catalyst supports should not only have high surface areas but also possess high thermal stabilities. For this matter, zirconia support was used. The support was first meshed to 45-60 mesh size and then calcined at 1073 K for 4 h in muffle furnace prior to the addition of the metals.

### 3.3.2. Preparation of Co-Ce/ZrO<sub>2</sub> catalyst

The experimental set-up shown in Figure 3.1, which was used in catalyst preparation by incipient to wetness impregnation method, consists of three parts for;

- Evacuating the support,
- Introducing the precursor solution onto the support, and
- Drying.

For incipient wetness impregnation, five grams of support was placed in the Buchner flask and kept under vacuum both before and during the addition of precursor solution(s). Trapped air in the pores of the support could prevent penetration of the solutions. In order to eliminate this problem and give a uniform distribution of the active component, vacuum pump was used; before impregnating the solution, the support material was mixed by using ultrasonic mixer under vacuum for 25 min.

To obtain Co-CeZrO<sub>2</sub> catalyst, impregnation of aqueous precursor solution of Ce (cerium (III) nitrate hexahydrate), at pre-calculated concentration determined according to the targeted metal loading, was performed first. This was followed by heat treatment at 773 K for 4 h in muffle furnace and impregnation of aqueous cobalt (II) nitrate hexahydrate solution. In both impregnation steps, a Masterflex computerized-drive peristaltic pump was used to feed the precursor solution (ca. 0.6 mL/g support) to the vacuum flask at a rate of 5 mL/min via silicone tubing. The slurry was mixed by an ultrasound mixer during the impregnation in order to maintain uniform distribution of the precursor solutions. After the

precursor solution was added, the slurry was ultrasonically mixed for additional 90 min. The thick slurry obtained was dried at 388 K overnight at each impregnation step.

### 3.3.3. Pretreatment

The catalysts were first calcined *in situ* under the flow of dry air (30 mL/min) for 4 h at 773 K and subsequently reduced *in situ* under the flow of H<sub>2</sub> (50 mL/min) for 2 h at the same temperature. Before calcination, the temperature was risen to 773 K under argon flow (25 mL/min) with temperature increase rate of 10 K/min. Argon flow was also introduced between calcination and reduction periods for 30 minutes in order to prevent the mixing of dry air and hydrogen. After reduction, the argon flow was adjusted to 5 mL/min and the system was left overnight prior to the reaction tests.

Prior to the FTIR-DRIFTS experiments, an *in situ* activation (re-reduction) pretreatment was also conducted in order to activate the catalyst. Four different pretreatment procedures were applied as given in Table 3.5. All the pretreatments were performed on 5%Co-2%Ce/ZrO<sub>2</sub>.

In pretreatment 1, catalyst sample pre-reduced *ex situ* was heated to 393 K with 20 K/min heating rate under 45 mL/min He flow. Then, sample was flushed 45 mL/min He flow at 393 K for 20 minutes followed by cooling to the room temperature under He flow.

In pretreatment 2, catalyst sample pre-reduced *ex situ* was heated to 573 K with 20 K/min heating rate under 45 mL/min He flow. Then, the sample was flushed 45 mL/min He for one hour at 573 K and cooled down to the room temperature under the same flow.

In pretreatment 3, catalyst sample prerduced *ex situ* was heated to 573 K with 20 K/min heating rate under 45 mL/min He flow. Then, the sample was reduced under 10% H<sub>2</sub>/He mixture of 45 mL/min He flow for one hour at 573 K and cooled down to the room temperature under 45 mL/min He flow.

In pre-treatment 4, catalyst sample pre-reduced *ex situ* was heated to 573 K with 20 K/min heating rate under 45 mL/min He flow. Then, the sample was reduced under 50

mL/min 10% H<sub>2</sub>/He mixture of 45 mL/min He flow for one hour at 573 K. Then, H<sub>2</sub> flow was stopped and the temperature was increased to 593 K in one minute. At 593 K, sample was flushed with 45 mL/min He for one hour and cooled down to the room temperature under the same flow.

Table 3.5. FTIR-DRIFTS pretreatment procedures.

<b>Pretreatment</b>	<b>Procedure</b>
1	20 min He flow at 393 K
2	One hour He flow at 573 K
3	One hour reduction under 10% H <sub>2</sub> /He flow at 573 K
4	One hour reduction under 10% H <sub>2</sub> /He flow at 573 K followed by one hour He flush at 593 K

### 3.4. Catalyst Characterization

#### 3.4.1. Temperature Programmed Oxidation (TPO)

TPO experiments were conducted on spent 5%Co-2%Ce-ZrO<sub>2</sub> catalyst samples with the following procedure: (i) The spent catalyst sample (~25 mg) was outgassed at 383 K for one hour and then at 298 K overnight to eliminate humidity and trapped gasses, (ii) The sample was subjected to 50 ml/min flow of 5%O<sub>2</sub>-95%He mixture at 1 bar, and then heated to 1023 K with 2 K/min heating rate in order to complete coke oxidation. Results from repeated experiments showed that the TPO profiles were reproducible.

#### 3.4.2. Raman Spectroscopy

Raman Spectroscopy analysis was conducted on spent 5%Co-2%Ce-ZrO<sub>2</sub> catalyst samples with the following operation parameters: 514 nm 20 mW Ar<sup>+</sup> laser as the excitation source; laser intensity of ~2 mW; 5 s acquisition time; a total of 20 accumulation per spectrum. Before measurements, Raman spectrum was calibrated by using a silicon wafer peak at 520 cm<sup>-1</sup>. All the samples were analyzed under atmospheric condition without pre-treatment with the de-focusing technique.

### 3.4.3. X-Ray Photoelectron Spectroscopy (XPS)

XPS analyses were applied over both freshly reduced 5%Co-2%Ce/ZrO<sub>2</sub>, 5%Co-3%Ce/ZrO<sub>2</sub>, 10%Co-2%Ce/ZrO<sub>2</sub> and 10%Co-3%Ce/ZrO<sub>2</sub> and spent 5%Co-2%Ce/ZrO<sub>2</sub> catalyst samples. All binding energies were referenced to the C1s line. For data analysis, the peak intensities were estimated by calculating the integral of each peak, after subtraction of the S-shaped Shirley-type background, and by fitting the curve to a combination of Lorentzian (30%) and Gaussian (70%) lines.

### 3.4.4. FTIR Spectroscopy

The FTIR-DRIFTS system described in Section 3.2.2.7 was used for characterization via CO adsorption.

Table 3.6. List of FTIR-DRIFTS experiments for characterization.

Experiment	Catalyst	Temperature (K)	Feed Composition (%) with He as balance		
			CH <sub>4</sub>	CO <sub>2</sub>	CO
CO adsorption	ZrO <sub>2</sub>	298	-	-	1
CO adsorption	2%Ce/ZrO <sub>2</sub>	298	-	-	1
CO adsorption	5%Co/ZrO <sub>2</sub>	298	-	-	1
CO adsorption	5%Co-2%Ce/ZrO <sub>2</sub>	298	-	-	1
CO adsorption	5%Co-3%Ce/ZrO <sub>2</sub>	298	-	-	1
CO adsorption	10%Co-2%Ce/ZrO <sub>2</sub>	298	-	-	1
CO adsorption	10%Co-3%Ce/ZrO <sub>2</sub>	298	-	-	1

## 3.5. Reaction Tests

### 3.5.1. Blank Tests

Blank tests were conducted to ensure that the material of construction, quartz disc and the reactor did not interfere with the reaction test outputs. The results indicated that

quartz disc and the reactor were inert under the conditions used in the reaction experiments.

### 3.5.2. CDRM Performance and Kinetic Tests

The effects of temperature,  $\text{CH}_4/\text{CO}_2$  feed ratio and space velocity on the performance of Co-Ce/ $\text{ZrO}_2$  catalysts in  $\text{CO}_2$  reforming of methane has been studied. Over the in situ reduced samples, first the argon flow was changed from 5 mL/min to 25 mL/min, then the furnace temperature was risen to the reaction temperature with rate of 10 K/min. Meanwhile, the GC operation procedure was followed. After both the GC and the system temperature were ready, the reactions were performed at the temperature interval of 873-973 K with  $\text{CH}_4/\text{CO}_2$  ratios of 1/1, 2/1, 1/2 and space velocities of 30000, 20000 and 10000 mL/h.g-catalyst. Data for 15 minutes, 1, 2, 4 and 6 h time-on-stream (TOS) were obtained. Then, 5 data for feed analysis were obtained after waiting for 15 minutes for the feed gases to mix completely. Experiments performed in this section are shown at Table 3.7 in detail.

FTIR-DRIFT system was also used to analyze both the performance of the Co-Ce/ $\text{ZrO}_2$  catalysts and the CDRM reaction mechanism on their surface as well. The list of the experiments performed for this purpose are given in Table 3.8.

The kinetic behaviors of 5%Co-2%Ce/ $\text{ZrO}_2$  and 10%Co-2%Ce/ $\text{ZrO}_2$  on CDRM was also parametrically tested as a function of temperature and partial pressures of  $\text{CH}_4$ ,  $\text{CO}_2$ , CO and  $\text{H}_2$ . The experiments were performed under differential conditions at atmospheric pressure using 12 mg catalyst. Low conversion levels and the absence of transport effects, which are necessary for obtaining intrinsic kinetic information, were guaranteed by varying the space velocity between 500000 and 750000 mL/h.g-catalyst.

In determination of the apparent activation energies, the reactions were carried out with a feed composition of  $\text{CH}_4/\text{CO}_2=1/1$  at the temperature interval of 853-893 K.

The partial pressure dependencies of reactants were examined at 873 K by maintaining a constant partial pressure of 0.08 atm of one reactant and varying the pressure

of the other. Argon was used to adjust atmospheric pressure and constant total flow during the tests. The various gas feed compositions used are listed in Table 3.9.

Table 3.7. Parameters for performance experiments over Co-Ce/ZrO<sub>2</sub> catalyst system.

<b>Reaction Temperature (K)</b>	<b>CH<sub>4</sub>/CO<sub>2</sub> Ratio</b>	<b>Space Velocity (mL/h.g-catalyst)</b>
973	1/1	20000
923	1/1	20000
873	1/1	20000
973	2/1	20000
923	2/1	20000
873	2/1	20000
973	1/2	20000
923	1/2	20000
873	1/2	20000
973	1/1	10000
973	1/1	30000
973	2/1	10000
973	2/1	30000
973	1/2	10000
973	1/2	30000

The effect of adding products CO and H<sub>2</sub> to feed stream was investigated in mixed flow tests through the experiments conducted with varying the partial pressure of one product in the feed stream, which consisted of constant reactant partial pressures as 0.08 atm at 873 K. The feed gas compositions used for product effect are listed in Table 3.10.

Power type rate expression and possible surface reaction models were utilized to explain the mechanistic features for CDRM. Additionally, the effect of Co/Ce loading ratio on parameters of both power type rate and other possible rate expressions was investigated.

Table 3.8. List of FTIR-DRIFTS experiments for performance and kinetics.

Experiment	Catalyst	Temperature (K)	Feed Composition (%) with He as balance		
			CH <sub>4</sub>	CO <sub>2</sub>	CO
CO <sub>2</sub> adsorption	ZrO <sub>2</sub>	298	-	10	-
CO <sub>2</sub> adsorption	ZrO <sub>2</sub>	373	-	10	-
CO <sub>2</sub> adsorption	ZrO <sub>2</sub>	573	-	10	-
CO <sub>2</sub> adsorption	ZrO <sub>2</sub>	573	-	40	-
CO <sub>2</sub> adsorption	5%Co-2%Ce/ZrO <sub>2</sub>	573	-	40	-
CH <sub>4</sub> adsorption	5%Co-2%Ce/ZrO <sub>2</sub>	573	40	-	-
Reaction	5%Co-2%Ce/ZrO <sub>2</sub>	573	40	40	-
Reaction	5%Co-3%Ce/ZrO <sub>2</sub>	573	40	40	-
Reaction	10%Co-2%Ce/ZrO <sub>2</sub>	573	40	40	-
Reaction	10%Co-3%Ce/ZrO <sub>2</sub>	573	40	40	-
Reaction	5%Co-2%Ce/ZrO <sub>2</sub>	573	40	20	-
Reaction	5%Co-3%Ce/ZrO <sub>2</sub>	573	40	20	-
Reaction	10%Co-2%Ce/ZrO <sub>2</sub>	573	40	20	-
Reaction	10%Co-3%Ce/ZrO <sub>2</sub>	573	40	20	-
Reaction	5%Co-2%Ce/ZrO <sub>2</sub>	573	20	40	-
Reaction	5%Co-3%Ce/ZrO <sub>2</sub>	573	20	40	-
Reaction	10%Co-2%Ce/ZrO <sub>2</sub>	573	20	40	-
Reaction	10%Co-3%Ce/ZrO <sub>2</sub>	573	20	40	-

Table 3.9. List of kinetic parameters for determining power law type rate equation.

CH <sub>4</sub> /CO <sub>2</sub> Ratio	W <sub>cat</sub> /F <sub>CH<sub>4</sub></sub> (g.s.mmol <sup>-1</sup> )	Partial Pressures (atm)	
		CH <sub>4</sub>	CO <sub>2</sub>
0.25	8.82	0.02	0.08
0.25	7.35	0.02	0.08
0.25	5.376	0.02	0.08
0.5	4.594	0.04	0.08
0.5	3.675	0.04	0.08
0.5	2.94	0.04	0.08
0.75	2.94	0.06	0.08
0.75	2.45	0.06	0.08
0.75	1.96	0.06	0.08
1	2.205	0.08	0.08
1	1.96	0.08	0.08
1	1.47	0.08	0.08
1.33	2.205	0.08	0.06
1.33	1.96	0.08	0.06
1.33	1.47	0.08	0.06
1.5	2.205	0.08	0.053
1.5	1.96	0.08	0.053
1.5	1.47	0.08	0.053
2	2.016	0.08	0.04
2	1.68	0.08	0.04
2	1.344	0.08	0.04
4	2.205	0.08	0.02
4	1.96	0.08	0.02
4	1.47	0.08	0.02

Table 3.10. List of kinetic parameters to determine the effect of H<sub>2</sub> and CO partial pressures.

<b>W<sub>cat</sub>/F<sub>CH4</sub></b> <b>(g.s.mmol<sup>-1</sup>)</b>	<b>Partial Pressures (atm)</b>			
	<b>CH<sub>4</sub></b>	<b>CO<sub>2</sub></b>	<b>CO</b>	<b>H<sub>2</sub></b>
1.47	0.08	0.08	0.015	-
1.47	0.08	0.08	0.030	-
1.47	0.08	0.08	0.045	-
1.47	0.08	0.08	0.060	-
1.47	0.08	0.08	0.075	-
1.47	0.08	0.08	0.090	-
1.47	0.08	0.08	-	0.015
1.47	0.08	0.08	-	0.030
1.47	0.08	0.08	-	0.045
1.47	0.08	0.08	-	0.060
1.47	0.08	0.08	-	0.075

## 4. RESULTS AND DISCUSSION

The aim of the current work is to design and develop effective non-PGM based CDRM catalysts, to confirm the roles of each component, to determine optimum reaction conditions for the highest performance, and to reveal the details of CDRM reaction mechanism. In this context, the results of this study will be presented and discussed in four sections:

- Characterization and CDRM performance of Co-Ce/ZrO<sub>2</sub> catalyst,
- The effects of Co/Ce loading ratio and reaction conditions on CDRM performance of Co-Ce/ZrO<sub>2</sub> catalysts,
- Kinetic and mechanistic features of CDRM over Co-Ce/ZrO<sub>2</sub> catalysts, and
- FTIR-DRIFT studies over Co-Ce/ZrO<sub>2</sub> catalysts.

### 4.1. Characterization and CDRM Performance of Co-Ce/ZrO<sub>2</sub> Catalyst

CDRM over 5%Co-2%Ce/ZrO<sub>2</sub> catalyst was analyzed and discussed in this section. It should be noted that small part of the work presented here includes the results of the studies conducted in M.Sc. thesis by Aysun İpek Paksoy (Paksoy, 2010), and the whole work in this section was published as a paper (Paksoy *et al.*, 2015).

#### 4.1.1. Characterization of Co-Ce/ZrO<sub>2</sub> Catalyst

Freshly reduced catalyst samples were characterized by SEM-EDX and HRTEM aiming to study micro-structural properties of the catalysts and dispersion of Co and Ce.

The SEM-EDX mapping image (Figure 4.1) shows well dispersed metal particles, Co and Ce, on the freshly-reduced catalyst sample. HRTEM results at higher magnifications (Figure 4.2), indicated local change in Ce/Co surface ratio. Average Ce/Co surface ratio calculated by using HRTEM-EDX data on different locations of two freshly reduced samples is 1.7, and the highest observed ratio is 3.59. The detailed analysis results of the two selected locations, shown in Figure 4.2, are given in Table 4.1 as examples.



Figure 4.1. Co-Ce-Zr mapping of freshly reduced 5%Co-2%Ce/ZrO<sub>2</sub> catalyst.

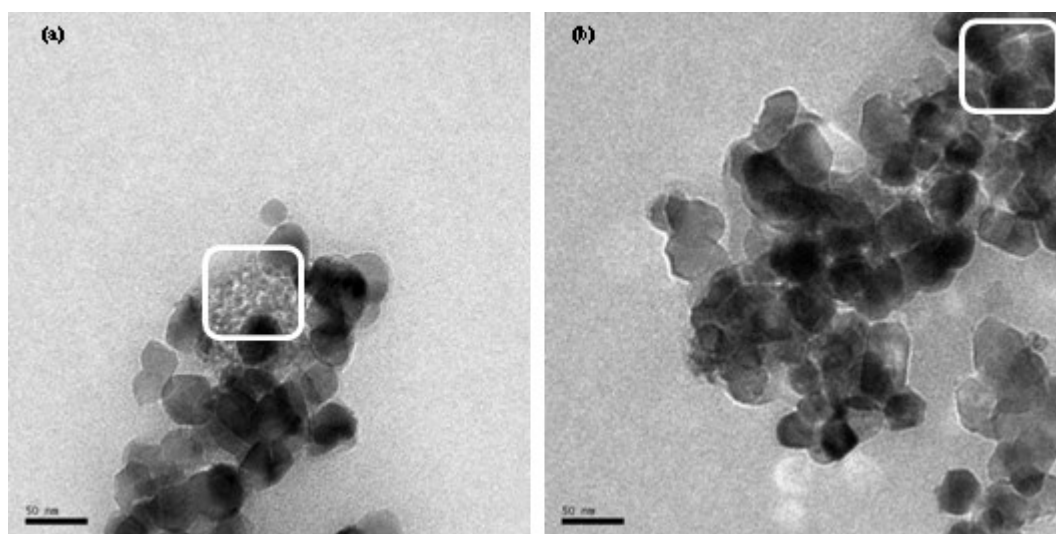


Figure 4.2. HRTEM images of selected regions on freshly reduced catalyst sample.

Table 4.1. HRTEM-EDX analysis results for the areas in Figure 4.2a and b.

Figure	Ce wt.%	Co wt.%	Ce/Co	Ce at.%	Co at.%	Ce/Co
4.2a	6.57	1.83	3.59	1.23	0.82	1.50
4.2b	5.06	3.24	1.56	1.26	1.92	0.86

The Ce3d XP spectrum of the freshly reduced and spent Co-Ce/ZrO<sub>2</sub> catalyst samples were obtained and analyzed aiming to understand the redox ability of CeO<sub>x</sub> formations in the freshly reduced sample and how it is changed during the reaction. XP spectra of the spent catalyst samples which were used under reaction conditions yielding the highest, at 973 K with CH<sub>4</sub>/CO<sub>2</sub> feed ratio of 2, and the lowest, at 873 K with CH<sub>4</sub>/CO<sub>2</sub> feed ratio of 1, coke formation are compared with that obtained from the freshly reduced sample.

The Ce3d XPS results of the freshly reduced sample are in accordance with the literature (Figure 4.3) but peaks are slightly shifted to higher binding energies. There are three main 3d<sub>5/2</sub> peaks at about 887.43 (v), 892.55 (v<sup>2</sup>) and 902.69 (v<sup>3</sup>) eV and three main 3d<sub>3/2</sub> peaks at about 906.21 (u), 912.5 (u<sup>2</sup>) and 919.79 (u<sup>3</sup>) eV, which are attributed to the Ce<sup>4+</sup> state, while the peaks at about 883.01 (v<sub>0</sub>), 890.21 (v<sup>1</sup>), 904.67 (u<sub>0</sub>) and 909.12 (u<sup>1</sup>) eV belong to unique photoelectron features of the Ce<sup>3+</sup> state (Leppelt *et al.*, 2006).

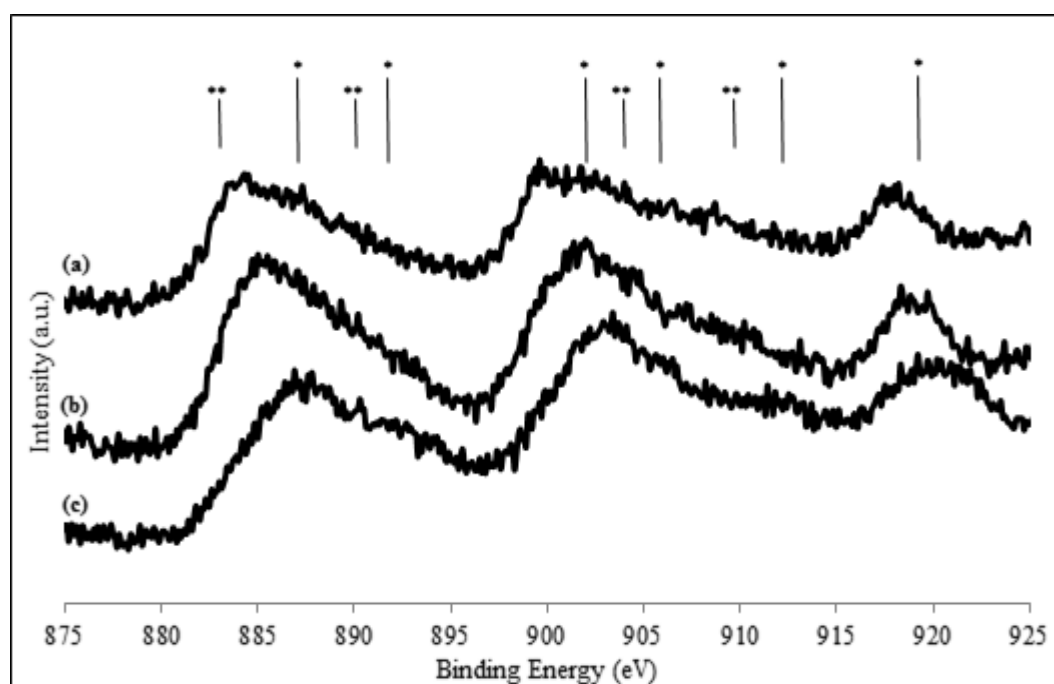


Figure 4.3. XP spectrum of Ce3d region of 5%Co-2%Ce/ZrO<sub>2</sub> catalyst (a) tested at 973 K and CH<sub>4</sub>/CO<sub>2</sub> feed ratio of 2/1, (b) tested at 873 K and CH<sub>4</sub>/CO<sub>2</sub> feed ratio of 1/1, and (c) freshly calcined and reduced (\*: Ce<sup>4+</sup>, \*\*: Ce<sup>3+</sup>).

After deconvolution of the spectrum, the degree of ceria reduction was evaluated from the ratio of the sum of integrated peak areas of  $v_0$ ,  $u_0$ ,  $u^1$  and  $v^1$  peaks to the sum of the integrated peak areas of all peaks. According to the given Equation 4.1,

$$[\text{Ce}^{3+}] = \frac{I\text{-Ce}^{3+}}{(I\text{-Ce}^{3+} + I\text{-Ce}^{4+})} \quad (4.1)$$

where  $I\text{-Ce}^{3+}$  and  $I\text{-Ce}^{4+}$  represent the sum of intensities of two doublets resulting from  $\text{Ce}_2\text{O}_3$  and three doublets resulting from  $\text{CeO}_2$ , respectively (Leppelt *et al.*, 2006), the amount of  $\text{Ce}^{3+}$  present on freshly reduced Co-Ce/ZrO<sub>2</sub> catalyst is estimated as 11.6%.

The binding energies attributed to  $\text{Ce}^{4+}$  and  $\text{Ce}^{3+}$  states for the spent catalyst samples are given in Table 4.2. Peaks belonging to both spent catalyst samples were observed to have a shift to lower binding energies when compared to the peaks from the freshly reduced catalyst sample. However, all binding energies found from the deconvolution analysis are in accordance with literature indicating there is no significant possibility of alloy formation (Leppelt *et al.*, 2006).

Table 4.2. The Ce valance-binding energy (eV) relation for different reaction conditions.

Reaction Conditions	Ce Valance	Binding Energy, eV
T=873 K, CH <sub>4</sub> /CO <sub>2</sub> =1/1	Ce <sup>4+</sup>	919.86, 912.03, 906.63, 902.84, 892.88, 886.88
	Ce <sup>3+</sup>	909.78, 905.07, 891.02, 882.02
T=973 K, CH <sub>4</sub> /CO <sub>2</sub> =2/1	Ce <sup>4+</sup>	918.06, 908.8, 902.69, 899.29, 889.63, 884.01
	Ce <sup>3+</sup>	905.49, 900.86, 886.72, 880.42

The deconvolution analysis indicated that the degree of ceria reduction is 13.8% for the catalyst tested at 973 K with 2/1 CH<sub>4</sub>/CO<sub>2</sub> feed ratio, but it is 8.7% for the one tested at 873 K with 1/1 CH<sub>4</sub>/CO<sub>2</sub> feed ratio, proving Ce's ability to store oxygen when the feed is rich in oxygen source; i.e. at higher CO<sub>2</sub> concentrations in the feed. This eases the utilization of surface oxygen; during reaction, Ce acts as a buffer regulating surface oxygen transfer from support to Co sites through redox cycle.

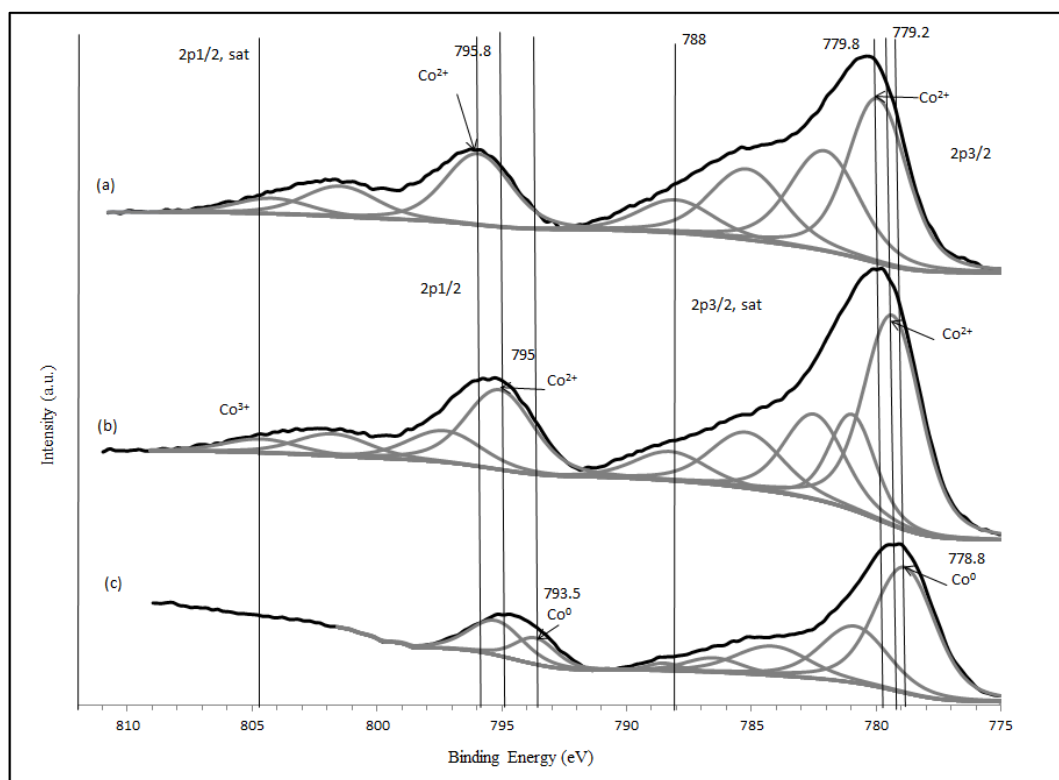


Figure 4.4. XP spectrum of Co2p region of 5%Co-2%Ce/ZrO<sub>2</sub> catalyst (a) tested at 973 K and CH<sub>4</sub>/CO<sub>2</sub> feed ratio of 2/1, (b) tested at 873 K and CH<sub>4</sub>/CO<sub>2</sub> feed ratio of 1/1, and (c) freshly calcined and reduced.

Figure 4.4 shows the Co2p XP spectra obtained from freshly reduced and spent catalyst samples. The two peaks, appearing in the spectrum of the freshly reduced sample (Figure 4.4c) at 778.8 eV and 793.5 eV, separated by 14.7 eV, may be attributed to the Co2p<sub>3/2</sub> and Co2p<sub>1/2</sub> spin-orbit peaks, respectively, of the Co<sup>0</sup> phase, indicating the metallic nature of the reduced catalyst surface. However, as the FWHM of the Co<sup>0</sup> peak is < 1.5 eV, in addition to the other deconvoluted peaks corresponding to the main and satellite peaks of the Co<sup>2+</sup> and Co<sup>3+</sup> phases, the features attributed to the metal phase are also thought to contain oxide phases (Dominguez *et al.*, 2010; Chai *et al.*, 2005; Lin *et al.*, 2010; Watanabe *et al.*, 2013). The Co2p XP spectra of both spent catalyst samples inform us about the variation of the Co oxidation state during reaction. The absence of Co<sup>0</sup> 2p<sub>3/2</sub> and 2p<sub>1/2</sub> spin-orbit peaks indicates, in addition to the oxide phases present on the freshly reduced catalyst surface, there is further Co oxide formation during reaction. As can be seen from Figure 4.4a and 4.4b, the spectra of the spent samples used in reactions conducted at 973 and 873 K, respectively, involve Co2p<sub>3/2</sub> and Co2p<sub>1/2</sub> spin-orbit peaks

and their satellite features belonging to cobalt oxide phases. It is very difficult to distinguish between the  $\text{Co}^{2+}$  and  $\text{Co}^{3+}$  oxide phases due to the small shifts ( $\sim 0.5$  eV) between their peaks. On the other hand, as it has been reported that when Co is deposited onto other oxides the XPS Co2p lines of  $\text{Co}^{2+}$  shift to higher BE values, and  $\text{Co}^{2+}$  has characteristic satellites which are more pronounced in CoO than in  $\text{Co}_3\text{O}_4$  (Dominguez *et al.*, 2010; Chai *et al.*, 2005; Lin *et al.*, 2010; Watanabe *et al.*, 2013), the peaks shown in Figure 4.4 are attributed to  $\text{Co}^{2+}$  phase.

When the surface metal site is covered even by a thin carbon layer, this site is not seen in metal mapping and the metal's surface concentration, evaluated by EDX, decreases. Considering this fact, a simple methodology, which utilizes a comparative analysis of Co and Ce site concentrations measured on the freshly reduced and spent samples through metal mapping (Figure 4.5) and SEM-EDX, was used to investigate the functions of Co and Ce sites in CDRM. The idea behind the methodology is the fact that carbon covers the site whose primary function is hydrogen production from methane/methyl groups, like methane dehydrogenation, forming carbon as the side product. A mild set of CDRM conditions, 873 K with the  $\text{CH}_4/\text{CO}_2$  feed ratio of 1/1 and space velocity of 20000 mL/h.g-catalyst, leading very limited carbon formation was used in preparation of the spent sample. A comparative analysis of EDX results showed that carbon formation is more pronounced on Co sites. The EDX results, on the average, showed that the atomic percentage of Ce is decreased from 0.55 to 0.47 upon 6 h TOS CDRM test, meaning ca. 15% of the surface Ce is covered by carbon. On the other hand, under the same conditions, the decrease in Co atomic percentage is from 4.1 to 2.28, meaning ca. 44% of Co is covered by carbon. The results clearly showed carbon blockage is significantly more severe on Co centers, confirming the primary function of the Co sites is hydrogen production, whose side product is deposited carbon. The Co and Ce metal mapping images also confirmed this outcome. It should be noted that the carbon covered Ce sites most probably are the ones present in close vicinity of the Co sites on which carbon formed may extend to the neighboring Ce centers.

It is known that the type and amount of coke deposited on the catalyst during CDRM plays an important role in the catalyst performance through affecting its activity and selectivity. In order to understand the effect of local surface Ce concentration on

prevention of coke formation, SEM-EDX analyses were performed on spent catalysts used in reaction tests at temperatures of 873 and 973 K,  $\text{CH}_4/\text{CO}_2$  feed ratios of 1/1 and 2/1 with the space velocity of 20000 mL/h.g-catalyst.

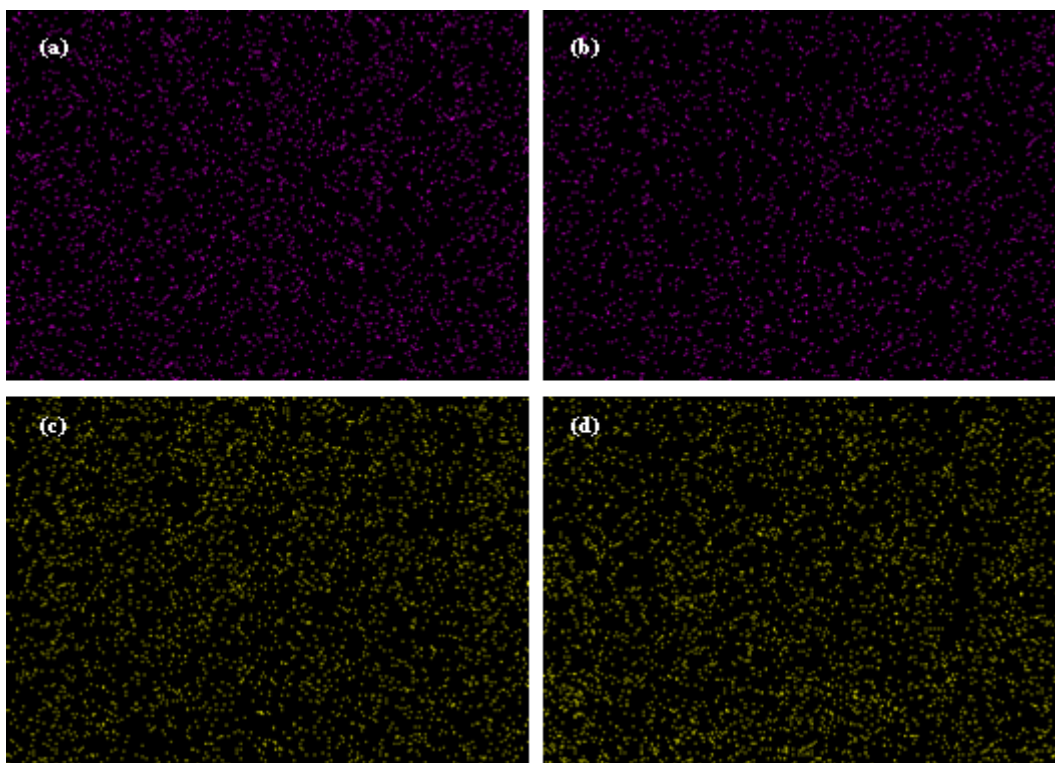


Figure 4.5. Co mapping of (a) freshly reduced catalyst, (b) spent sample used during the reaction performed at 873 K and  $\text{CH}_4/\text{CO}_2=1/1$ , Ce mapping of (c) freshly reduced catalyst, (d) spent sample used during the reaction performed at 873 K and  $\text{CH}_4/\text{CO}_2=1/1$ .

Two distinct, namely coked and coke-free, regions observed for each one of the spent Co-Ce catalyst samples, tested under four different reaction conditions, are presented as examples (Figure 4.6). EDX analyses (Table 4.3) performed for both regions on each sample reveal that Ce/Co surface molar ratio of coked parts is lower than that of the coke-free parts. The results confirmed that the presence of ceria on the surface creates an additional storage capacity for oxygen coming from  $\text{ZrO}_2$  support, which is known to catalyze  $\text{CO}_2$  disintegration generating surface oxygen (Wang and Lu, 1998). Ce centers go through continuous reduction/oxidation cycle during the reaction; they act as a buffer for surface oxygen, regulating and enhancing oxygen transfer to Co centers (Ozkara-Aydinoglu and Aksoylu, 2010). This transfer removes deposited carbon through oxidation

and makes catalytic centers more carbon resistant. It is observed from the images that formation of carbon is favored for the regions with low Ce/Co ratio. It should be noted that there may be also a possibility of increased Co-Ce interaction.

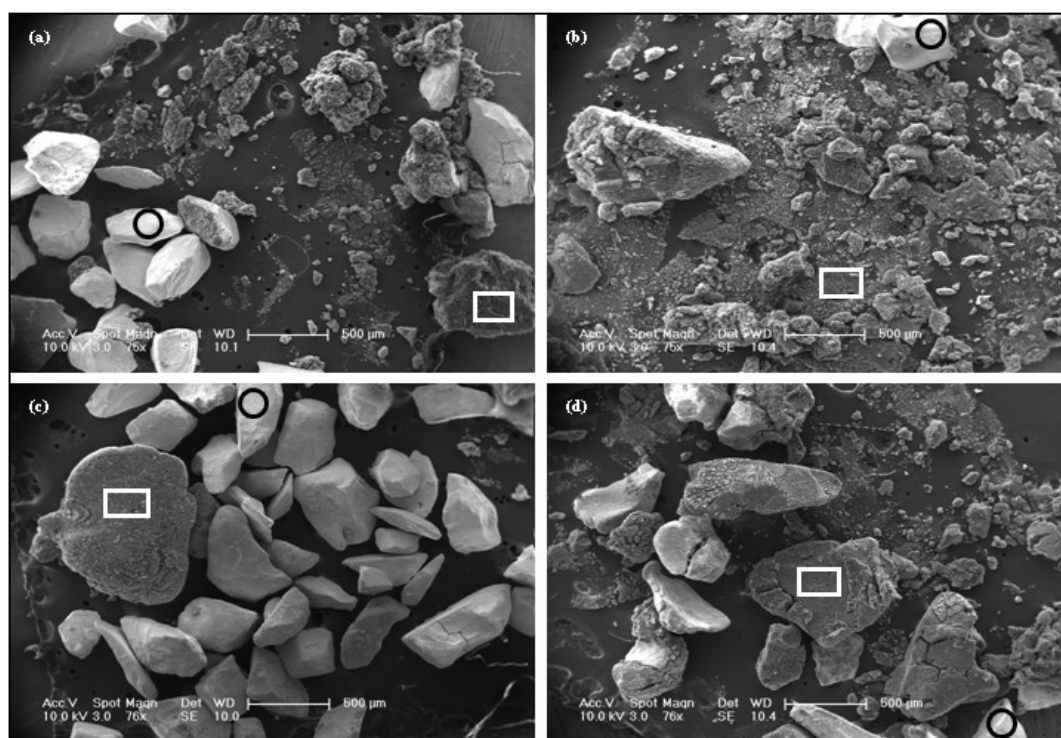


Figure 4.6. SEM images of catalyst samples used during the reactions performed at (a) 973 K and  $\text{CH}_4/\text{CO}_2=1/1$ , (b) 973 K and  $\text{CH}_4/\text{CO}_2=2/1$ , (c) 873 K and  $\text{CH}_4/\text{CO}_2=1/1$ , (d) 873 K and  $\text{CH}_4/\text{CO}_2=2/1$  (circles for coke-free regions, rectangles for coked regions).

Many studies have shown that during CDRM, surface oxygen (or oxygen-containing species) originating from  $\text{CO}_2$ , oxidize carbon species formed by  $\text{CH}_4$  decomposition on the metallic sites. Therefore, the rate of carbon accumulation on the catalyst surface is determined by the relative rates of the generation and oxidative removal of carbon species. Excess carbon deposition will occur when the former is faster than the latter (Ruckenstein and Wang, 2002; Dominguez *et al.*, 2010). SEM analyses (Figure 4.7) obtained from the spent samples tested at different temperature and  $\text{CH}_4/\text{CO}_2$  feed ratios gave information about the relation between reaction conditions, yielding changes in the relative rates of carbon generation and removal, and the type and abundance of carbon deposition.

Table 4.3. Ce and Co surface atomic percentages of the spent catalysts obtained by SEM-EDX analysis.

<b>Reaction Conditions</b>	<b>Ce% Coked part</b>	<b>Co% Coked part</b>	<b>Ce/Co Coked part</b>	<b>Ce% Coke-free part</b>	<b>Co% Coke-free part</b>	<b>Ce/Co Coke-free part</b>
T=973 K, CH <sub>4</sub> /CO <sub>2</sub> =1/1	0.35	1.25	0.28	1.89	3.10	0.61
T=973 K, CH <sub>4</sub> /CO <sub>2</sub> =2/1	0.43	0.97	0.44	1.42	3.15	0.45
T=873 K, CH <sub>4</sub> /CO <sub>2</sub> =1/1	0.56	2.03	0.28	1.39	2.60	0.54
T=873 K, CH <sub>4</sub> /CO <sub>2</sub> =2/1	0.24	0.89	0.27	1.40	2.79	0.50

High level of carbon deposition was observed on the spent sample tested at 973 K with 1/1 CH<sub>4</sub>/CO<sub>2</sub> feed ratio, indicating that condition favors carbon formation more than carbon oxidation.

When the CH<sub>4</sub>/CO<sub>2</sub> feed ratio was increased to 2/1 while keeping the temperature and space velocity fixed, the highest coke deposition was observed. In addition to the temperature effect, another reason for higher coke accumulation is the higher amount of carbon source in the feed relative to the oxygen source, led by the increased methane concentration in the feed. Consequently, coke deposition is strongly favored when CH<sub>4</sub>/CO<sub>2</sub> feed ratio and reaction temperature are both high.

On the other hand, it was seen that coke formation decreased with a decrease in reaction temperature in 873-973 K temperature region. From the SEM image of the sample tested at 873 K, with the CH<sub>4</sub>/CO<sub>2</sub> feed ratio of 1/1 and space velocity of 20000 mL/h.g-catalyst, the lowest carbon deposition was observed. It should be noted that Boudouard reaction favored at low temperatures was thought not significant except CDRM tests conducted at 873 K. Although the temperature parameter was still 873 K, the increased,

2/1, ratio of  $\text{CH}_4/\text{CO}_2$  in the feed caused carbon formation, indicating relatively limited carbon oxidation activity.

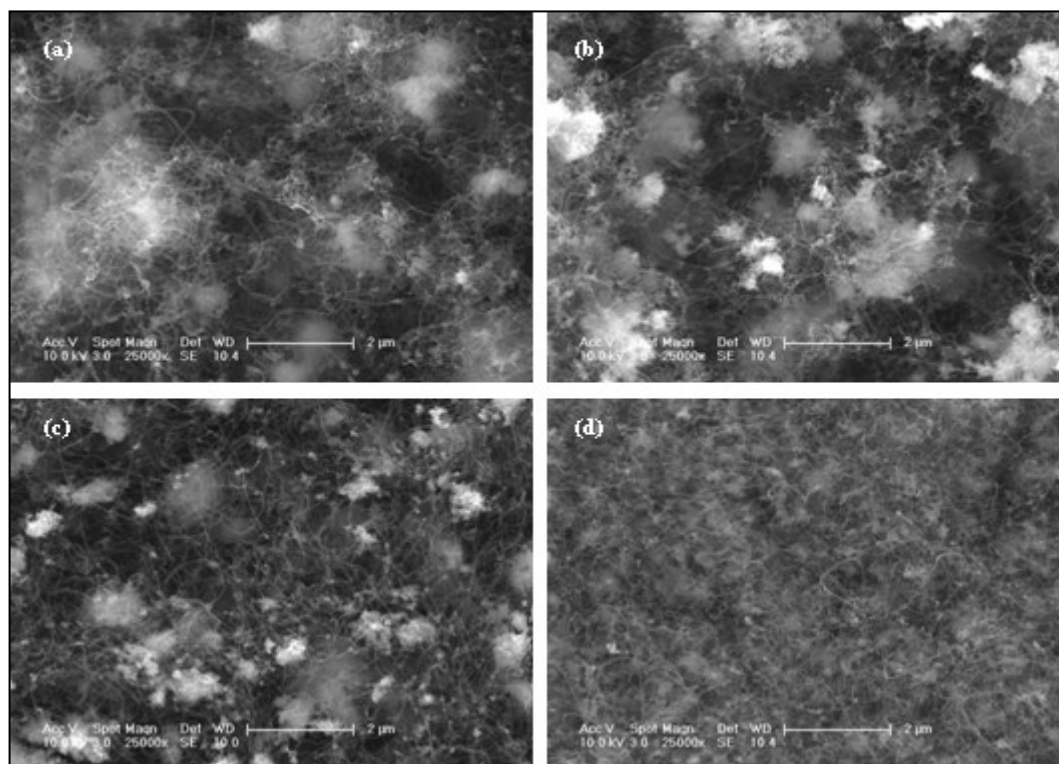


Figure 4.7. SEM images of the catalyst samples used during the reaction at space velocity of 20000 mL/h g-catalyst and at (a) 973 K,  $\text{CH}_4/\text{CO}_2=1/1$ , (b) 973 K,  $\text{CH}_4/\text{CO}_2=2/1$ , (c) 873 K,  $\text{CH}_4/\text{CO}_2=1/1$ , and (d) 873 K,  $\text{CH}_4/\text{CO}_2=2/1$ .

The structure of the deposited carbon formed on the spent catalyst samples was further characterized by Raman spectroscopy and Temperature Programmed Oxidation (TPO). The catalyst samples yielding the highest, at 973 K with  $\text{CH}_4/\text{CO}_2$  feed ratio of 2, and the lowest, at 873 K with  $\text{CH}_4/\text{CO}_2$  feed ratio of 1, coke formation were chosen for analysis. The Raman spectra of both spent catalyst samples given in Figure 4.8 show two well defined bands at around 1344 and 1580  $\text{cm}^{-1}$ , which are attributed to the D band, associated with the disordered structural mode of crystalline carbon species, and G band, corresponding to the graphitic carbon with high degree of symmetry, respectively (Dominguez *et al.*, 2010; Wragg *et al.*, 2013; Sousa *et al.*, 2012). The relative intensity of D and G bands ( $I_D/I_G$ ) gives information about the degree of crystallinity; smaller  $I_D/I_G$  value indicates higher crystallinity (Dominguez *et al.*, 2010). The  $I_D/I_G$  values were

calculated as 0.83 and 1.13 for the catalyst samples spent at 873 and 973 K, respectively; pointing out that the coke formed during reaction at 873 K has higher degree of graphitization.

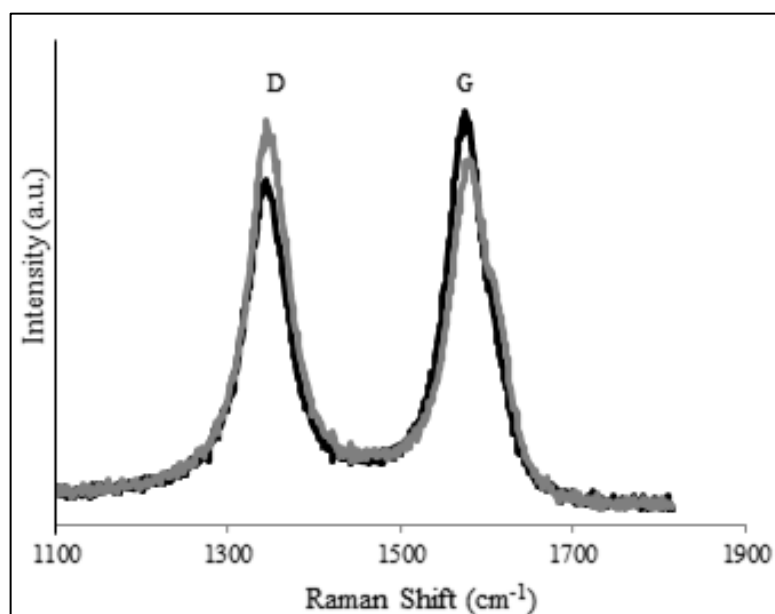


Figure 4.8. Raman spectra of the catalyst samples used during the reaction with space velocity of 20000 mL/h.g-catalyst at 973 K,  $\text{CH}_4/\text{CO}_2=2/1$ (black curve), and 873 K,  $\text{CH}_4/\text{CO}_2=1/1$ (grey curve).

In TPO tests, it is widely accepted that amorphous carbon species are combusted at lower temperatures, i.e. below 773 K, than crystalline ones (Dominguez *et al.*, 2010; Sousa *et al.*, 2012; Vicente *et al.*, 2014; Daza *et al.*, 2009). The TPO profile (Figure 4.9) of the catalyst tested at 973 K with 2/1  $\text{CH}_4/\text{CO}_2$  ratio, reveals a wide and asymmetric peak that begins around 550 K and ends around 750 K. According to the deconvolution results this wide peak encompasses 4 peaks at 628, 652, 673 and 703 K which are all attributed to the amorphous coke. On the other hand, in accordance with the Raman spectroscopy results, the TPO profile of the catalyst used at 873 K records a wider peak between 670 and 900 K, with 3 major peaks at 758, 810 and 838 K. The higher oxidation temperatures of the deposited carbon on that sample indicates an increase in degree of crystallinity in the carbon structure. The peak evolved at 758 K may be attributed to monoatomic coke, and the latter two major peaks may be assigned to filamentous coke with different degree of crystallization, getting closer to pure graphitic structures with the increase in oxidation

temperature (Vicente *et al.*, 2014). Thus, a combined evaluation of SEM images, Raman results and TPO profiles of spent catalyst samples clearly confirms the formation of different carbon structures on the catalyst samples during CDRM, and indicates that the fraction of different carbon types depends on the reaction conditions.

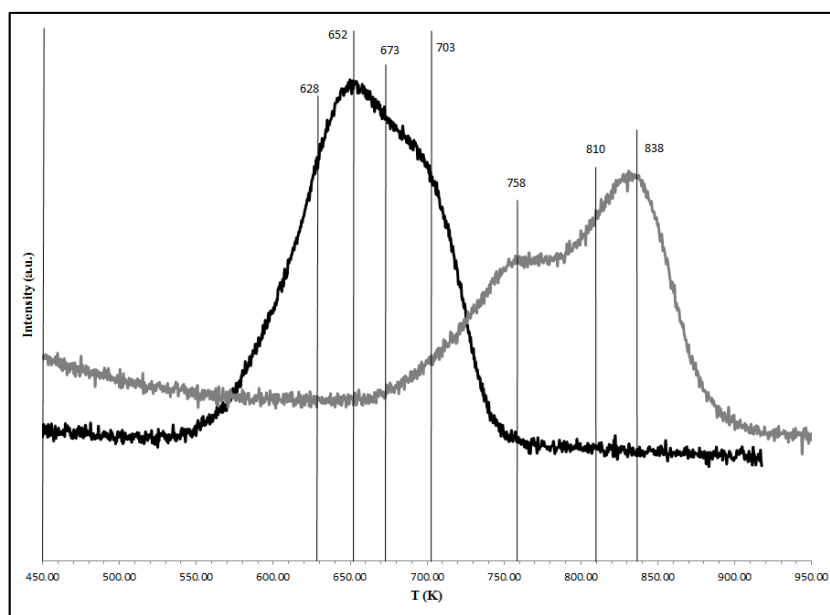


Figure 4.9. TPO of the catalyst samples used during the reaction at space velocity of 20000 mL/h.g-catalyst and at 973 K,  $\text{CH}_4/\text{CO}_2=2/1$ (black curve), and 873 K,  $\text{CH}_4/\text{CO}_2=1/1$ (grey curve).

#### 4.1.2. Performance Tests

A parametric CDRM performance study was conducted on Co-Ce/ZrO<sub>2</sub> system considering reaction temperature,  $\text{CH}_4/\text{CO}_2$  feed ratio and space velocity as the parameters.  $\text{H}_2/\text{CO}$  ratio in the product stream was used as the measure of selectivity. As the syngas fed to Fischer-Tropsch reactor yields valuable olefins when its  $\text{H}_2/\text{CO}$  ratio is close to 1, obtaining  $\text{H}_2/\text{CO}$  ratio in CDRM product closer to 1 is widely accepted advantageous. The activity of the catalyst was studied and discussed in terms of both  $\text{CH}_4$  and  $\text{CO}_2$  conversions, and  $\text{H}_2$  yield achieved.

No severe activity loss was observed during the performed experiments. The  $\text{CH}_4$  conversion results of the reaction tests carried at  $\text{CH}_4/\text{CO}_2$  feed ratio of 2/1, which was

expected to cause the highest activity loss due to the higher loading of CH<sub>4</sub>, indicated only 25% decrease at most in terms of methane conversion during the time-on-stream (TOS) experiments (Figure 4.10). This activity loss was consistent with the carbon deposition observed in SEM analysis (Figure 4.7). Main activity loss was observed for the first 15 minutes TOS for all temperature levels indicating coke formation was more rapid than carbon oxidation reaction on the freshly reduced sample, leading to an activity decrease (Figure 4.10). When the rates of methane dehydrogenation and oxidation of carbon formed on Co sites become compatible, the activity level is stabilized. The activity and selectivity profiles indicate that the performance of the catalyst is very stable when the CH<sub>4</sub>/CO<sub>2</sub> feed ratio is 1/1 for the whole temperature range except at 873 K, which hints limited carbon removal ability compared to methane dehydrogenation at low temperatures (Figure 4.11).

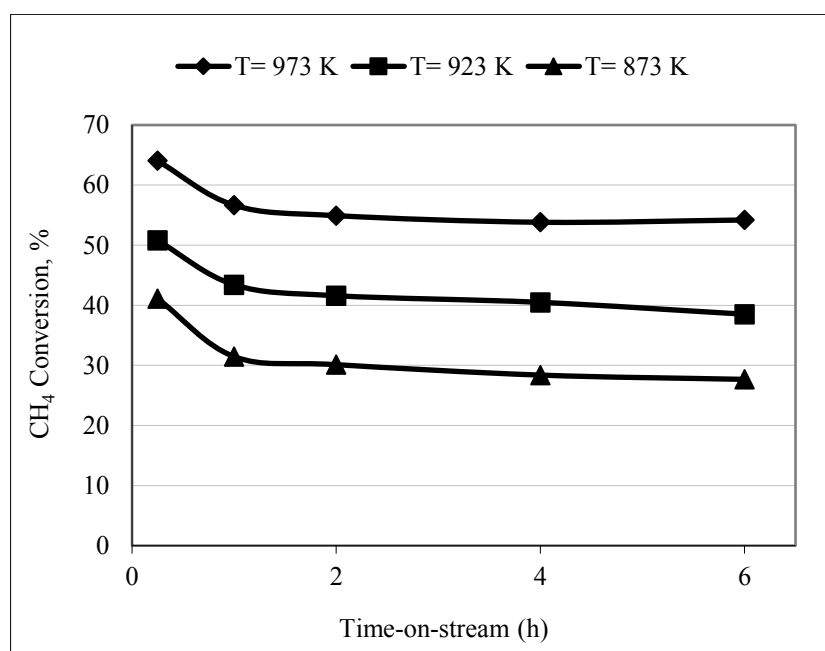


Figure 4.10. Time-on-stream activity profiles of the catalyst in terms of CH<sub>4</sub> conversion for CH<sub>4</sub>/CO<sub>2</sub> feed ratio of 2/1.

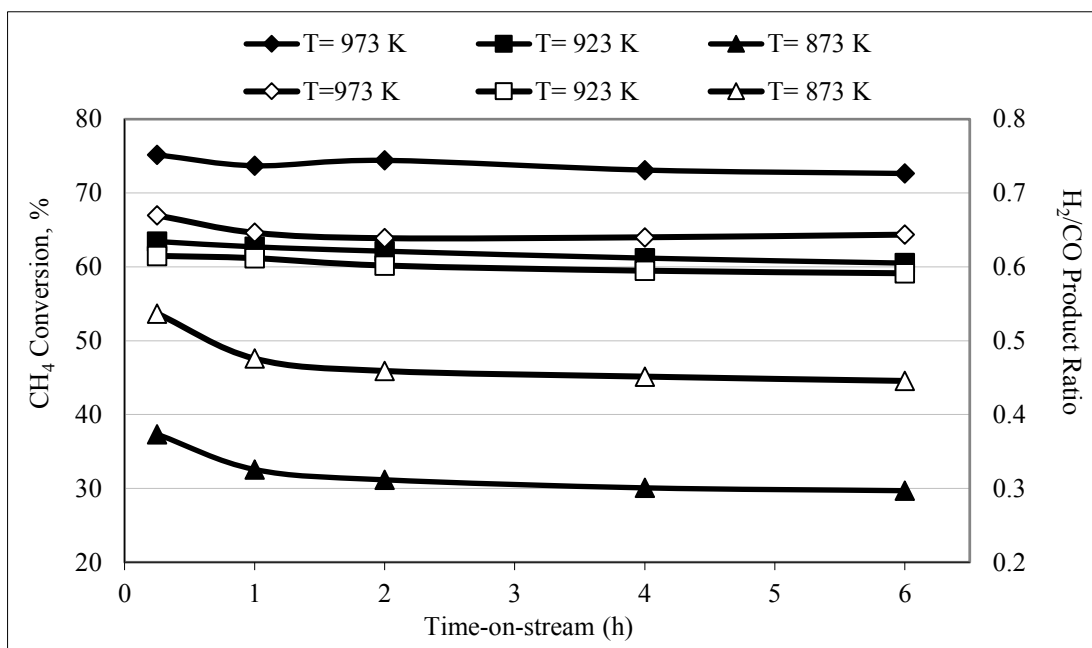


Figure 4.11. Time-on-stream activity and selectivity profiles of the catalyst in terms of CH<sub>4</sub> conversion and H<sub>2</sub>/CO product ratio, respectively, for CH<sub>4</sub>/CO<sub>2</sub> feed ratio of 1/1 (filled symbols: conversion; hollow symbols: selectivity).

4.1.2.1. The Effect of Reaction Temperature. The effect of temperature on catalyst performance was analyzed for the temperature range of 873-973 K in a detailed fashion by using feeds having CH<sub>4</sub>/CO<sub>2</sub> ratios of 1/2, 1/1 and 2/1 for 20000 mL/h.g-catalyst space velocity.

The effects of temperature and CH<sub>4</sub>/CO<sub>2</sub> feed ratio on CH<sub>4</sub> and CO<sub>2</sub> conversion, CH<sub>4</sub>/CO<sub>2</sub> activity ratio and H<sub>2</sub>/CO product ratio are shown in Figure 4.12a-d based on the performance values obtained at the end of 6 h. TOS. For all cases studied, both CH<sub>4</sub> and CO<sub>2</sub> conversion values (Figure 4.12a and b) increased with the increase in temperature. At CH<sub>4</sub>/CO<sub>2</sub> feed ratio of 1/1, for example, methane conversions at the end of 6 h TOS were 30%, 61% and 73% for the reaction temperatures of 873 K, 923 K and 973 K, respectively (Figure 4.12a). Carbon dioxide conversions, which were higher than that of methane, were measured as 41%, 70% and 83% at 873 K, 923 K and 973 K, respectively (Figure 4.12b). It should be noted that the percentage decline in activity with reaction time was inversely proportional to increase in reaction temperature. Therefore, it can be concluded that surface oxygen generation rate increases sharply relative to carbon formation with an increase in

temperature. Additionally, the activation of surface carbon formed may be more favorable at higher reaction temperatures.

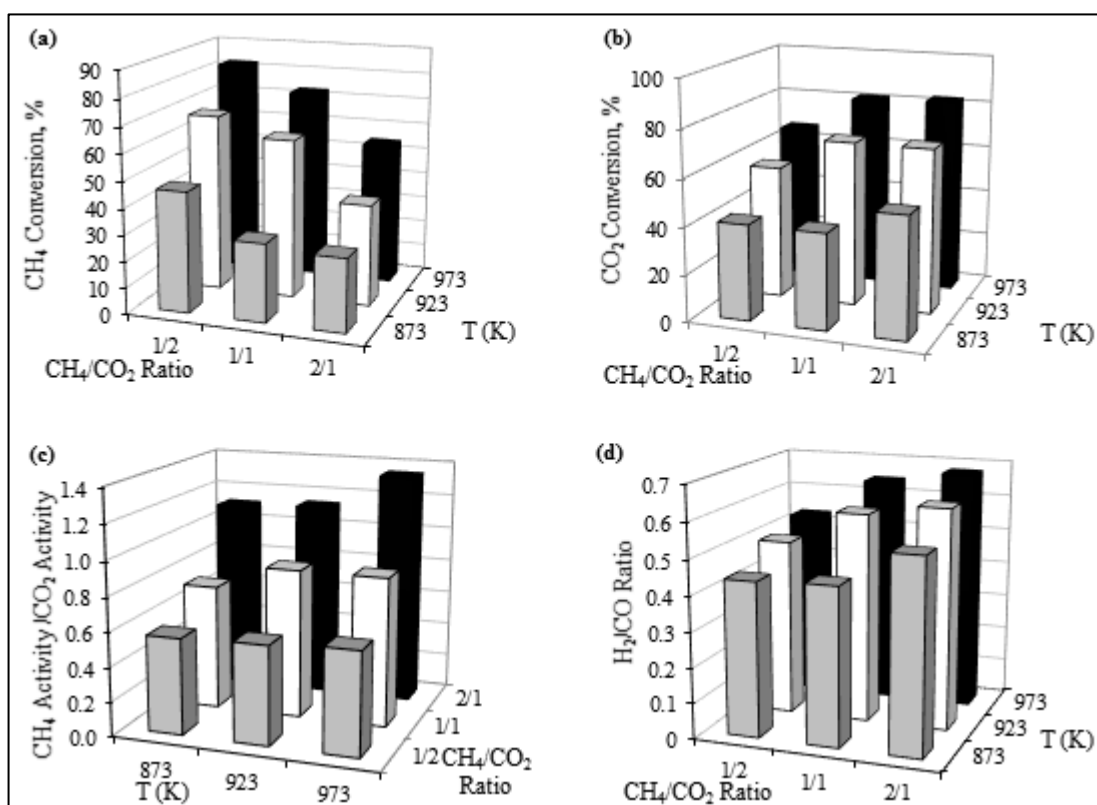


Figure 4.12. The effect of reaction temperature and CH<sub>4</sub>/CO<sub>2</sub> feed ratio on (a) CH<sub>4</sub> conversion, (b) CO<sub>2</sub> conversion, (c) CH<sub>4</sub> activity/CO<sub>2</sub> activity ratio, and (d) H<sub>2</sub>/CO product ratio at the end of 6 h TOS.

The temperature increase resulted in an increase in the ratio of CH<sub>4</sub> activity to CO<sub>2</sub> activity as the methane decomposition reaction favored at high temperatures (Figure 4.12c). The highest observed ratio was 1.35 and it was obtained for the reaction at 973 K with CH<sub>4</sub>/CO<sub>2</sub> feed ratio of 2/1. Consequently, both H<sub>2</sub> yield and H<sub>2</sub>/CO product ratio (Figure 4.12d) increase with the increase in temperature. Stabilized H<sub>2</sub>/CO product ratio, at the end of 6 h TOS, was 0.64 at 973 K, 0.59 at 923 K and 0.45 at 873 K for the CH<sub>4</sub>/CO<sub>2</sub> feed ratio of 1/1. On the other hand, increase in CH<sub>4</sub> activity relative to that of CO<sub>2</sub> caused higher level of coke deposition which may lead to reactor blockage.

TOS data for H<sub>2</sub> yield (Figure 4.13) for the reactions carried out between 873 and 973 K at CH<sub>4</sub>/CO<sub>2</sub> feed ratio of 1/1 reflect the effect of coke deposition. It is evident that coke may form either through methane dehydrogenation or Boudouard reaction. At the beginning of the reaction, surface concentrations of the species are stabilized and the effect of temperature could not be fully observed; as an example, the yield at the end of 1<sup>st</sup> hour-on-stream was the highest for the test conducted at 873 K. However, with the increase in TOS, Boudouard reaction favored at low temperatures may become relatively significant leading lower H<sub>2</sub> yields at 873 K compared to yields at higher temperatures. The slight increase in “CH<sub>4</sub> activity/CO<sub>2</sub> activity” ratio with temperature (Figure 4.12c) supports the dominance of CH<sub>4</sub> dehydrogenation, while relatively higher increase in H<sub>2</sub>/CO product ratio with the increase in temperature may indicate the suppression of Boudouard reaction at higher temperatures.

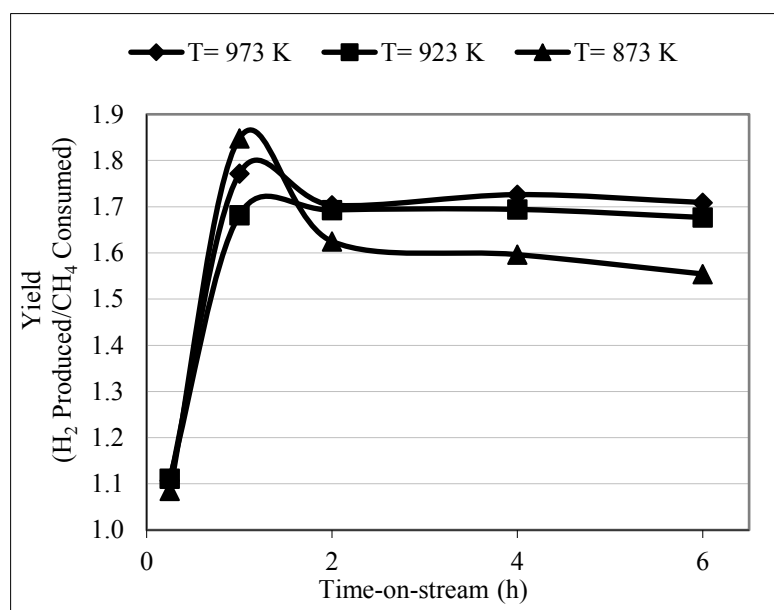


Figure 4.13. Time-on-stream profile of H<sub>2</sub> yield (H<sub>2</sub> produced/CH<sub>4</sub> consumed) obtained at CH<sub>4</sub>/CO<sub>2</sub> feed ratio of 1/1 and 20000 mL/h.g-catalyst.

Conclusively, it was clearly observed that increasing temperature resulted in increasing activity and selectivity towards hydrogen as well as increasing coke deposition for Ce-Co catalyst in CDRM.

4.1.2.2. The Effect of CH<sub>4</sub>/CO<sub>2</sub> Feed Ratio. The effect of CH<sub>4</sub>/CO<sub>2</sub> feed ratio on the activity and selectivity of the Co-Ce catalyst has been studied in a detailed fashion. For the reactions carried out at the same temperature and space velocity, CH<sub>4</sub> activity losses over time were lower at the CH<sub>4</sub>/CO<sub>2</sub> feed ratio of 1/2 and 1/1 but significantly high for the feed ratio of 2/1 (Figure 4.14). As reaction proceeded, CH<sub>4</sub> conversion decreased by only 3% for the feed ratios of 1/2 and 1/1, whereas the decrease was 15% for the feed ratio of 2/1 at 973 K. The limited activity loss at lower CH<sub>4</sub>/CO<sub>2</sub> feed ratios can be attributed to the higher loading of the oxygen source, carbon dioxide. With increased CO<sub>2</sub> feeding rate, carbon formed as the side product of CDRM could be easily cleaned away, resulting in less coke deposition and therefore limited activity loss. This effect is also in agreement with the results of SEM-EDX analysis showing the effect of CH<sub>4</sub>/CO<sub>2</sub> feed ratio on deposited carbon (Figure 4.6 and 4.7).

The CH<sub>4</sub>/CO<sub>2</sub> feed ratio of 1/2 yielded the highest methane conversion values, whereas the lowest carbon dioxide conversion and H<sub>2</sub>/CO product ratio values were obtained for the whole temperature range for that feed ratio (Figure 4.12a, b and d). CH<sub>4</sub>/CO<sub>2</sub> feed ratio of 2/1, on the other hand, had an opposite effect on catalyst activity and selectivity; it yielded the highest carbon dioxide conversion values and H<sub>2</sub>/CO product ratios with the lowest methane conversions observed for the conditions tested. For reactions conducted at 973 K, methane conversion values were 82%, 73% and 54% for the feed ratios of 1/2, 1/1 and 2/1, respectively (Figure 4.12a). Carbon dioxide conversion values, on the other hand, were 67% at 1/2 feed ratio, 82% at 1/1 feed ratio and 83% at 2/1 feed ratio (Figure 4.12b). At the end of 6 hours-on-stream, the highest H<sub>2</sub>/CO product ratio, 0.68, was obtained for 2/1 feed ratio whereas the lowest ratio, 0.53, was recorded for the reaction with 1/2 feed ratio (Figure 4.12d). It was clearly observed that both conversion and H<sub>2</sub>/CO product ratio values were sufficiently high for the tests conducted using 1/1 feed ratio.

When CH<sub>4</sub>/CO<sub>2</sub> feed ratio was increased, because of higher loading of hydrocarbon, CH<sub>4</sub> activity increased while CO<sub>2</sub> activity decreased (Figure 4.14), leading to an increase in CH<sub>4</sub>/CO<sub>2</sub> activity ratio (see Figure 4.12c). Considering also the increase in H<sub>2</sub> yield, based on CH<sub>4</sub> fed (not shown), one can explain the enhanced H<sub>2</sub> selectivity in the product stream. However, the increase in CH<sub>4</sub>/CO<sub>2</sub> activity ratio caused coke deposition, as there

was not enough oxygen source to clean away the formed carbon and, therefore, H<sub>2</sub> yield, based on CH<sub>4</sub> consumed, was decreased.

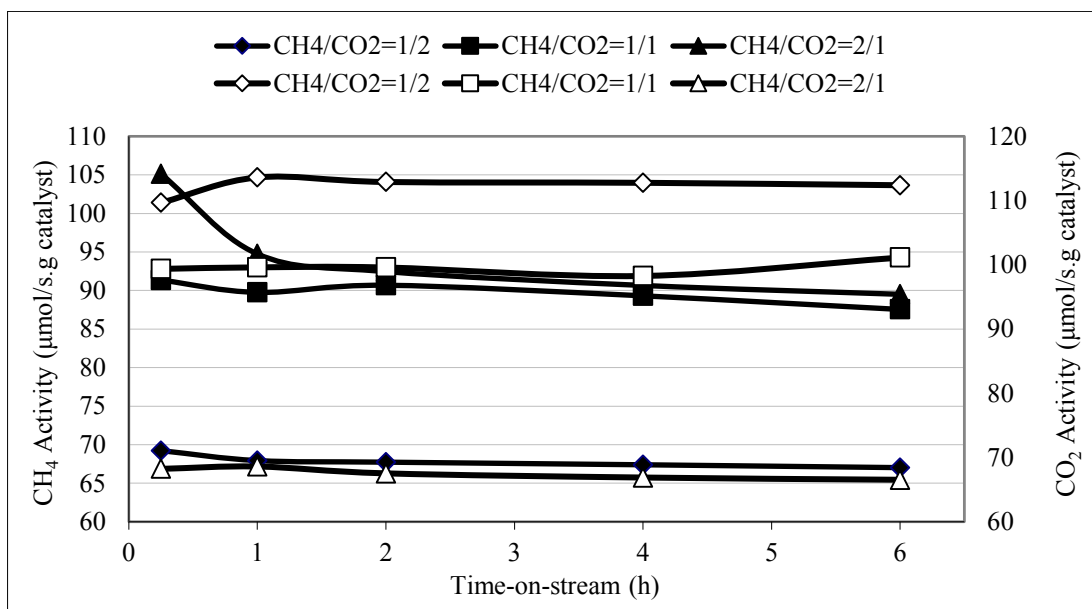


Figure 4.14. CH<sub>4</sub> and CO<sub>2</sub> activities at 973 K for 20000 mL/h.g-catalyst (filled symbols: CH<sub>4</sub> activity; hollow symbols: CO<sub>2</sub> activity).

It was clear that CH<sub>4</sub>/CO<sub>2</sub> feeding ratio has a serious effect on both activity and selectivity of the Ce-Co catalyst. Evaluating activities and coke deposition in a combined fashion indicates that 1/1 feed ratio can be taken as a suitable value for the current catalyst.

**4.1.2.3. The Effect of Space Velocity.** The effect of space velocity on the CDRM performance of Co-Ce system was investigated for three different space velocities, 10000 mL/h.g-catalyst, 20000 mL/h.g-catalyst and 30000 mL/h.g-catalyst at 973 K for CH<sub>4</sub>/CO<sub>2</sub> feed ratio values between 0.5 and 2 (Figure 4.15). Similar activity trends were observed for all space velocities tested (not shown).

As the space velocity increased from 10000 mL/h.g-catalyst to 30000 mL/h.g-catalyst, both CH<sub>4</sub> and CO<sub>2</sub> conversion values decreased for all feed compositions (Figure 4.15a and b). The decrease was 5% for the CH<sub>4</sub>/CO<sub>2</sub> feed ratio of 1/1 and most of the decrease was observed when the space velocity was changed from 10000 to 20000 mL/h.g-catalyst. At the end of 6<sup>th</sup> hour-on-stream, methane conversions for the feed ratio of 1/1

were recorded as 78%, 73% and 71% for the space velocities of 10000, 20000 and 30000 mL/h.g-catalyst, respectively.

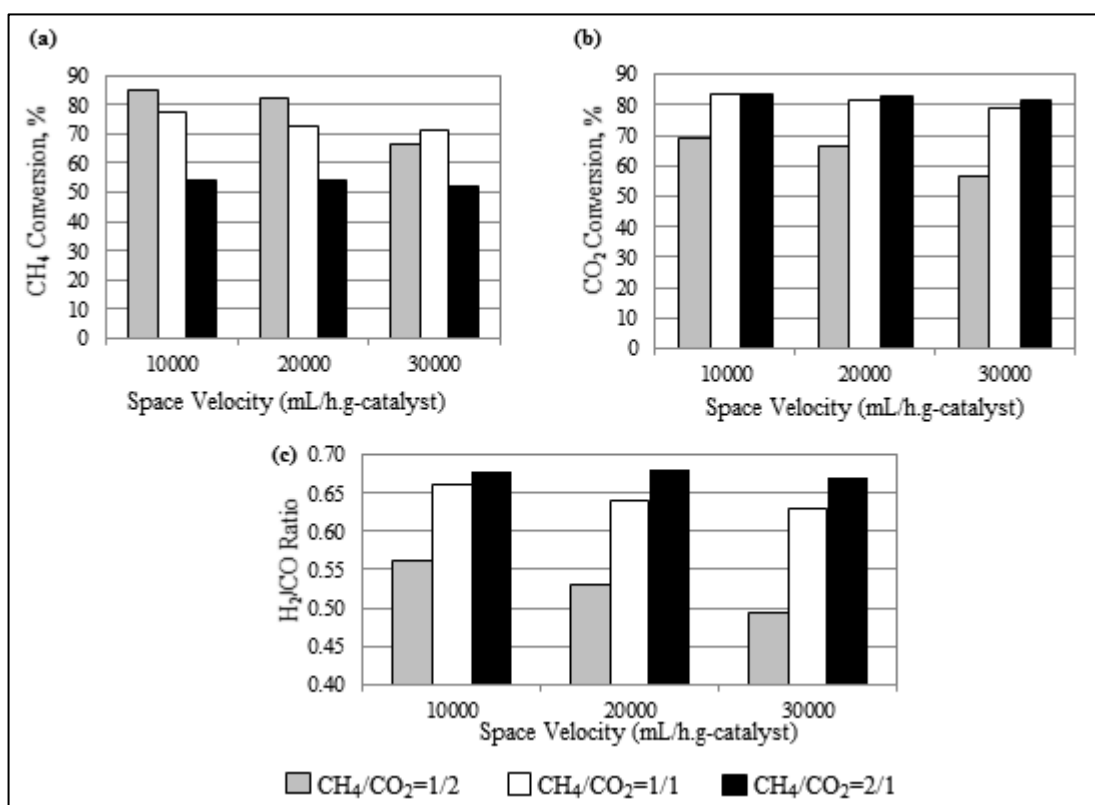


Figure 4.15. Activity and selectivity trends at 973 K as a function of CH<sub>4</sub>/CO<sub>2</sub> feed ratios and space velocities (a) CH<sub>4</sub> conversions, (b) CO<sub>2</sub> conversions, and (c) H<sub>2</sub>/CO product ratio.

It was interesting to notice that the effect of space velocity was observed more significantly as the CH<sub>4</sub>/CO<sub>2</sub> feed ratio was decreased. This can be explained by the comparative analysis of methane dehydrogenation and surface carbon oxidation rates. The increase in oxygen source resulted in closer oxidation and dissociation rates leading stable CDRM activity.

There were no major changes observed for H<sub>2</sub>/CO product ratio for the CH<sub>4</sub>/CO<sub>2</sub> feed ratios of 1/1 and 2/1 in response to changes in space velocity (Figure 4.15c). As the space velocity was increased from 10000 to 30000 mL/h.g-catalyst, H<sub>2</sub>/CO product ratio only decreased from 0.66 to 0.64 and 0.68 to 0.67 for CH<sub>4</sub>/CO<sub>2</sub> feed ratios of 1/1 and 2/1,

respectively. However, H<sub>2</sub>/CO product ratio became 0.49 for CH<sub>4</sub>/CO<sub>2</sub> feed ratio of 1/2 at 30000 mL/h.g-catalyst, which was 0.56 at 10000 mL/h.g-catalyst.

Based on the results of the experiments carried out, the increase in space velocity resulted in a decrease in both CH<sub>4</sub> and CO<sub>2</sub> conversions and H<sub>2</sub>/CO product ratio for all CH<sub>4</sub>/CO<sub>2</sub> feed ratios applied.

#### 4.1.3. Stability Test

The 72 hours stability test was performed over 5%Co-2%Ce-ZrO<sub>2</sub> at 873 K with the CH<sub>4</sub>/CO<sub>2</sub> feed ratio of 1/1 and space velocity of 20000 mL/h.g-catalyst. Despite very limited coke formation, which was characterized by TPO and Raman analysis, the catalyst showed no deactivation (Figure 4.16) during 72 h TOS.

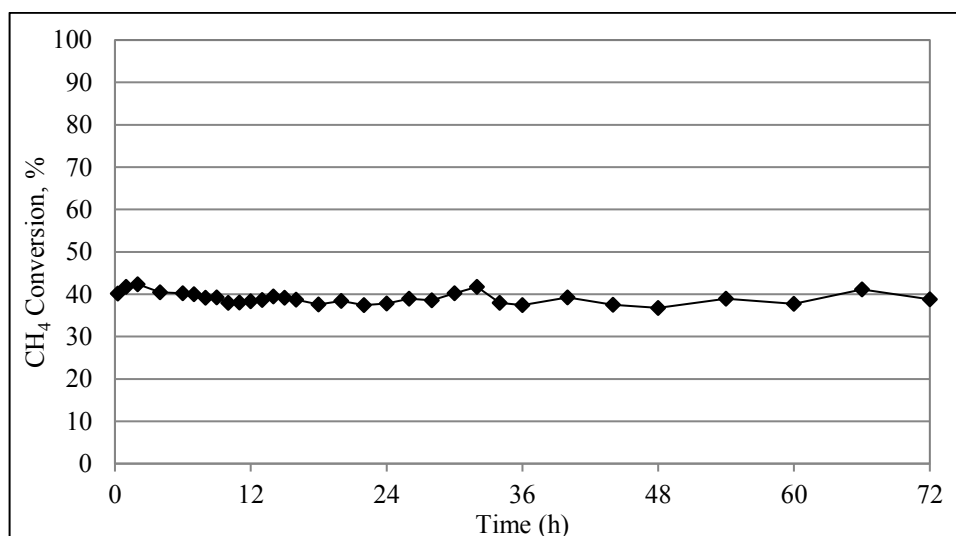


Figure 4.16. Stability test over 5%Co-2%Ce/ZrO<sub>2</sub> (873 K, CH<sub>4</sub>/CO<sub>2</sub>=1/1, space velocity=20000 mL/h.g-catalyst).

## 4.2. The Effects of Co/Ce Loading Ratio and Reaction Conditions on CDRM Performance of Co-Ce/ZrO<sub>2</sub> Catalysts

The overall purpose of this section is to analyze the link between Co/Ce ratio and CDRM performance, and to confirm the roles of Co, Ce and ZrO<sub>2</sub> in Co-Ce/ZrO<sub>2</sub> system.

In this context, catalysts with different Co and Ce loadings were prepared, HRTEM-EDX and XPS techniques were utilized for their detailed characterization, and their parametric CDRM performance analyses at different temperatures (873 K, 923 K and 973 K) and  $\text{CH}_4/\text{CO}_2$  feed ratios (1/2, 1/1 and 2/1) were carried out. This section has been submitted to *Applied Catalysis B: Environmental* as a manuscript of a research paper.

#### 4.2.1. Characterization of Co-Ce/ZrO<sub>2</sub> System

Micro-structural properties of Co-Ce/ZrO<sub>2</sub> system and dispersion of Co and Ce on catalyst samples were analyzed by HRTEM and EDX. The existence of Co, Ce and ZrO<sub>2</sub> particles were verified via EDX analysis given in Figure 4.17. The HRTEM images in the same figure also expressed that Co and Ce particles are typically at size of 5-10 nm, whereas ZrO<sub>2</sub> particles are at size of 20-50 nm.

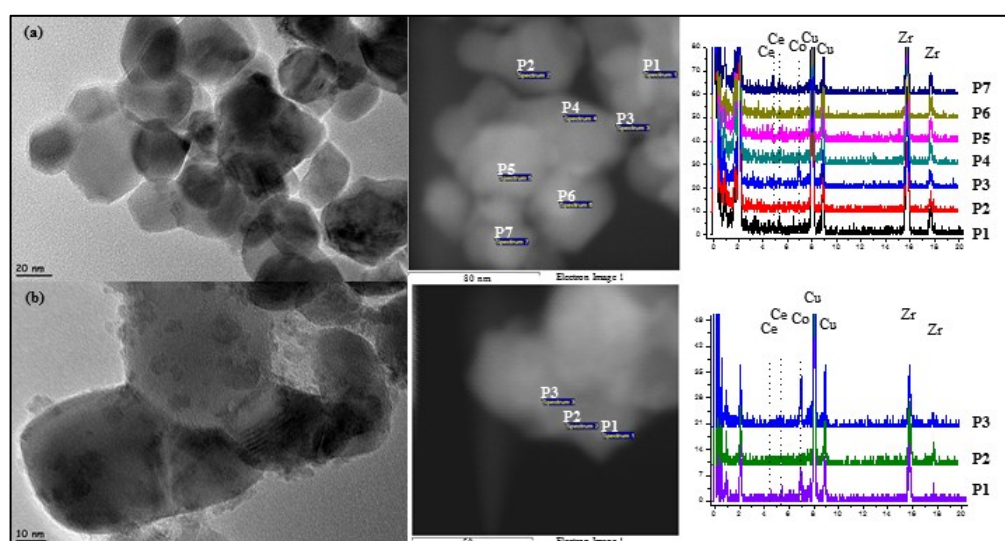


Figure 4.17. HRTEM area images and EDX results for (a) 5%Co-2%Ce/ZrO<sub>2</sub> and (b) 10%Co-3%Ce/ZrO<sub>2</sub> catalysts.

The nanobeam diffraction analysis applied to HRTEM images for 5%Co-2%Ce/ZrO<sub>2</sub> catalyst sample (Figure 4.18a) gave d-spacing values corresponding to monoclinic zirconia of (1 1 0) and (0 2 2) planes. In another region of the same sample, d-spacing value for CoO in (1 1 1) plane was detected in addition to that of monoclinic zirconia of (1 1 0) plane (Figure 4.18b).

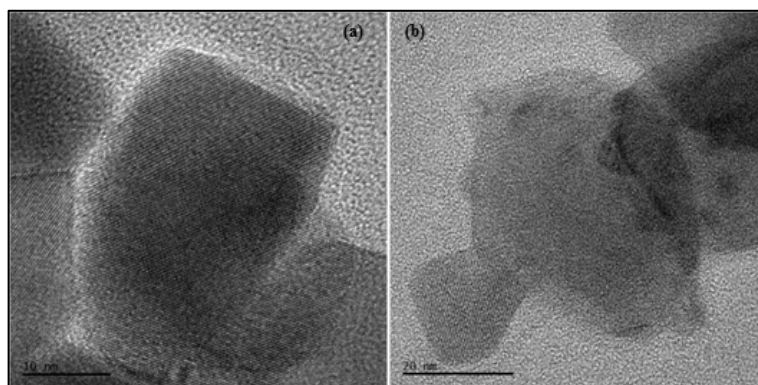


Figure 4.18. HRTEM images of 5%Co-2%Ce/ZrO<sub>2</sub> catalyst.

The comparison of HRTEM area images in Figure 4.19 for 5%Co-2%Ce/ZrO<sub>2</sub>, 10%Co-2%Ce/ZrO<sub>2</sub> and 10%Co-3%Ce/ZrO<sub>2</sub> revealed that in general Co/Ce ratio does not impose significant micro-physical changes on catalyst surface.

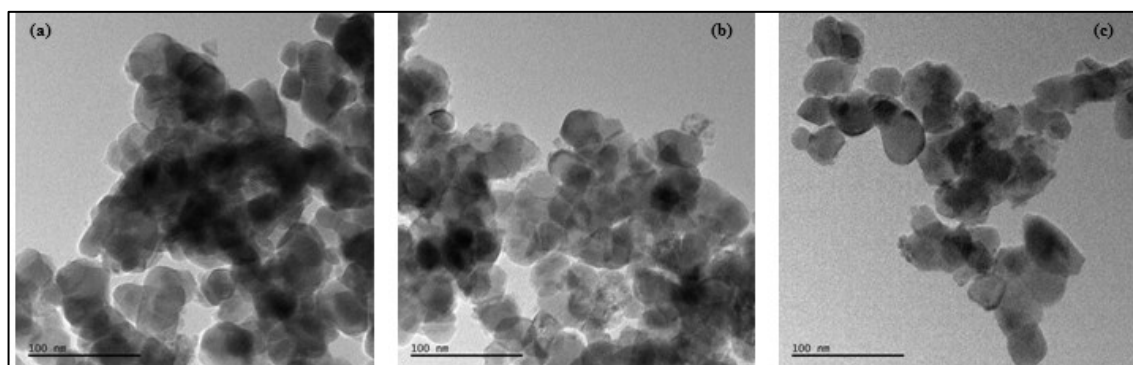


Figure 4.19. HRTEM area images for (a) 5%Co-2%Ce/ZrO<sub>2</sub>, (b) 10%Co-2%Ce/ZrO<sub>2</sub>, and (c) 10%Co-3%Ce/ZrO<sub>2</sub> catalysts.

In the previous study, HRTEM analysis was utilized to indicate that local Co/Ce ratio changes along catalyst surface for 5%Co-2%Ce/ZrO<sub>2</sub> catalyst. Additionally, from SEM-EDX analysis, local Co/Ce surface molar ratio-coke formation relation was confirmed, and it was noted that carbon is favored for the regions with high Co/Ce ratio (See Section 4.1). The mapping results obtained in this study verified these findings by showing nonhomogeneous dispersion of Co particles and even distribution of Ce particles (Figure 4.20). The EDX-Line analysis utilized for another region of the 5%Co-2%Ce/ZrO<sub>2</sub> catalyst sample also highlighted that Ce particles are well dispersed but low in amount; whereas Co

particles are found as clusters (Figure 4.21). This phenomenon was also valid for the other tested catalyst samples. According to HRTEM-EDX results, for example, Co/Ce ratio values ranged in between 0.18 and 2.63 (wt./wt.%) for 10%Co-3%Ce/ZrO<sub>2</sub> catalyst. It might be suggested that Co particles partially cover Ce particles during its impregnation.

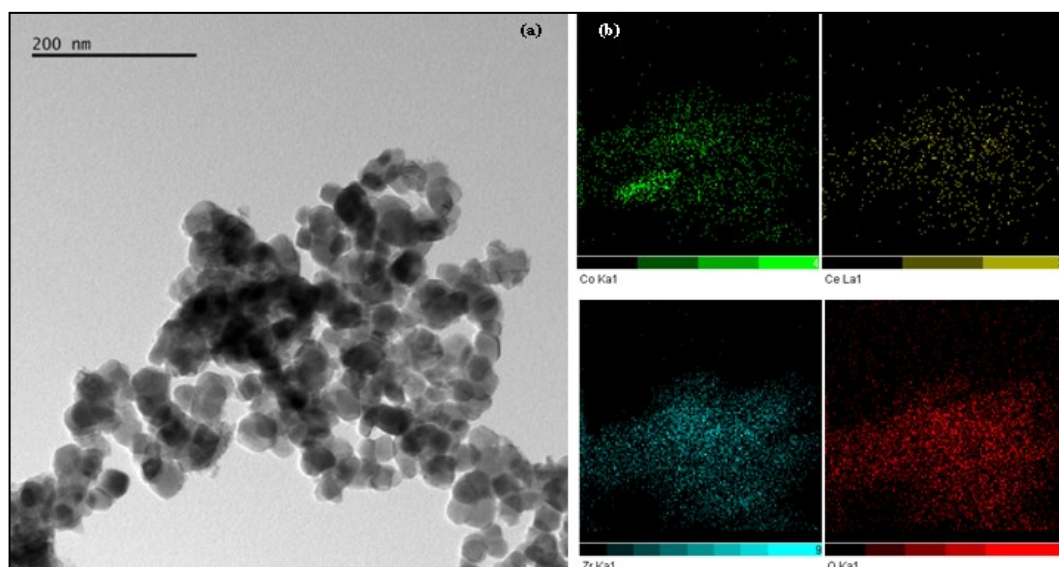


Figure 4.20. (a) HRTEM image of 5%Co-2%Ce/ZrO<sub>2</sub> catalyst, (b) Co, Ce, Zr and O mapping of the region.

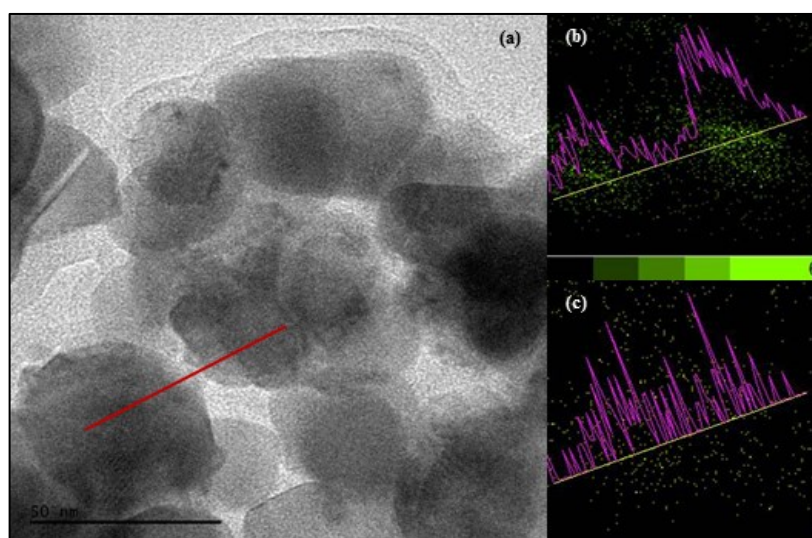


Figure 4.21. (a) HRTEM image of 5%Co-2%Ce/ZrO<sub>2</sub> catalyst, (b) Co EDX-Line and mapping analysis, and (c) Ce EDX-Line and mapping analysis of the selected region, indicated by a line in (a).

In order to analyze the redox ability of  $\text{CeO}_x$  formations and how it is affected by Co/Ce ratio, the Ce3d XP spectra of the freshly reduced and spent Co-Ce/ZrO<sub>2</sub> catalyst samples were obtained (Figure 4.22). Overall surface Ce%, on atomic basis, was calculated as 13.2, 17.8, 9.6 and 16.3 for the 5%Co-2%Ce/ZrO<sub>2</sub>, 5%Co-3%Ce/ZrO<sub>2</sub>, 10%Co-2%Ce/ZrO<sub>2</sub>, and 10%Co-3%Ce/ZrO<sub>2</sub> catalysts, respectively. For 10%Co-2%Ce/ZrO<sub>2</sub>, this explains the lower intensity values, which are expected because of the highest Co/Ce ratio (Figure 4.22). In literature, three main 3d<sub>5/2</sub> peaks at about 882.5 (v), 888.8 (v<sup>2</sup>) and 898.3 (v<sup>3</sup>) eV and three main 3d<sub>3/2</sub> peaks at about 901 (u), 907.4 (u<sup>2</sup>) and 916.6 (u<sup>3</sup>) eV, belonging to the Ce<sup>4+</sup> state were reported, while the peaks at about 880.5 (v<sub>0</sub>), 885.4 (v<sup>1</sup>), 898.8 (u<sub>0</sub>) and 904 (u<sup>1</sup>) eV were matched to Ce<sup>3+</sup> state (Leppelt *et al.*, 2006). The binding energies attributed to Ce<sup>4+</sup> and Ce<sup>3+</sup> states, given in Table 4.4, were found in accordance with literature for all catalyst samples; as there is no shift in the binding energies of the Ce peaks compared to those of the literature, the results point out that for the catalyst samples tested, alloy formation is of very small probability.

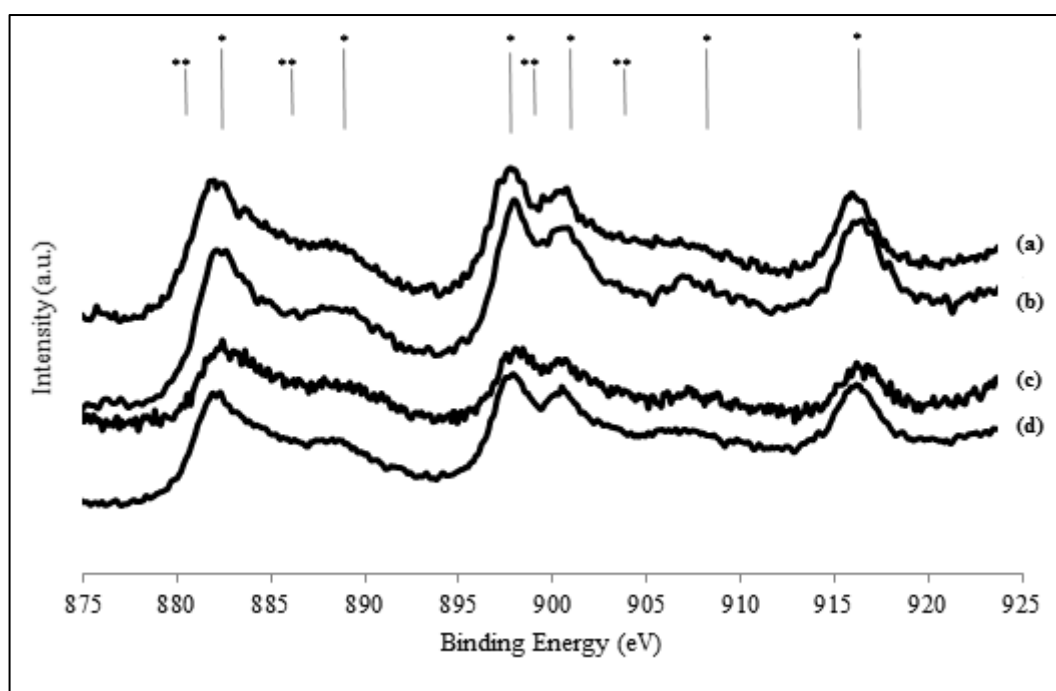


Figure 4.22. XP spectra of Ce3d region for freshly calcined and reduced (a) 5%Co-2%Ce/ZrO<sub>2</sub>, (b) 5%Co-3%Ce/ZrO<sub>2</sub>, (c) 10%Co-2%Ce/ZrO<sub>2</sub>, and (d) 10%Co-3%Ce/ZrO<sub>2</sub> (\*: Ce<sup>4+</sup>, \*\*: Ce<sup>3+</sup>).

Table 4.4. The Ce valance-binding energy (eV) relation for different catalyst samples.

Catalyst	Ce Valance	Binding Energy, eV
5%Co-2%Ce/ZrO <sub>2</sub>	Ce <sup>4+</sup>	916.06, 907.22, 900.56, 897.54, 888.57, 882.5
	Ce <sup>3+</sup>	903.47, 898.92, 884.85, 879.36
5%Co-3%Ce/ZrO <sub>2</sub>	Ce <sup>4+</sup>	916.75, 907.7, 901.07, 898.29, 889.37, 882.68
	Ce <sup>3+</sup>	903.43, 898.65, 885.72, 880.63
10%Co-2%Ce/ZrO <sub>2</sub>	Ce <sup>4+</sup>	916.39, 907.76, 900.85, 897.79, 889.1, 882.4
	Ce <sup>3+</sup>	904.13, 899.44, 885.43, 879.56,
10%Co-3%Ce/ZrO <sub>2</sub>	Ce <sup>4+</sup>	916.15, 906.96, 900.54, 897.62, 888.46, 881.88
	Ce <sup>3+</sup>	902.69, 899.09, 884.54, 879.77

The degree of ceria reduction was evaluated after deconvolution of each spectra by taking the ratio of the sum of integrated areas of  $v_0$ ,  $u_0$ ,  $u^1$  and  $v^1$  peaks to the sum of the integrated peak areas of all peaks, as given in Equation 4.1 (Leppelt *et al.*, 2006). It was argued that higher degree of ceria reduction leads to an increase of the oxygen vacancy content and hence, increases the mobility of oxygen ions (Melchionna and Fornasiero, 2014). The deconvolution analysis established the degrees of ceria reduction as 27.8, 26.5, 22.1 and 27.7% for the 5%Co-2%Ce/ZrO<sub>2</sub>, 5%Co-3%Ce/ZrO<sub>2</sub>, 10%Co-2%Ce/ZrO<sub>2</sub>, and 10%Co-3%Ce/ZrO<sub>2</sub> catalysts, respectively. The lowest degree of ceria reduction estimated for 10%Co-2%Ce/ZrO<sub>2</sub> might be explained by its highest Co/Ce ratio. Therefore, it is suggested that not only Ce amount but also the Co/Ce ratio should play a role in CDRM performance -and perhaps CDRM kinetics- of the Co-Ce catalysts.

To obtain information about support defects on catalysts, O1s spectra was utilized (Figure 4.23). Accordingly, the peak at 528-530 eV corresponds to lattice oxygen of CeO<sub>2</sub>, ZrO<sub>2</sub> and CoO phases (Deng *et al.*, 2016; Fu *et al.*, 2015; Piumetti *et al.*, 2016; Moses *et al.*, 2007), whereas peaks at 531-533 eV belongs to adsorbed oxygen and lattice oxygen vacancies, which are formed as a result of highly polarized oxygen atoms at the surface and interphase of low coordination numbered nanocrystallites (Fu *et al.*, 2015; Holgado *et al.*, 2000; Cai *et al.*, 2016). Blue shift of the spectrum for 10%Co-2%Ce/ZrO<sub>2</sub> can be attributed to doping effect on support (Cai *et al.*, 2016). Since the lowest intensity values were already observed at Ce3d spectrum for this catalyst (Figure 4.22), this might hint that

cerium atoms are incorporated in zirconia lattice which causes oxygen vacancies (Cai *et al.*, 2016). Additionally, the highest asymmetry of the spectrum was observed for this catalyst due to lattice oxygen vacancies and adsorbed oxygen (Renuka *et al.*, 2016).

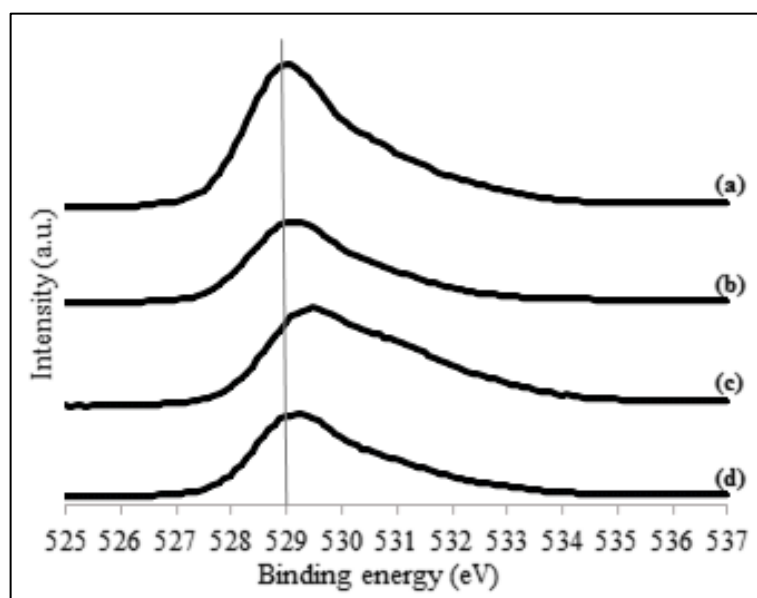


Figure 4.23. XP spectra of O1s region for freshly calcined and reduced (a) 5%Co-2%Ce/ZrO<sub>2</sub>, (b) 5%Co-3%Ce/ZrO<sub>2</sub>, (c) 10%Co-2%Ce/ZrO<sub>2</sub>, and (d) 10%Co-3%Ce/ZrO<sub>2</sub>.

Differentiation of cobalt species having different oxidation states and correlation of their (relative) amounts to catalytic properties, especially when they are in interaction with support, is known to be a challenging task (Lin *et al.*, 2010). The XP spectra of Co2p region, given in Figure 4.24 for all catalyst samples, was analyzed in detail. The peaks at 778.8 and 793.7 eV, separated by 14.9 eV, which were reported as Co2p<sub>3/2</sub> and Co2p<sub>1/2</sub> peaks, respectively, of Co<sup>0</sup> phase in literature (Chai *et al.*, 2005; Lin *et al.*, 2010), indicate the metallic nature of catalyst surface. Surface metallic Co concentrations were calculated as 41.1, 44.1, 37.0 and 35.0% for 5%Co-2%Ce/ZrO<sub>2</sub>, 5%Co-3%Ce/ZrO<sub>2</sub>, 10%Co-2%Ce/ZrO<sub>2</sub>, and 10%Co-3%Ce/ZrO<sub>2</sub> catalysts, respectively, highlighting the possibility of metal oxidation for catalysts having higher Co loading. Co oxide phases are reported as hard to distinguish due to the small shifts in their binding energy values (Watanabe *et al.*, 2013; Biesinger *et al.*, 2011). The Co2p<sub>3/2</sub> peak at 780-781 eV corresponds to oxide states of Co (Hilmen *et al.*, 1999; Wang *et al.*, 2011) and the peak with no satellite was stated as a signature of Co<sup>3+</sup> phase (Varga *et al.*, 2015). On the other hand, the peak with an intense

satellite at a distance of 6 eV was attributed to  $\text{Co}^{2+}$  phase in CoO (Weidler *et al.*, 2016; Lin *et al.*, 2010). As can be clearly seen from Figure 4.24,  $\text{Co}^{2+}$  peaks with their satellite features for CoO are present in spectra of all catalysts. HRTEM analysis (Figure 4.18b) has also verified the existence of CoO. The red shift of the  $\text{Co}^{2+}$  peak positions from 781 to 780.4 eV for the catalysts with higher Co loading verifies that Co species in these samples are more oxidized (Konsolakis *et al.*, 2015). It should be noted that the peak at 782.5 eV, which is only observed for 10%Co-2%Ce/ZrO<sub>2</sub>, is attributed to  $\text{Co}(\text{OH})_2$  and  $\text{Co}_3\text{O}_4$  (Biesinger *et al.*, 2011; Yang *et al.*, 2010) which contain both  $\text{Co}^{3+}$  and  $\text{Co}^{2+}$  species.

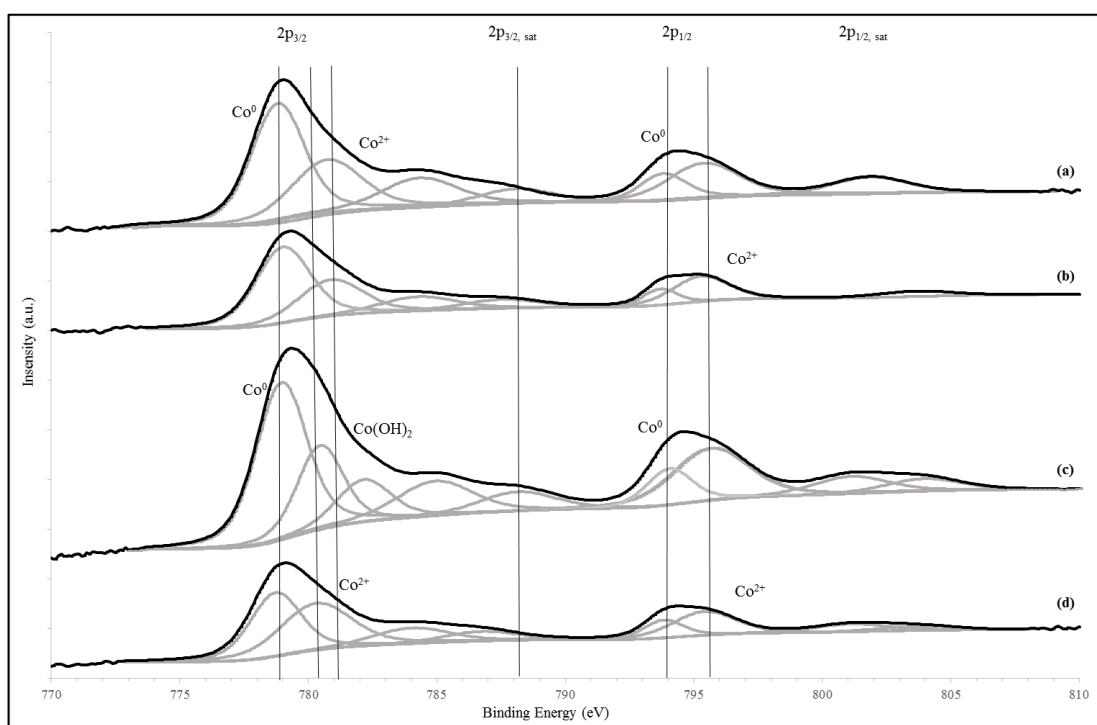


Figure 4.24. XP spectra of Co2p region for freshly calcined and reduced (a) 5%Co-2%Ce/ZrO<sub>2</sub>, (b) 5%Co-3%Ce/ZrO<sub>2</sub>, (c) 10%Co-2%Ce/ZrO<sub>2</sub>, and (d) 10%Co-3%Ce/ZrO<sub>2</sub>.

#### 4.2.2. CDRM Performance of Co-Ce/ZrO<sub>2</sub> System

Aiming to understand the roles of each species and to observe the effect of Co and Ce loading on CDRM performance of Co-Ce/ZrO<sub>2</sub> system, 5%Co-2%Ce/ZrO<sub>2</sub>, 5%Co-3%Ce/ZrO<sub>2</sub>, 10%Co-2%Ce/ZrO<sub>2</sub> and 10%Co-3%Ce/ZrO<sub>2</sub> were parametrically tested for their CDRM activity and selectivity at different temperatures (873 K, 923 K and 973 K) and CH<sub>4</sub>/CO<sub>2</sub> feed ratios (1/1, 1/2 and 2/1) at fixed, 20000 mL/h.g-catalyst, space velocity.

In this context, CH<sub>4</sub> and CO<sub>2</sub> conversion, activity, H<sub>2</sub> yield and selectivity were obtained for all the above mentioned samples. H<sub>2</sub>/CO product ratio, for which values closer to 1 is accepted advantageous as the syngas with H<sub>2</sub>/CO=1 fed to Fischer-Tropsch reactor yields valuable olefins, is considered as a measure of selectivity.

6 h time-on-stream (TOS) data obtained over the catalysts in the performance tests conducted at 973 K with 1/1 CH<sub>4</sub>/CO<sub>2</sub> feed ratio (Figure 4.25) shows that the highest CH<sub>4</sub> and CO<sub>2</sub> activity values, 76 and 89 μmol/s.g-catalyst, respectively, were recorded for the catalyst with 10% Co and 2% Ce loading. High activity values were also noted for 10%Co-3%Ce/ZrO<sub>2</sub> catalyst. However, the tests conducted over these catalysts resulted in more carbon deposition than the ones over 5% Co-loaded samples. Increased carbon deposition yielded higher CH<sub>4</sub> activity loss values as well; the percentage activity losses at the end of 6 h TOS were calculated as 7% and 5% for 10%Co-2%Ce/ZrO<sub>2</sub> and 10%Co-3%Ce/ZrO<sub>2</sub>, respectively. The stability problem stands as an obstacle for the industrial use of these catalysts, and it points out that Co is mainly related to CH<sub>4</sub> dehydrogenation activity (See Section 4.1), and that there is not enough surface oxygen to clean away carbon formed by CH<sub>4</sub> dehydrogenation due to relatively low amount of Ce and ZrO<sub>2</sub> for high Co loaded samples. Therefore, it can indirectly be seen that both Ce and ZrO<sub>2</sub> have roles in surface oxygen production/transfer. It should be noted that the reason of low surface Ce concentration for high Co-loaded samples, measured in above mentioned HRTEM-EDX and Ce3d XPS analyses, is explained by Co formations covering Ce sites during catalyst preparation, which is evident in HRTEM images/analyses. The lack of Co-Ce synergistic interaction, which allows oxygen storage and transfer between species, should also be noted for the catalysts with higher Co/Ce ratio. Moreover, catalysts with 10% Co loading were found to contain more oxidized Co species according to Co2p XPS results which may lead to catalyst deactivation due to metal sintering (Nagaoka *et al.*, 2004; Souza *et al.*, 2014; Ayodele *et al.*, 2015; Ruckenstein and Wang, 2002). On the other hand, low activity values observed in the performance tests over 5%Co-3%Ce/ZrO<sub>2</sub> catalyst for the first two hours TOS can be explained by the relatively lower CH<sub>4</sub> dehydrogenation activity compared to that of CO<sub>2</sub> dissociation, which also strengthened the idea that Co is primarily effective in CH<sub>4</sub> dehydrogenation. The unaffected CO<sub>2</sub> activation indicated that ZrO<sub>2</sub> is responsible for surface oxygen production by CO<sub>2</sub> dissociation; since the support of this catalyst is less covered by metals compared to those with 10% Co loading. Therefore,

ceria's role is mainly the transfer of this surface oxygen by creating a continuous oxidation/reduction cycle; relatively limited CO<sub>2</sub> activity decrease compared to that of CH<sub>4</sub> also supports that explanation.

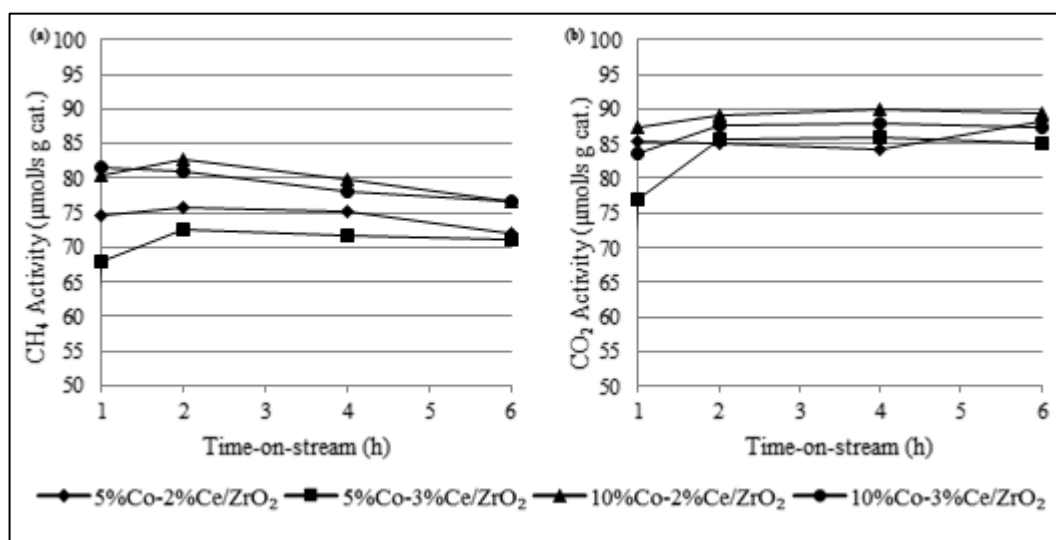


Figure 4.25. Activity profiles of tested catalysts at 973 K with 1/1 CH<sub>4</sub>/CO<sub>2</sub> feed ratio  
(a) CH<sub>4</sub> activity, and (b) CO<sub>2</sub> activity.

When the selectivity profiles of all catalysts were compared for the tests conducted at 973 K with 1/1 CH<sub>4</sub>/CO<sub>2</sub> feed ratio (Figure 4.26), it was seen that the catalyst with 10% Co and 2% Ce loading gave the highest H<sub>2</sub>/CO product ratio throughout 6 h TOS. However, the values decreased sharply and stable product ratio could not be obtained for that sample. The same trend was also observed for the tests conducted over 10%Co-3%Ce/ZrO<sub>2</sub> and 5%Co-3%Ce/ZrO<sub>2</sub> catalysts, preventing their possible long-term use. On the other hand, the catalyst with 5% Co and 2% Ce loading gave the most stable selectivity profile, which can be explained through the balance between C-formation and C-oxidation led by enhanced mobility of surface oxygen, verified by XPS analysis.

Since CDRM contains many side reactions favored at different temperature levels, changing the temperature affects the performance of catalysts. Carbon forming reactions - Boudouard reaction and methane decomposition- and oxygen producing reaction - dissociative adsorption of CO<sub>2</sub>- are the most important reactions affecting the CDRM performance; dissociative CO<sub>2</sub> adsorption leading surface oxygen needs to be at least as

fast as the former ones in order to prevent coke deposition. Boudouard reaction is an exothermic reaction favored at low temperatures, whereas methane decomposition is favored at high temperatures (Gallego *et al.*, 2008a). Considering these trends, performance tests were applied by keeping the feed ratio as 1/1 but decreasing the CDRM temperature in order to grasp the performance characteristics in 873-973 K range. For all tested catalysts, both  $\text{CH}_4$  and  $\text{CO}_2$  activity values and  $\text{H}_2/\text{CO}$  product ratios decreased with the decrease in temperature. The activity order of the tested catalysts also changed with the decrease in temperature, pointing out the effect of metal and promoter content in rates of side reactions.

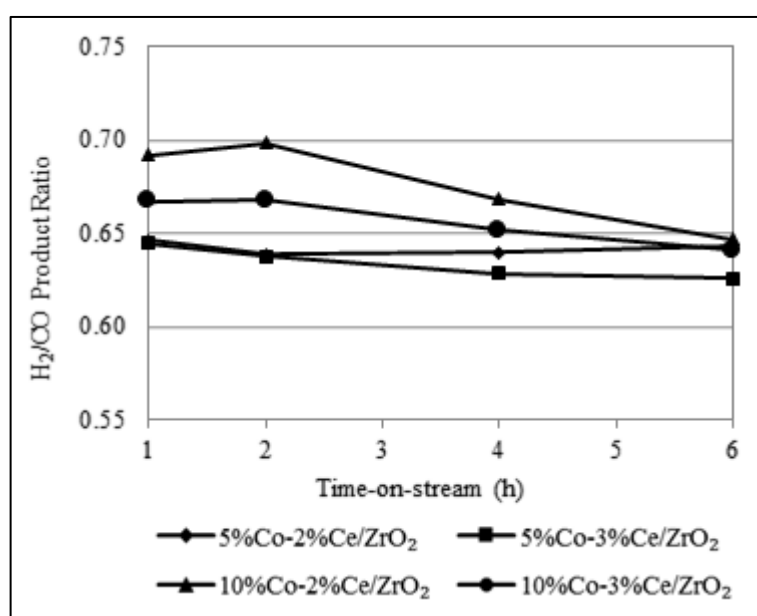


Figure 4.26. Selectivity profiles of tested catalysts at 973 K with 1/1  $\text{CH}_4/\text{CO}_2$  feed ratio.

At 923 K, 10%Co-2%Ce/ZrO<sub>2</sub>, the catalyst with the highest Co/Ce ratio, showed a very unstable  $\text{CH}_4$  activity, which might be related to its high Co loading, and therefore, favored  $\text{CH}_4$  decomposition which caused coke accumulation (Figure 4.27). The highest  $\text{CH}_4$  and  $\text{CO}_2$  activity values and  $\text{H}_2/\text{CO}$  product ratio, on the other hand, were obtained over 10%Co-3%Ce/ZrO<sub>2</sub> catalyst underlining the positive effect of both Ce and  $\text{Ce}^{3+}$ , as indicated by the XPS analysis results of that sample, on both CDRM activity and selectivity. Ce limits the activity loss related to coke deposition. Additionally, the selectivity values for the catalysts with 10% Co loading varied a lot as the reaction proceeded proving that the rate of carbon removal was less than that of carbon formation.

More stable activity and selectivity profiles were obtained for the catalysts with 5% Co loading. It was also interesting to note that the effect of Ce on both activity and selectivity was less noticeable for the catalysts with 5% Co loading. This might hint that Ce is less utilized when there are more reduced Co species, since surface  $\text{Co}^0$  concentrations were recorded as highest for 5% Co loaded catalysts in XPS analysis.

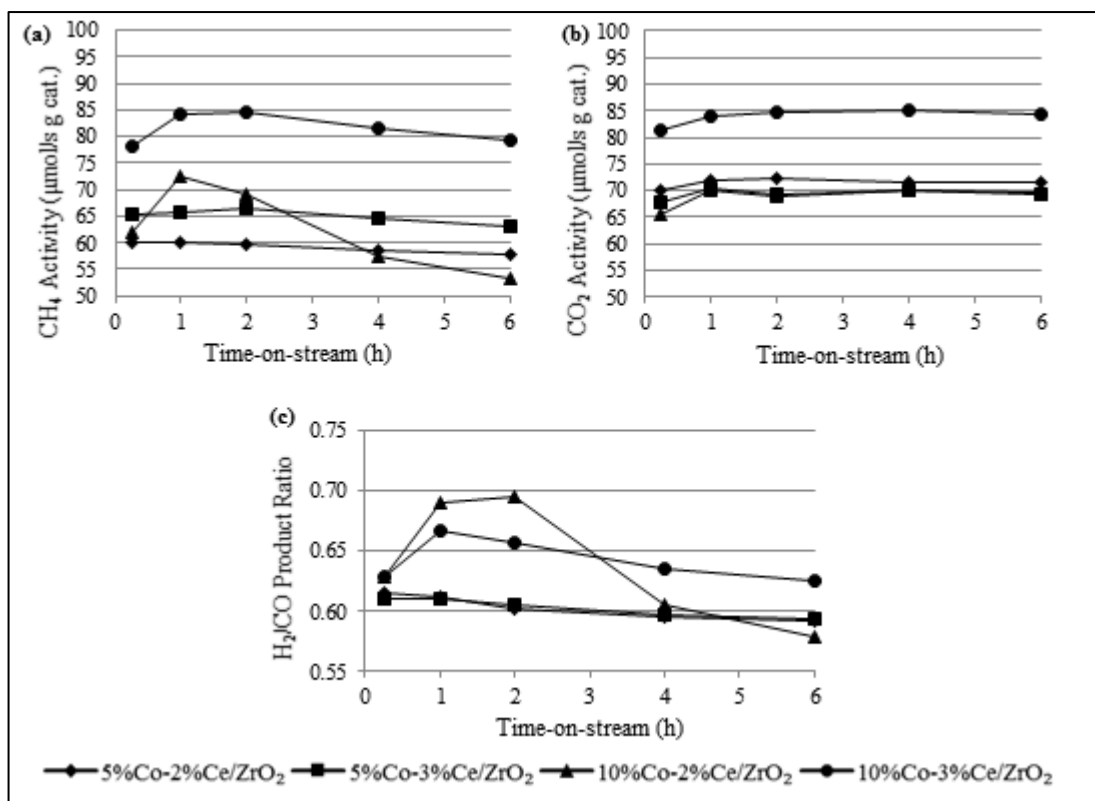


Figure 4.27. Activity and selectivity profiles of tested catalysts at 923 K with 1/1 CH<sub>4</sub>/CO<sub>2</sub> feed ratio (a) CH<sub>4</sub> activity, (b) CO<sub>2</sub> activity, and (c) H<sub>2</sub>/CO product ratio.

When the temperature was further decreased to 873 K (Figure 4.28), the highest CH<sub>4</sub> and CO<sub>2</sub> activity values were recorded for 5%Co-3%Ce/ZrO<sub>2</sub> and 10%Co-3%Ce/ZrO<sub>2</sub>, respectively, at 6 h TOS. This difference most probably stemmed from the relative change in the rates of CO<sub>2</sub> dissociation and CH<sub>4</sub> decomposition. It should also be noted that CDRM activities of the catalysts with 10% Co loading decreased more with the decline in temperature, compared to other catalysts; confirming the role of Co on CH<sub>4</sub> decomposition which is less favored at low temperatures. At 6 h TOS, 21% loss in CH<sub>4</sub> activity values was calculated for 10%Co-3%Ce/ZrO<sub>2</sub>, which might result from carbon accumulation.

From the parametric temperature analysis, it might also be concluded that carbon is deposited at sites that are active in CH<sub>4</sub> dehydrogenation (See Section 4.1), since CH<sub>4</sub> activity loss was faster than that of CO<sub>2</sub>, especially for the catalysts with 10% Co loading.

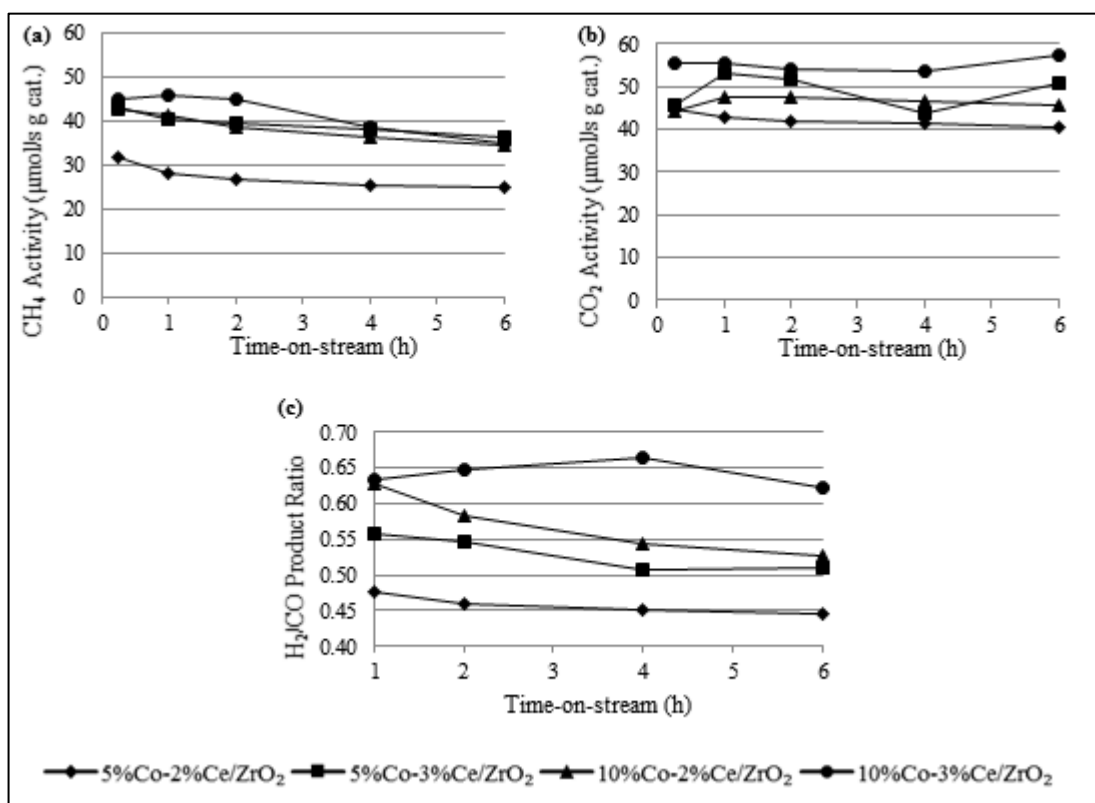


Figure 4.28. Activity and selectivity profiles of tested catalysts at 873 K with 1/1 CH<sub>4</sub>/CO<sub>2</sub> feed ratio (a) CH<sub>4</sub> activity, (b) CO<sub>2</sub> activity, and (c) H<sub>2</sub>/CO product ratio.

CH<sub>4</sub>/CO<sub>2</sub> feeding ratio is another important CDRM parameter as CO<sub>2</sub> acts as the oxygen source whereas excess CH<sub>4</sub> favors carbon formation. In addition to performance tests conducted with CH<sub>4</sub>/CO<sub>2</sub>=1/1, performance tests were also conducted for two other feed ratios, 1/2 and 2/1, to analyze how the effect of Co/Ce loading on CDRM performance was enhanced or suppressed by feed composition. It should be noted that as reactant flow rates would be different for each CH<sub>4</sub>/CO<sub>2</sub> feed ratio, conversion values, through which the results with different reactant flow rates can be compared, are used for discussion.

Increasing CH<sub>4</sub> source in the feed, i.e. using CH<sub>4</sub>/CO<sub>2</sub>=2/1, mainly caused stability problem through coke deposition, especially during first 2 hours of the reaction for all temperature levels. For example, the activity loss in terms of CH<sub>4</sub> conversion was recorded as 41% for the test conducted over 10%Co-2%Ce/ZrO<sub>2</sub> at 973 K (Figure 4.29a). The lowest activity loss at this temperature was noted as 19% over 5%Co-2%Ce/ZrO<sub>2</sub>. As 5%Co-2%Ce/ZrO<sub>2</sub> and 10%Co-2%Ce/ZrO<sub>2</sub> are the catalysts having the highest and lowest Ce<sup>3+</sup> concentrations, respectively, and as the highest deactivation was observed for 10% Co loaded catalysts, which have higher concentration of oxidized Co species; the combined evaluation of characterization and performance tests results revealed that Co/Ce ratio should play a plausible role in CDRM mechanism, which is in accordance with the literature (Ayodele *et al.*, 2015; Ruckenstein and Wang, 2002).

On the other hand, the increase in the feeding rate of CO<sub>2</sub>, i.e. using CH<sub>4</sub>/CO<sub>2</sub>=1/2, created a noticeable decrease in the activity losses in terms of both CH<sub>4</sub> and CO<sub>2</sub> conversions at 2 h TOS. This might have occurred because when the feed was rich in oxygen source, surface oxygen formation and its effective transfer to Co sites -via CO<sub>2</sub> dissociation on ZrO<sub>2</sub> forming surface oxygen followed by transfer of surface oxygen to Co sites regulated by Ce- prevented coke accumulation. At 973 K, where CH<sub>4</sub> dehydrogenation was mostly favored, the combined effect of ZrO<sub>2</sub> and Ce can be more clearly observed (Figure 4.29b); CH<sub>4</sub> conversion dropped only by 3% for the test conducted on the catalyst with the lowest Co/Ce ratio and relatively high ZrO<sub>2</sub> content, i.e. 5%Co-3%Ce/ZrO<sub>2</sub>. The percentage activity loss increased with the increase in Co/Ce loading ratio and became 10% for the catalyst with the highest Co/Ce ratio, i.e. 10%Co-2%Ce/ZrO<sub>2</sub>.

At the feed ratio of CH<sub>4</sub>/CO<sub>2</sub>=2/1, suffering from lack of surface oxygen to clean away formed carbon on active sites also led to lower conversion values, in terms of both CH<sub>4</sub> and CO<sub>2</sub>, compared to those recorded for the other feed ratios (Figure 4.29c). Conversion values at the end of 6 h TOS, on the other hand, were close to each other for all tested catalysts at each temperature level. At 973 K, for example, 6 h TOS CH<sub>4</sub> conversion values were 34.1%, 33.3%, 34.9% and 35.2% for 5%Co-2%Ce-ZrO<sub>2</sub>, 10%Co-2%Ce-ZrO<sub>2</sub>, 5%Co-3%Ce-ZrO<sub>2</sub> and 10%Co-3%Ce-ZrO<sub>2</sub>, respectively. At CH<sub>4</sub>/CO<sub>2</sub> feed ratio of 1/2, the highest conversion values were recorded for the catalysts with 10% Co loading at all

temperature levels showing that increased oxygen source in the feed can overcome the rapid coke formation that would be led by high CH<sub>4</sub> dehydrogenation activity of the catalysts having high Co loading.

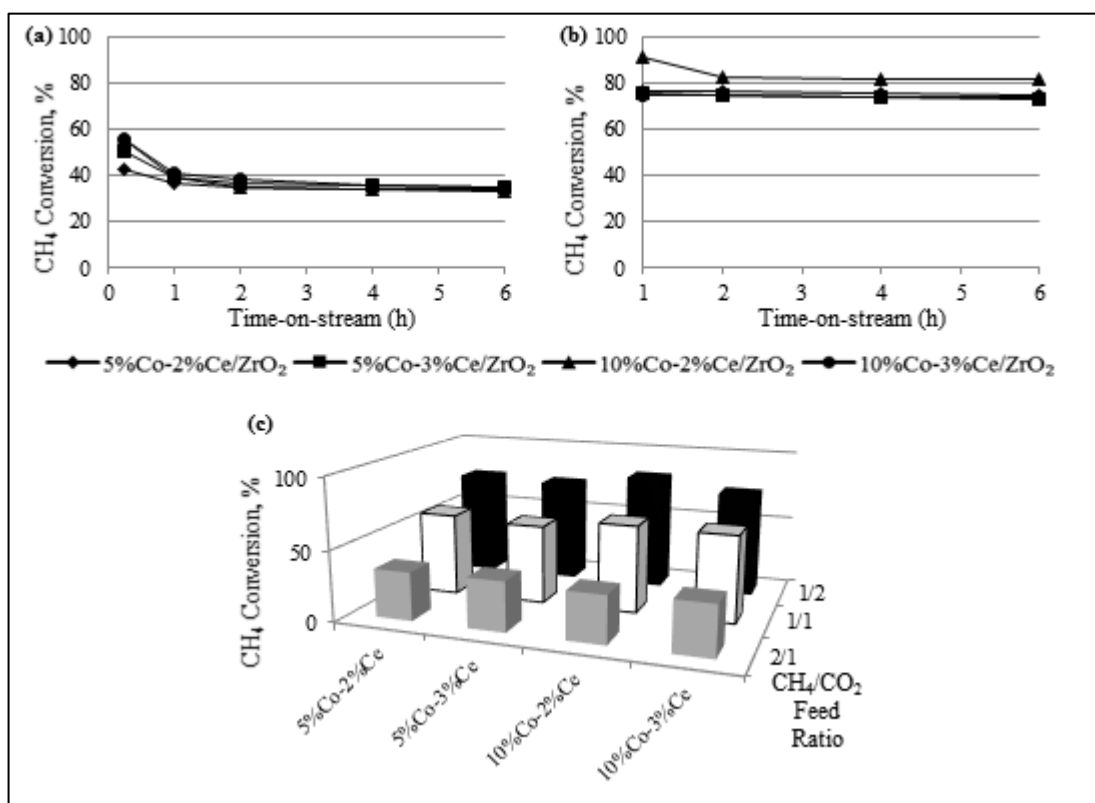


Figure 4.29. Activity profiles in terms of CH<sub>4</sub> conversion for tested catalysts at 973 K (a) with the feed ratio of 2/1, (b) with the feed ratio of 1/2, and (c) for all tested feed ratios.

For the tests conducted at CH<sub>4</sub>/CO<sub>2</sub> feeding ratio of 2/1, it was also clearly noticed that the catalysts with the same cobalt loading displayed exactly the same selectivity profiles at all temperatures (Figure 4.30). Therefore, it can be said that at CH<sub>4</sub>/CO<sub>2</sub> feed ratio of 2/1, CH<sub>4</sub> dehydrogenation performance plays the major role in determining the selectivity. It can additionally be concluded that Ce has limited effect on selectivity when there is not enough surface oxygen, underlining that Ce is only responsible for oxygen transfer but not its formation. When the CO<sub>2</sub> concentration in the feed was increased, the H<sub>2</sub>/CO product ratio values were converged to ca. 0.52 at the end of 6 h TOS for all tested catalysts at 973 K. It should be noted that selectivity shifted towards hydrogen with the decrease in temperature for the catalysts with 10% Co loading. Additionally, the results

indicated that Ce amount did not have a distinct impact on selectivity at 873 K for the catalysts with the same Co loading.

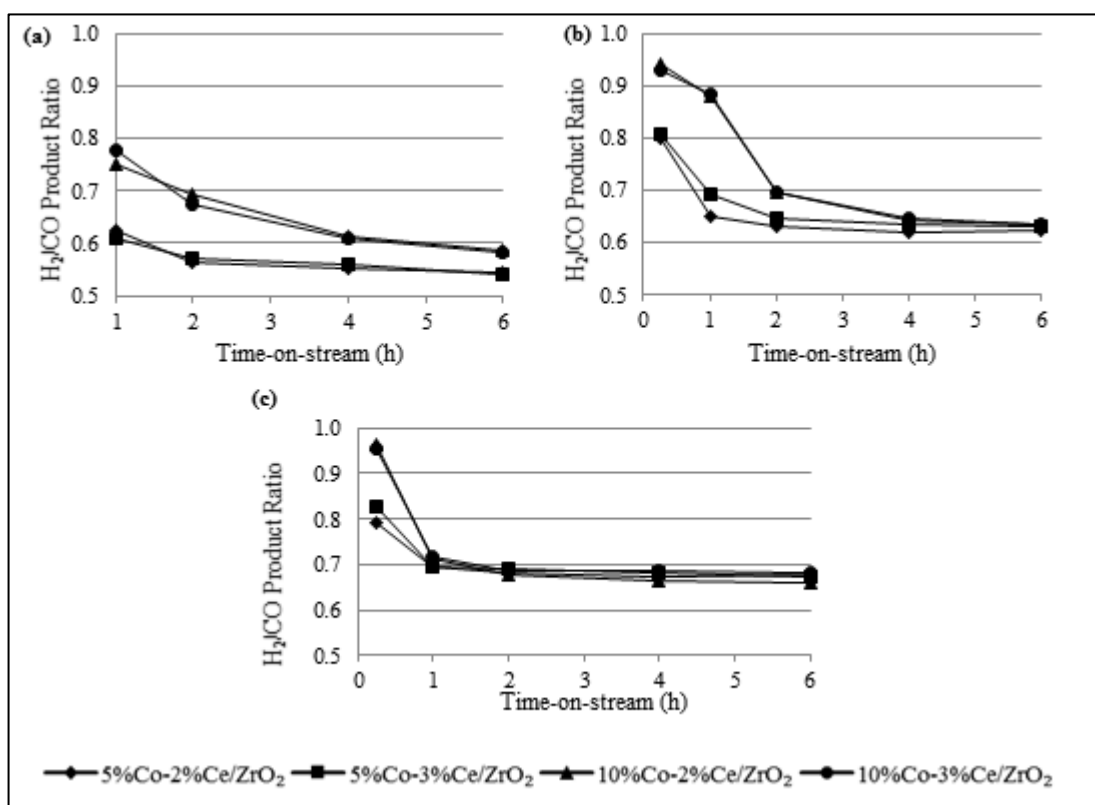


Figure 4.30. Selectivity profiles of tested catalysts with the feed ratio of 2/1 at (a) 873 K, (b) 923 K, and (c) 973 K.

### 4.3. Kinetic and Mechanistic Features of CDRM over Co-Ce/ZrO<sub>2</sub> Catalysts

As 10%Co-2%Ce/ZrO<sub>2</sub> and 5%Co-2%Ce/ZrO<sub>2</sub> catalysts were found to have the higher and most stable CDRM activity, respectively, this section aims to determine the CDRM kinetic behavior of these catalysts, and the effect of Co/Ce loading ratio on parameters of both power type rate and other possible rate expressions. It should be noted that most of the kinetic tests on 10%Co-2%Ce/ZrO<sub>2</sub> catalyst had been performed previously as the part of a M.Sc. study (Yassi, 2014). In the current thesis work, all the kinetic tests on 5%Co-2%Ce/ZrO<sub>2</sub> and additional kinetic tests, which were necessary for estimating the parameters of mechanistic models, on 10%Co-2%Ce/ZrO<sub>2</sub>; all optimization calculations for determination of kinetic model parameters, and mechanistic model

discrimination and parameter optimization for both 5%Co-2%Ce/ZrO<sub>2</sub> and 10%Co-2%Ce/ZrO<sub>2</sub> were performed.

The kinetic analysis was parametrically performed by varying temperature and partial pressures of both reactants and products. The rates were obtained from intrinsic kinetic data in the initial rate region by using differential method of data analysis; the reaction rates were calculated from conversion versus residence time data through the use of Equation 4.2, where  $r_{CH_4}$  is reaction rate in mmol/g.s,  $x_{CH_4}$  is methane conversion,  $F_{CH_4}$  is methane flow rate in the feed in mmol/s and  $W_{cat}$  is catalyst weight in g.

$$-r_{CH_4} = \frac{X_{CH_4}F_{CH_4}}{W_{cat}} \quad (4.2)$$

#### 4.3.1. The Apparent Activation Energies and Power-Law Type Rate Expression

The apparent activation energies were determined in the temperature range of 853-893 K based on consumption rates of CH<sub>4</sub> and CO<sub>2</sub> (Table 4.5).

Table 4.5. Apparent activation energies (kJ/mol) for Co-Ce/ZrO<sub>2</sub> catalysts.

Catalyst	CH <sub>4</sub>	CO <sub>2</sub>
5%Co-2%Ce/ZrO <sub>2</sub>	144	106.8
10%Co-2%Ce/ZrO <sub>2</sub>	61.3	50.5

It was noted that the activation barrier for CH<sub>4</sub> consumption is higher than that for CO<sub>2</sub> consumption for both catalysts, which is in agreement with reported values in literature (Özkara-Aydinoğlu and Aksoylu, 2013; Lemonidou and Vasalos, 2002; Wang and Lu, 1999; Souza *et al.*, 2001). This points out the possibility of higher rates for mechanistic reactions involving CO<sub>2</sub> compared to those involving CH<sub>4</sub>. When the activation barriers for both reactants over the catalysts were compared, it was observed that the values calculated for 10%Co-2%Ce/ZrO<sub>2</sub> catalyst are lower. Relatively harder CH<sub>4</sub> utilization compared to that of CO<sub>2</sub> over 5%Co-2%Ce/ZrO<sub>2</sub>, indicated by higher activation energy for CH<sub>4</sub>, is in accordance with our previous performance tests in which the carbon

formation observed in long time-on-stream tests on Co sites, responsible for CH<sub>4</sub> dehydrogenation, was found limited over 5%Co-2%Ce/ZrO<sub>2</sub> (See Section 4.1). This leads a decrease in need for surface oxygen utilization for cleaning away formed coke from the sites over 5%Co-2%Ce/ZrO<sub>2</sub>. Even though ceria plays an important role in regulating surface oxygen transfer, it was noted that Ce is less utilized when there are more reduced Co species on the surface of the catalyst (See Section 4.2). Therefore, excess surface oxygen on ZrO<sub>2</sub> support becomes unavoidable over 5%Co-2%Ce/ZrO<sub>2</sub>, which may suppress CO<sub>2</sub> activation on ZrO<sub>2</sub> causing a higher CO<sub>2</sub> activation barrier than that on 10%Co-2%Ce/ZrO<sub>2</sub>. The increase in CH<sub>4</sub> utilization over 10%Co-2%Ce/ZrO<sub>2</sub>, observed from the decrease in the activation barrier compared to that for 5%Co-2%Ce/ZrO<sub>2</sub>, eventually increases CO<sub>2</sub> utilization. On the other hand, the ratio of CH<sub>4</sub> activation barrier to that of CO<sub>2</sub> is lower for 10%Co-2%Ce/ZrO<sub>2</sub> catalyst yielding even higher CH<sub>4</sub> dehydrogenation activity than CO<sub>2</sub> dissociation, resulting in coke formation. This causes insufficient surface oxygen and therefore, higher coke deposition, verified by the recent performance tests (See Section 4.2). The lower Ce<sup>+3</sup> concentration, which is responsible for oxygen mobility and regulation, obtained from XPS results for 10%Co-2%Ce/ZrO<sub>2</sub> is also in accordance with the activation energy results (See Section 4.2). To sum up, CH<sub>4</sub> utilization is a key factor in CDRM, and it even indirectly affects CO<sub>2</sub> utilization. However, the effect of Co/Ce ratio on CDRM activity cannot be denied considering the dominant role of catalyst composition in forming a balance between C-formation and C-oxidation.

The influence of reactant partial pressures on CDRM rate over both catalysts was studied at atmospheric pressure for different CH<sub>4</sub>/CO<sub>2</sub> feed ratios and space velocities. The calculated reaction rates are given in Table 4.6.

It was seen that up to 1/1 CH<sub>4</sub>/CO<sub>2</sub> feed ratio, 'initial reaction rate-CH<sub>4</sub>/CO<sub>2</sub> feed ratio' is in direct relationship for both catalysts. However, decreasing trend in rate values was observed for increasing feed ratios for 5%Co-2%Ce/ZrO<sub>2</sub>, whereas a constant value was calculated for feed ratios above 1.33 for 10%Co-2%Ce/ZrO<sub>2</sub> (Figure 4.31). The decrease in initial rates of reaction for 5%Co-2%Ce/ZrO<sub>2</sub> catalyst for CH<sub>4</sub>/CO<sub>2</sub> feed ratio above 1 was expected since increasing CH<sub>4</sub> in the feed enhances CH<sub>4</sub> dehydrogenation. Co sites, where CH<sub>4</sub> dehydrogenation occurs, seem insufficient for high CH<sub>4</sub> concentration in

feed for the ratio above 1. This might also explain the constant initial reaction rate values in 10%Co-2%Ce/ZrO<sub>2</sub> catalyst for the feed ratio between 1.33 and 4. The Co clusters observed in previously conducted HRTEM studies might provide sufficient sites for CH<sub>4</sub> utilization (See Section 4.2). It should be noted that the comparative analysis of performance trends with respect to time in long time-on-stream (TOS) tests for the same catalysts may be different from the above mentioned trends due to both coke formation and surface oxygen utilization rates (See Section 4.2).

Table 4.6. Initial CDRM rates for Co-Ce/ZrO<sub>2</sub> catalysts (SV=500000, 600000 and 750000 mL/h.g-catalyst, TOS=90 min).

CH <sub>4</sub> /CO <sub>2</sub> Ratio	Partial Pressures (atm)		Reaction Rates (mmol/h.g-catalyst)	
	CH <sub>4</sub>	CO <sub>2</sub>	5%Co-2%Ce/ZrO <sub>2</sub>	10%Co-2%Ce/ZrO <sub>2</sub>
0.25	0.02	0.08	-	0.016958
0.5	0.04	0.08	0.024846	0.035967
0.75	0.06	0.08	0.036279	0.055038
1	0.08	0.08	0.076599	0.073811
1.33	0.08	0.06	0.075202	0.090157
1.5	0.08	0.053	0.057206	-
2	0.08	0.04	-	0.089073
4	0.08	0.02	-	0.088955

The reaction orders ( $\alpha$  and  $\beta$ ) and the apparent rate constant ( $k$ ) were estimated for the empirical power-law type rate expression in Equation 4.3 by using non-linear regression analysis applied to CH<sub>4</sub> reforming rates versus partial pressure data at 873 K, and are given in Table 4.7.

$$-r_{CH_4} = kP_{CH_4}^{\alpha}P_{CO_2}^{\beta} \quad (4.3)$$

It was observed that the reaction orders with respect to CH<sub>4</sub> were higher than those with respect to CO<sub>2</sub> for both catalysts, suggesting that the mechanistic step(s) involving CH<sub>4</sub> and/or its constituents may be rate determining steps (RDS). The small negative order for CO<sub>2</sub> in 10%Co-2%Ce/ZrO<sub>2</sub> catalyst underlined the inhibitory effect of CO<sub>2</sub> on H<sub>2</sub>

(and/or CO) production for this catalyst (Bradford and Vannice, 1999). This difference in  $\beta$  values showed that the active steps including CO<sub>2</sub> strongly depend on the catalyst composition.

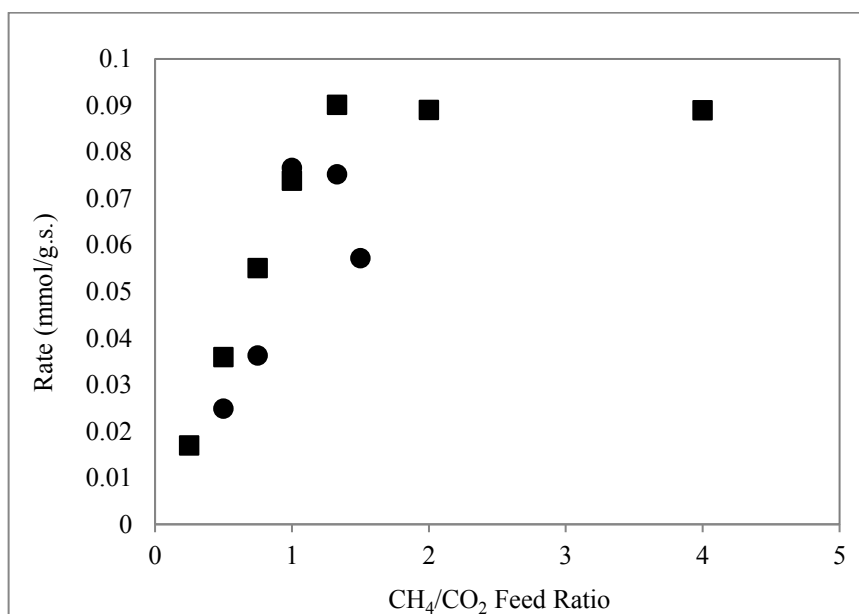


Figure 4.31. Variation of reaction rates according to feed ratio (●:5%Co-2%Ce/ZrO<sub>2</sub>; ■: 10%Co-2%Ce/ZrO<sub>2</sub>).

Table 4.7. Estimated reaction rate parameters.

Catalyst	Reaction Orders		k
	$\alpha$	$\beta$	
5%Co-2%Ce/ZrO <sub>2</sub>	1.63	0.29	9.0549 mmol.g <sup>-1</sup> .s <sup>-1</sup> .atm <sup>-1.92</sup>
10%Co-2%Ce/ZrO <sub>2</sub>	1.12	-0.12	0.9859 mmol.g <sup>-1</sup> .s <sup>-1</sup> .atm <sup>-1.00</sup>

#### 4.3.2. The Product Influence on CDRM Rate

The effect of products, CO and H<sub>2</sub>, on rate were investigated through conducting mixed feed experiments for which the partial pressure of one product in the feed stream was varied while keeping reactant partial pressures constant as 0.08 atm at 873 K.

Increasing CO content in the feed first caused an up-and-down (wavy) trend in intrinsic rates (Figure 4.32a) for both catalysts. However, the CO content for which this trend starts, and the amplitude of the changes differed depending on the Co/Ce ratio of the catalyst. For example, according to the results of the CO content range, 0-9%; 4% CO in the feed yielded the highest intrinsic rate, 0.0865 mmol/s.g-catalyst over 10%Co-2%Ce/ZrO<sub>2</sub>, while the lowest rate, 0.0165 mmol/s.g-catalyst, was measured over 5%Co-2%Ce/ZrO<sub>2</sub> for the same CO content. This can be seen as an indication of different reaction mechanisms and/or different rate determining steps for the catalysts, most probably due to disparate properties (i.e. dispersion, oxidation state of active sites) of their surface verified by XPS and HRTEM analyses (See Section 4.2).

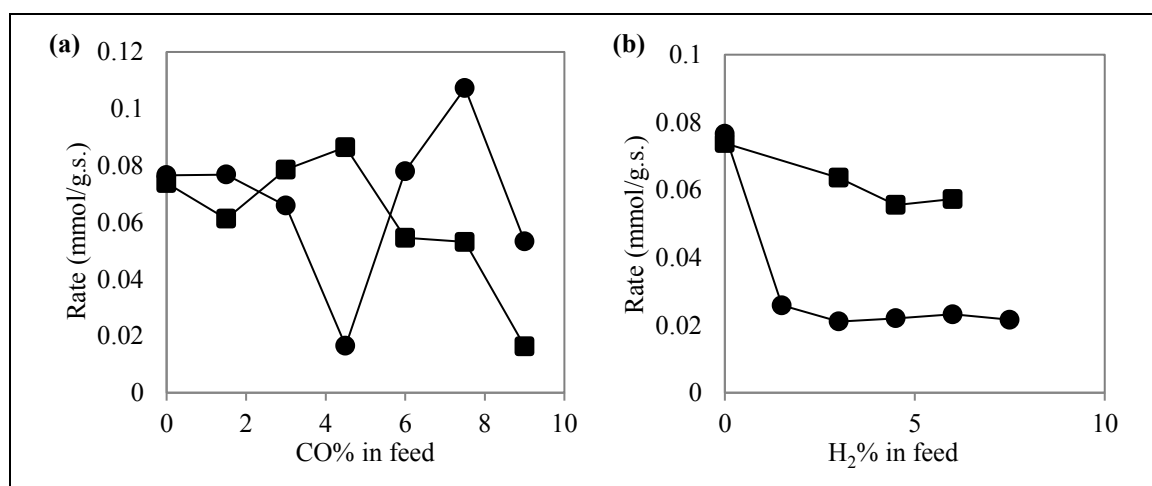


Figure 4.32. Variation of intrinsic rate according to (a) CO, and (b) H<sub>2</sub> content in the feed (●: 5%Co-2%Ce/ZrO<sub>2</sub>; ■: 10%Co-2%Ce/ZrO<sub>2</sub>).

In mixed feed runs, introducing H<sub>2</sub> to the feed, on the other hand, created an inhibitory effect on CDRM rate (Figure 4.32b). This might be explained by the presence of H<sub>2</sub> in the feed slowing down the mechanistic steps involving CH<sub>4</sub> or its constituents, which are catalyzed by Co sites, via adsorption competition. For Ni-based CDRM catalysts, it was proposed that Ni-H produced on catalysts reach equilibrium state with the product hydrogen formed in the reaction (Cui *et al.*, 2007; Ozkara-Aydinoğlu and Aksoylu, 2013), and therefore, the reaction steps involving the hydrogen species on the catalyst surface were the rapid or equilibrium steps. Same phenomenon might be valid for Co-H in this system. Since Co sites are found rather insufficient in quantity for 5%Co-2%Ce/ZrO<sub>2</sub>, this

effect was more severe (Figure 4.32b); the intrinsic rate decreased by 72% when 3% H<sub>2</sub> was introduced to the feed stream. The decrease in the activity was calculated as 14% for CDRM on 10%Co-2%Ce/ZrO<sub>2</sub> catalyst for the same H<sub>2</sub> level in the feed. Further H<sub>2</sub> addition created no significant effect on reaction rates (Figure 4.32b).

### 4.3.3. Surface Reaction Models

Expressing CDRM kinetics as a power-law model is simple for application but inadequate over a wide range of partial pressure data. Therefore, to understand the mechanistic nature of the reaction, the validity of possible Langmuir-Hinshelwood (LH) and Eley-Rideal (ER) type of reaction models, listed in Table 4.8, were also tested for each catalyst. Model 1 is based on ER type mechanism taking the reaction of adsorbed CO<sub>2</sub> with CH<sub>4</sub> in the gas phase as rate determining step (Mark *et al.*, 1997). In Model 2, which has been proposed for Ni and Co based catalysts, on the other hand, CO formation is considered as rate determining. This model is based on the stepwise mechanism, in which decomposition of methane to hydrogen and active carbon is followed by the conversion of this active carbon with CO<sub>2</sub> to 2 CO (Wang and Lu, 1999; Ayodele *et al.*, 2016). Model 3 is derived from the LH type mechanism with CH<sub>4</sub> dissociation as the rate determining step (Zhang and Verykios, 1994). In Model 4, it is assumed that both reactants are adsorbed and the rate determining step is the surface reaction between the adsorbed reactants to form products, H<sub>2</sub> and CO (Mark *et al.*, 1997). Model 5 is another LH type rate expression (Olsbye *et al.*, 1997). With the addition of the inhibiting effect of CO in the denominator to Model 1, Model 6 is formed. In another ER type model, Model 7, the reaction between CH<sub>x</sub> and CO<sub>2,g</sub> is considered as rate-limiting at low pressures of carbon dioxide (Mark *et al.*, 1997; Olsbye *et al.*, 1997). The inhibiting effect of both CO and CH<sub>4</sub> is considered in Model 8. Model 9 considers the inhibitory effect of H<sub>2</sub> by formulating an ER type mechanism with dissociation of CH<sub>4</sub> as the rate determining step (Pakhare *et al.*, 2014). Model 10, on the other hand, is derived as an appropriate dual site model for a Co-based catalyst (Ayodele *et al.*, 2016). The K<sub>i</sub> values in all models stand for the adsorption coefficients for each species. It should be noted that the first eight models were tested for Pt-Ni catalyst in our previous work (Ozkara-Aydinoğlu and Aksoylu, 2013) and Models 9 and 10 are additionally considered in the current work, as those models have been reported as the plausible mechanisms on Co-based catalysts involving H<sub>2</sub> effect on CDRM.

Table 4.8. Rate expressions tested in this study.

Model No.	Rate Equation	Reference
1	$-r_{CH_4} = \frac{kK_{CO_2}P_{CH_4}P_{CO_2}}{(1 + K_{CO_2}P_{CO_2})}$	Mark <i>et al.</i> , 1997
2	$r_{CH_4} = \frac{kP_{CH_4}P_{CO_2}}{(1 + K_1P_{CH_4})(1 + K_2P_{CO_2})}$	Wang and Lu, 1999; Ayodele <i>et al.</i> , 2016
3	$r_{CH_4} = \frac{aP_{CH_4}P_{CO_2}^2}{(P_{CO_2} + bP_{CO_2}^2 + cP_{CH_4})^2}$	Zhang and Verykios, 1994
4	$-r_{CH_4} = \frac{kK_{CO_2}K_{CH_4}P_{CH_4}P_{CO_2}}{(1 + K_{CO_2}P_{CO_2} + K_{CH_4}P_{CH_4})^2}$	Mark <i>et al.</i> , 1997
5	$-r_{CH_4} = \frac{kP_{CH_4}P_{CO_2}}{(1 + K_1P_{CH_4} + K_2P_{CO_2})(1 + K_3P_{CO_2})}$	Olsbye <i>et al.</i> , 1997
6	$-r_{CH_4} = \frac{kK_{CO_2}P_{CH_4}P_{CO_2}}{(1 + K_{CO_2}P_{CO_2} + K_{CO}P_{CO})}$	<i>Derived from Model 1</i>
7	$-r_{CH_4} = \frac{kK_{CH_4}P_{CH_4}P_{CO_2}^m}{(1 + K_{CH_4}P_{CH_4})}$	Mark <i>et al.</i> , 1997; Olsbye <i>et al.</i> , 1997
8	$-r_{CH_4} = \frac{kP_{CH_4}^m P_{CO_2}^n}{(1 + K_{CO_2}P_{CO_2} + K_{CO}P_{CO} + K_{CH_4}P_{CH_4})}$	Inhibitory effect of CO and CH <sub>4</sub> included
9	$r_{CH_4} = \frac{kK_{CH_4}P_{CH_4}}{\left(1 + K_{CH_4}P_{CH_4} + \frac{P_{CO}^2}{K_{CO_2}P_{CO_2}} + \frac{\sqrt{P_{H_2}}}{\sqrt[4]{K_{H_2}}}\right)^2}$	Pakhare <i>et al.</i> , 2014
10	$r_{CH_4} = \frac{kP_{CO_2}\sqrt{P_{CH_4}}}{(1 + \sqrt{(K_{CH_4}P_{CH_4})})(1 + K_{CO_2}P_{CO_2})}$	Ayodele <i>et al.</i> , 2016

The experimental CH<sub>4</sub> consumption rate data for both catalysts were fitted to the listed models and the validity of them was determined through nonlinear regression analysis by utilizing Levenberg-Marquardt algorithm provided in the POLYMATH 5.1 software. Variance value and physical meaningfulness of the constants were considered as the basis in model discrimination. In this context, models with poor correlation coefficients, negative parameter values or 95% confidence interval greater than the parameter itself were excluded. The effect of Co/Ce ratio in the CDRM mechanism was also investigated through comparative analysis of the models found plausible, and the calculated parameters in model discrimination analysis.

Model 1 was found appropriate for the CDRM kinetics on both catalysts (Table 4.9 and 4.10). For 5%Co-2%Ce/ZrO<sub>2</sub> catalyst, this model gave the lowest squared error meaning that CH<sub>4</sub> is weakly adsorbed and the surface coverage of methane is relatively low for this sample at the pressures studied. When the parameters estimated for both catalysts were compared, it was noticed that the k values are similar. However, K<sub>CO<sub>2</sub></sub> was calculated to be much higher for 10%Co-2%Ce sample, suggesting CO<sub>2</sub> adsorption on that sample is stronger. This might result from the higher surface oxygen defects of zirconia observed on this sample via O1s spectra of XPS analysis (See Section 4.2), since CO<sub>2</sub> dissociation is promoted at support defect sites (Bradford and Vannice, 1999).

Table 4.9. Model parameters obtained for 5%Co-2%Ce/ZrO<sub>2</sub> catalyst.

Model No.	Rate Parameters	$\sigma^2$ (mmol.g <sup>-1</sup> .s <sup>-1</sup> ) <sup>2</sup>
1	k=0.937 mmol.g <sup>-1</sup> .s <sup>-1</sup> .atm <sup>-1</sup> K <sub>CO<sub>2</sub></sub> =101.9 atm <sup>-1</sup>	1.711 × 10 <sup>-4</sup>
3	a=133.1 mmol.g <sup>-1</sup> .s <sup>-1</sup> .atm <sup>-3</sup> b=101.9 atm <sup>-2</sup> c=4.369 atm <sup>-1</sup>	5.092 × 10 <sup>-4</sup>
9	k=0.982 mmol.g <sup>-1</sup> .s <sup>-1</sup> .atm <sup>-1</sup> K <sub>CH<sub>4</sub></sub> =0.979 atm <sup>-1</sup> K <sub>CO<sub>2</sub></sub> =1009.9 atm <sup>-1</sup> K <sub>H<sub>2</sub></sub> =0.0017 atm <sup>-1</sup>	4.725 × 10 <sup>-4</sup>
10	k=7.846 mmol.g <sup>-1</sup> .s <sup>-1</sup> .atm <sup>-1</sup> K <sub>CH<sub>4</sub></sub> =1.908 atm <sup>-1</sup> K <sub>CO<sub>2</sub></sub> =11.099 atm <sup>-1</sup>	8.778 × 10 <sup>-4</sup>

The other common model for both catalysts was determined as Model 3. For both catalysts, the adsorption parameters related to CO<sub>2</sub> are higher than those related to CH<sub>4</sub>, indicating strong adsorption of CO<sub>2</sub>. Comparing the CO<sub>2</sub> adsorption parameters obtained for both catalysts pointed out that CO<sub>2</sub> utilization is higher on 5%Co-2%Ce/ZrO<sub>2</sub>. This might be explained by the higher Ce<sup>3+</sup> concentration on this catalyst (See Section 4.2) yielding enhanced oxygen mobility, as it was stated that CO<sub>2</sub> dissociation depends on the quantity and mobility of oxygen present in the surface (Melchionna and Fornasiero, 2014;

Bobrova *et al.*, 2016). It should be stated that this model gave the least squared error among the other tested models for 10%Co-2%Ce/ZrO<sub>2</sub>. Therefore, it can be concluded that the parameters obtained for this model are more plausible in explaining CDRM behavior of this catalyst.

Table 4.10. Model parameters obtained for 10%Co-2%Ce/ZrO<sub>2</sub> catalyst.

Model No.	Rate Parameters	$\sigma^2$ (mmol.g <sup>-1</sup> .s <sup>-1</sup> ) <sup>2</sup>
1	k=0.972 mmol.g <sup>-1</sup> .s <sup>-1</sup> .atm <sup>-1</sup> K <sub>CO2</sub> =101000 atm <sup>-1</sup>	8.99 × 10 <sup>-5</sup>
3	a=2.047 mmol.g <sup>-1</sup> .s <sup>-1</sup> .atm <sup>-3</sup> b=5.286 atm <sup>-2</sup> c=0.062 atm <sup>-1</sup>	1.758 × 10 <sup>-5</sup>
6	k=1.072 mmol.g <sup>-1</sup> .s <sup>-1</sup> .atm <sup>-1</sup> K <sub>CO2</sub> =1010.9 atm <sup>-1</sup> K <sub>CO</sub> =765.55 atm <sup>-1</sup>	2.3 × 10 <sup>-4</sup>
8	k=110.51 mmol.g <sup>-1</sup> .s <sup>-1</sup> .atm <sup>-2</sup> m=1.0114 n=0.8496 K <sub>CH4</sub> =57.899 atm <sup>-1</sup> K <sub>CO2</sub> =73.859 atm <sup>-1</sup> K <sub>CO</sub> =101.99 atm <sup>-1</sup>	8.203 × 10 <sup>-4</sup>
9	k=23.188 mmol.g <sup>-1</sup> .s <sup>-1</sup> .atm <sup>-1</sup> K <sub>CH4</sub> =0.0446 atm <sup>-1</sup> K <sub>CO2</sub> =0.2009 atm <sup>-1</sup> K <sub>H2</sub> =10.149 atm <sup>-1</sup>	1.62 × 10 <sup>-4</sup>

Model 9 also fitted to the results obtained from the experiments conducted over both catalysts. The adsorption coefficient for H<sub>2</sub> is higher for 10%Co-2%Ce/ZrO<sub>2</sub> than that for 5%Co-2%Ce/ZrO<sub>2</sub>. This result and the previously mentioned more pronounced inhibitory effect of H<sub>2</sub> on 5%Co-2%Ce/ZrO<sub>2</sub> hints that though H<sub>2</sub> adsorption on 10%Co-2%Ce/ZrO<sub>2</sub> is higher than that on 5%Co-2%Ce/ZrO<sub>2</sub>, the ratio of H<sub>2</sub> adsorption coefficients for the catalysts ( $K^{10\text{Co}2\text{Ce}}_{\text{H}_2}/K^{5\text{Co}2\text{Ce}}_{\text{H}_2}$ ) is lower than the corresponding ratio of surface Co active

in methane activation steps,  $[\text{Co}]^{10\text{Co}2\text{Ce}}/[\text{Co}]^{5\text{Co}2\text{Ce}}$ . On the other hand, for 5%Co-2%Ce/ZrO<sub>2</sub> catalyst, noticeable effect of adsorption coefficient related to CO<sub>2</sub> on this mechanism was clearly observed, highlighting that higher Ce<sup>3+</sup> enhances oxygen mobility, and therefore CO<sub>2</sub> dissociation. It should also be noted that the comparative analysis between the adsorption parameters for CO<sub>2</sub> and CH<sub>4</sub>, and the adsorption parameters for CO<sub>2</sub> for both catalysts follow the similar trends as observed in Model 3.

For 5%Co-2%Ce/ZrO<sub>2</sub> catalyst, suitable parameters were also attained when Model 10 was applied. The results supported that CO<sub>2</sub> utilization is more pronounced than that of CH<sub>4</sub> for CDRM over this catalyst.

In addition to Model 1, 3 and 9, the parameters obtained from Models 6 and 8 were also appropriate for representing possible mechanisms for CDRM over 10%Co-2%Ce/ZrO<sub>2</sub>. It was interesting to notice that in Model 6, CO<sub>2</sub> adsorption is found to be stronger than that of CO, whereas in Model 8 the opposite is claimed. This might result from introducing CH<sub>4</sub> in denominator for its inhibiting effect. Additionally, in Model 8, the order of CH<sub>4</sub> was estimated to be higher than that of CO<sub>2</sub> like in power-law type rate expression. The orders of K values, K<sub>CH<sub>4</sub></sub> being lower than K<sub>CO<sub>2</sub></sub>, in this model also confirmed that CO<sub>2</sub> is more strongly adsorbed than CH<sub>4</sub> on the surface.

Consequently, the comparative analysis of meaningful surface reaction models for the catalysts and their optimized model parameters revealed that both Co/Ce ratio and support structure have severe effects on CDRM activity. The difference in parameter values of common models explaining CDRM mechanism over the catalysts may stem from the relative changes in the roles of their active sites.

#### 4.4. FTIR-DRIFT Studies over Co-Ce/ZrO<sub>2</sub> Catalysts

In order to obtain more information on the surface characteristics of each catalyst and to validate the plausible CDRM reaction pathway(s), FTIR-DRIFT studies were conducted.

#### 4.4.1. The Effect of Pretreatment on Catalyst Surface Characterization

Changes on the catalyst surface due to moisture uptake during the transfer of reduced sample to DRIFT cell prior to measurements may lead to erroneous results in FTIR-DRIFT analysis. In order to overcome this problem, *in situ* pretreatments aiming to reactivate/re-reduce the sample placed in DRIFT cell are needed. In the first part of this subchapter, the effect of 4 pretreatments, which were conducted *in situ* on 5%Co-2%Ce/ZrO<sub>2</sub>, on the catalyst surface was determined. The details of the pretreatment procedures are given in Experimental part (Chapter 3). In summary, the first pretreatment included heating up to 393 K under 45 mL/min He flow, then waiting for 20 minutes at this temperature so the catalyst can release the moisture on its surface. The second pretreatment differs from the first that the sample was heated up 573 K, and the waiting period was extended to 1 hour. In the 3<sup>rd</sup> pretreatment, following the He treatment, the catalyst was re-reduced *in situ* under 45 mL/min H<sub>2</sub> flow of at 573 K for 1 hour. In pretreatment 4, following re-reduction at 573 K, the temperature was risen to 593 K under He flow and waited for 1 h at this temperature aiming to flush the groups formed as a result of the re-reduction. After all pretreatments, the temperature of the system was decreased down to room temperature under He flow, then adsorption under the flow of 1% CO and balance He was applied for 30 minutes. This was followed by He flush for 30 minutes and the spectra at this stage were taken.

All spectra obtained following the He flush of CO adsorbed samples, which were pretreated through above mentioned pretreatments, were analyzed in detail (Figure 4.33). The comparative analysis shows that the peaks are observed at similar wavelengths indicating neither of the pretreatments have a significant impact on catalyst structure, and all of them are applicable for moisture removal.

It was stated that probe CO molecules can accept electron density from surface metal sites, resulting in metal-carbonyl complexes, which are characterized by IR absorption bands of CO at 2200-1800 cm<sup>-1</sup> (Morales *et al.*, 2007; Bachiller-Baeza *et al.*, 2013). At this interval, the peaks at 2115 and 2185 cm<sup>-1</sup>, which are seen at all spectra (Figure 4.33), corresponds to gas phase CO and adsorbed CO, respectively (Garcia-Diequez *et al.*, 2010; Ni *et al.*, 2012). The other common peaks at 1825, 1865, 1945, 1990 and 2015 cm<sup>-1</sup> can be

assigned to adsorbed CO on the sites of reduced Co samples (Jiang *et al.*, 2001), stretching vibrations of CO linearly bonded to the surface cobalt metal sites (Morales *et al.*, 2007) or bidentate bridging CO types (Ni *et al.*, 2012).

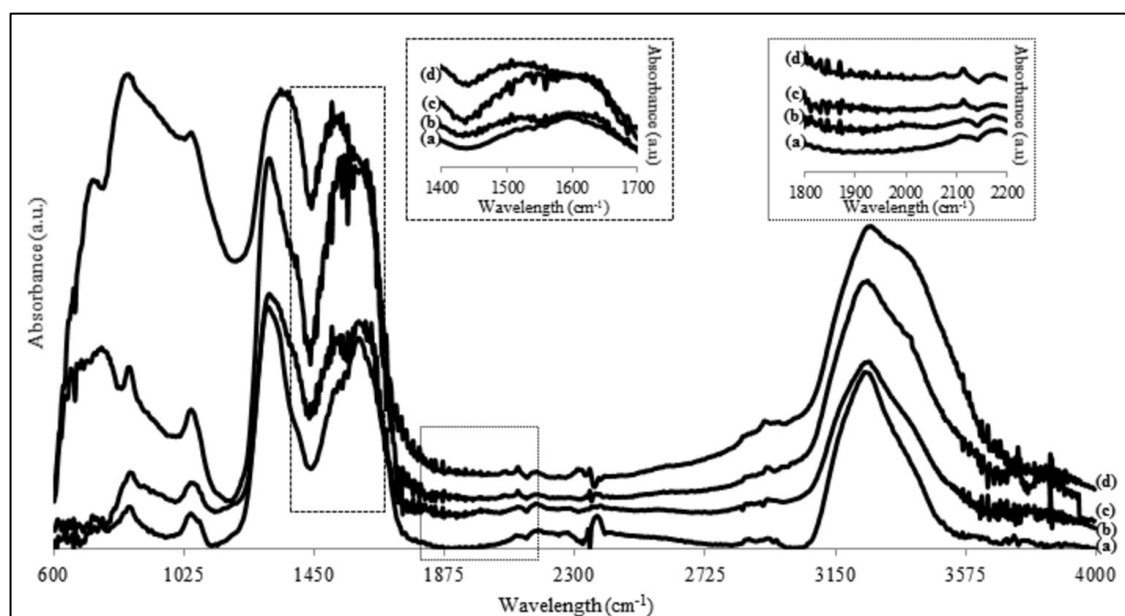


Figure 4.33. FTIR-DRIFT spectra upon He flush for 1% CO adsorption at room temperature for 5%Co-2%Ce/ZrO<sub>2</sub> catalyst with (a) pretreatment 1, (b) pretreatment 2, (c) pretreatment 3, and (d) pretreatment 4 (insets are the detailed views of the selected parts).

Adsorbed CO<sub>2</sub> indicated by the peak at 2328 cm<sup>-1</sup> was observed at each spectra (Ni *et al.*, 2012). Additionally, the peaks belonging to gas phase CO<sub>2</sub> at the band interval of 2310-2380 cm<sup>-1</sup> and rotation-vibration P and R bands of gas phase CO<sub>2</sub> at 2340 and 2360 cm<sup>-1</sup> are also common (Yung *et al.*, 2008; Bouarab *et al.*, 2004).

The peaks in the 1200-1600 cm<sup>-1</sup> band were ascribed to carbonates that might arise from the reduction of cobalt with CO (Pietrogiacomini *et al.*, 2000). It was noted that these peaks are common after 1% CO adsorption at each pretreatment. The peaks that are characteristic of unidentate carbonate at 1050, 1310 and 1512 cm<sup>-1</sup> were also recorded at each spectra (Grillo *et al.*, 2004; Khassin *et al.*, 2001).

Despite pretreatment, formate groups, identified at 1593 cm<sup>-1</sup>, were obtained at the spectra belonging to CO adsorption (Garcia-Dieguez *et al.*, 2010) after all tested

pretreatments. The peaks at 1554, 2890 and 2943  $\text{cm}^{-1}$  can also be ascribed to formate species (Ma *et al.*, 2005).

Another common peak at 3250  $\text{cm}^{-1}$  was ascribed to hydroxyl groups (Frank *et al.*, 2007). Since the magnitude and place of the peak did not change with the change in pretreatment, it was suggested that OH-groups are seen as a side product of CO adsorption, rather than as a result of any possible oxidation due to moisture uptake.

From the analysis of pretreatment method effect on catalyst structure, it was concluded that CO adsorption capacity is independent of the pretreatment method for Co-Ce/ZrO<sub>2</sub> catalysts.

#### 4.4.2. Surface Interaction of Each Species at Co-Ce/ZrO<sub>2</sub> System

A comparative analysis of the spectra obtained upon 1% CO adsorption at room temperature was applied on 5%Co-2%Ce/ZrO<sub>2</sub>, 5%Co/ZrO<sub>2</sub>, 2%Ce/ZrO<sub>2</sub> and ZrO<sub>2</sub> to display the differences in CO interactions with each component of Co-Ce/ZrO<sub>2</sub> catalyst.

Figure 4.34 includes the spectra obtained both just after CO adsorption and upon He flush treatment applied to CO adsorbed samples. On all samples, CO adsorption at room temperature yielded bands of CO<sub>(g)</sub> (2116 and 2172  $\text{cm}^{-1}$ ), CO<sub>2(g)</sub> (2345 and 2353  $\text{cm}^{-1}$ ), OH groups (3247  $\text{cm}^{-1}$ ) and some carbonate and formate groups (1040, 1050, 1360 and 1625  $\text{cm}^{-1}$ ) (Garcia-Dieguez *et al.*, 2010; Bourab *et al.*, 2004; Frank *et al.*, 2007; Khassin *et al.*, 2001). It should be noted that the intensity of all peaks decreased after He flush.

The higher intensities of CO<sub>(g)</sub> band at 2116 and 2172  $\text{cm}^{-1}$  observed in CO adsorption spectra and the significant decrease in intensities of those bands upon He flush for all samples indicate there is a weak interaction between CO and the possible sites of the Co-Ce/ZrO<sub>2</sub> system at room temperature; this result also hints that CO adsorption properties of the Co-Ce system should also be checked at elevated temperatures in order to see whether the steps involving (strongly) adsorbed CO in the CDRM reaction mechanism are not the rate determining steps but the rapid ones.

From the comparative analysis of the peaks obtained after CO adsorption for different catalyst samples, it was observed that the peaks corresponding to formate groups at 2960 and 2928  $\text{cm}^{-1}$  are more intense for 2%Ce/ZrO<sub>2</sub> sample. This might highlight the strong interaction of Ce with O-related groups. Additionally, the possibility that Ce might play a role in formate-groups included side-steps of CDRM mechanism should be considered.

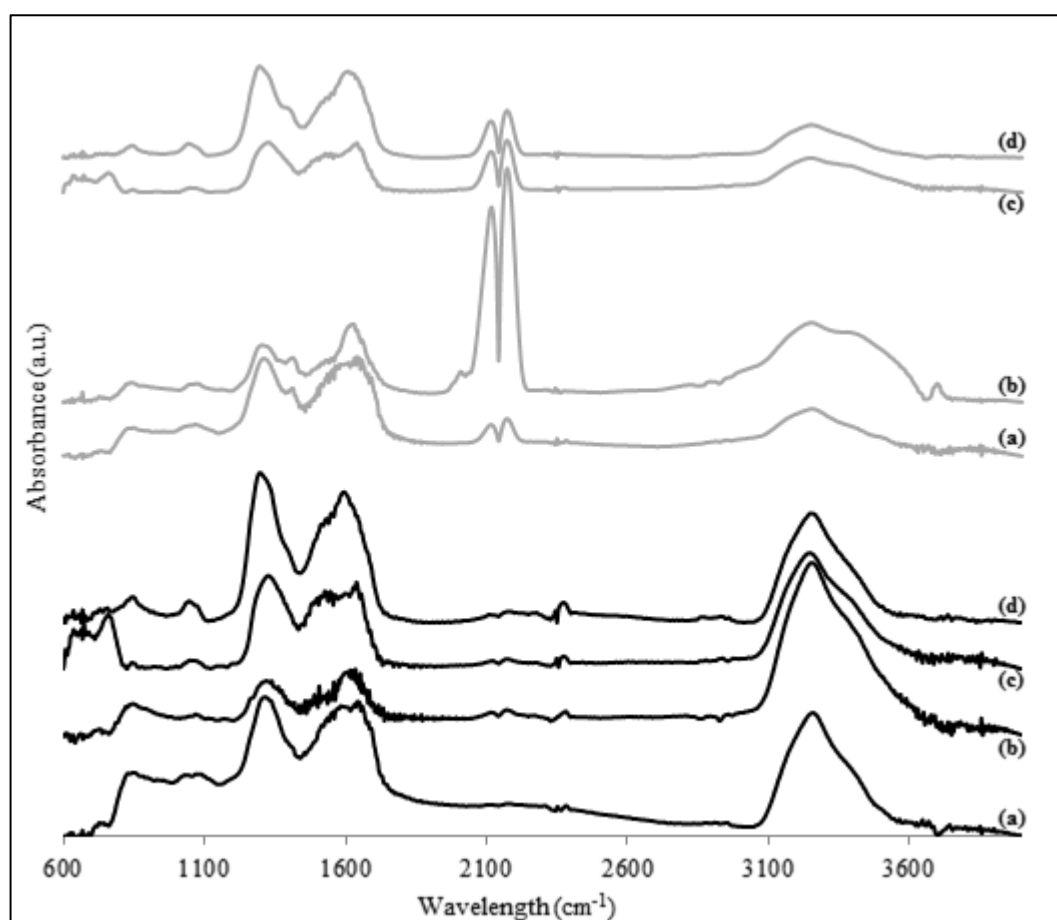


Figure 4.34. FTIR-DRIFT spectra obtained from 1% CO adsorption at room temperature for (a) ZrO<sub>2</sub>, (b) 2%Ce/ZrO<sub>2</sub>, (c) 5%Co/ZrO<sub>2</sub> and (d) 5%Co-2%Ce/ZrO<sub>2</sub> just after CO adsorption (grey spectra), and upon after He flush (black spectra).

Another outcome is that the peak at 1417  $\text{cm}^{-1}$  corresponding to unidentate carbonate is present at the spectra for all tested samples, except 5%Co/ZrO<sub>2</sub>; hinting that Co introduction to catalyst composition might suppress formation of some carbonate species

(Grillo *et al.*, 2004). The weakness of the interaction between these species and the catalyst samples was confirmed with diminishing of this peak after He flush treatment.

After He flush, the bidentate bridging CO peaks at 1850, 1870 and 1978  $\text{cm}^{-1}$  becomes more pronounced on 2%Ce/ZrO<sub>2</sub> sample (Ni *et al.*, 2012). Thus, it might be concluded that Ce-CO interaction is stronger than those between CO and the other components in Co-Ce/ZrO<sub>2</sub> system.

#### 4.4.3. CO Adsorption on Co-Ce/ZrO<sub>2</sub> Catalyst System

In order to investigate the changes occurred in the catalyst surface structure and the adsorption properties of the sites formed in response to the change in Co/Ce loading ratio, 1% CO adsorption at room temperature was conducted on 5%Co-2%Ce/ZrO<sub>2</sub>, 5%Co-3%Ce/ZrO<sub>2</sub>, 10%Co-2%Ce/ZrO<sub>2</sub> and 10%Co-3Ce%/ZrO<sub>2</sub> catalysts.

The peaks attributed to gas phase CO (Yung *et al.*, 2008) or adsorbed CO on metal or support sites, at 2115 and 2170  $\text{cm}^{-1}$ , were observed at the spectra for both just after CO adsorption and upon He flush treatment applied to CO adsorbed samples as given in Figure 4.35 (Westerman *et al.*, 2012; Khassin *et al.*, 2001). The peak at 2170  $\text{cm}^{-1}$  was also reported as CO adsorbed on Ce<sup>4+</sup> (Pozdnyakova *et al.*, 2006). The presence of bridge-bonded CO adsorbed on Co metallic sites was verified with the peaks observed at 1920 and 1935  $\text{cm}^{-1}$  (Bachiller-Baeza *et al.*, 20013; Song and Li, 2006). Linear-bonded CO was observed at 2020  $\text{cm}^{-1}$  for all catalysts (Morales *et al.*, 2007). It was interesting to note that the intensity of the peaks at 1800-2200  $\text{cm}^{-1}$  region, attributed to adsorbed CO, showed a sharper decrease after He flush for the catalysts with 10% Co loading, pointing out that CO adsorption is weaker for these catalysts.

For all tested catalysts, 1% CO adsorption at room temperature yielded peaks at 1060, 1305 and 1621  $\text{cm}^{-1}$  in 1000-1700  $\text{cm}^{-1}$  band, which is reported as OCO asymmetric and symmetric stretching vibrations region (Jacobs *et al.*, 2003). Those peaks are attributed to carbonate species (Yung *et al.*, 2008; Ma *et al.*, 2004). The peak at 1303  $\text{cm}^{-1}$  can specifically be noted as ion carbonate on m-ZrO<sub>2</sub> (Ma *et al.*, 2005). It should also be noted that the peak at 1401  $\text{cm}^{-1}$ , which corresponds to unidentate carbonate (Grillo *et al.*, 2004),

was only present at the spectra of 5%Co-2%Ce/ZrO<sub>2</sub>. However, this peak disappears after He flush treatment indicating weak interaction. For the other catalysts, on the other hand, the presence of unidentate carbonate species at 1521 cm<sup>-1</sup> (Khassin *et al.*, 2001) after CO adsorption was verified. It should also be noted that for the catalysts having same Co loading, this peak is more pronounced for the ones with higher Ce loading, hinting a relation between unidentate carbonate formation and ceria loading.

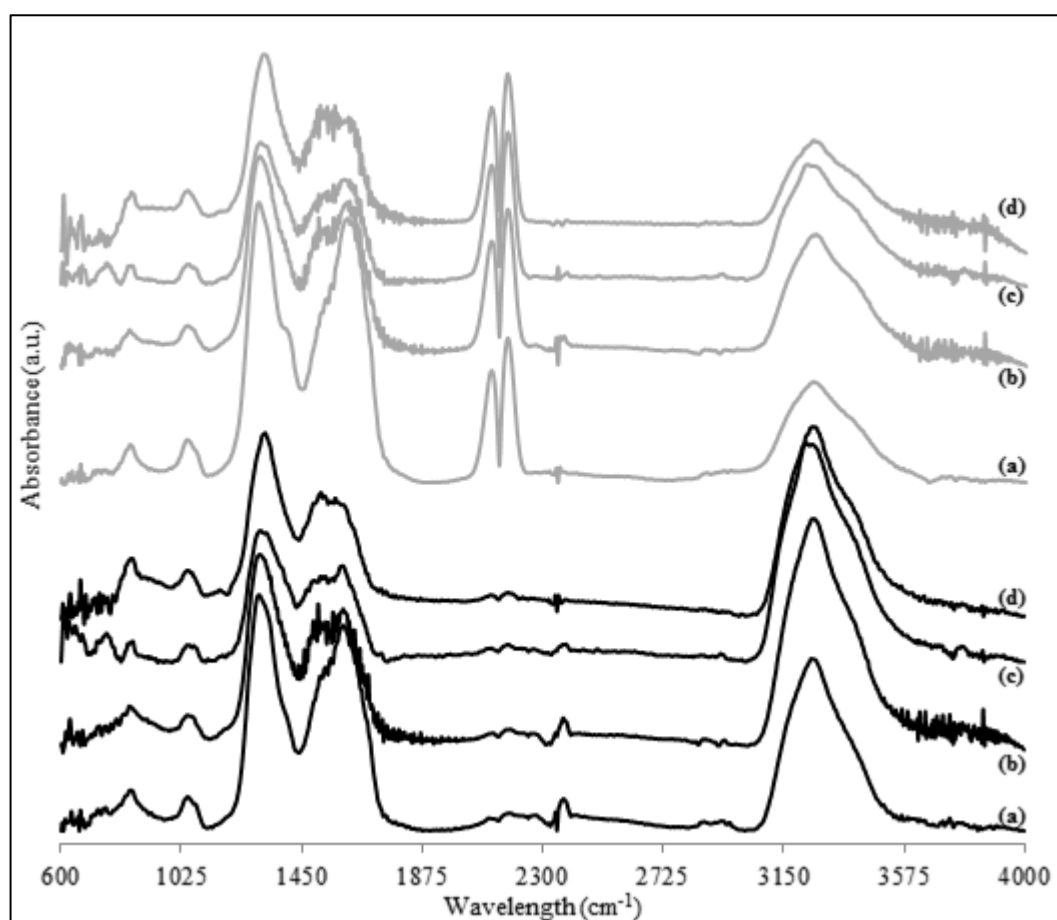


Figure 4.35. FTIR-DRIFT spectra from 1% CO adsorption at room temperature for (a) 5%Co-2%Ce/ZrO<sub>2</sub>, (b) 5%Co-3%Ce/ZrO<sub>2</sub>, (c) 10%Co-2%Ce/ZrO<sub>2</sub>, and (d) 10%Co-3%Ce/ZrO<sub>2</sub> just after CO adsorption (grey spectra), and upon He flush (black spectra).

The spectra for the tests performed both just after CO adsorption and upon He flush treatment applied to CO adsorbed samples included peaks at 2870, 2950 and 3250 cm<sup>-1</sup>, where the latter corresponds to OH groups and the others to formates (Frank *et al.*, 2007; Dulaurent and Bianchi, 2001). It is interesting to note that the intensity of the peak

attributed to OH groups increase upon He flush on all catalysts, which may reflect possible CO-catalyst surface interaction yielding OH-involving species.

The results obtained also showed that CO adsorption yielded peaks corresponding to gas phase (at 2343 and 2356  $\text{cm}^{-1}$ ) and adsorbed  $\text{CO}_2$  (at 2321 and 2333  $\text{cm}^{-1}$ ) (Solymosi *et al.*, 2005; Yung *et al.*, 2008; Das and Deo, 2012). It should be noted that the  $\text{CO}_{2(\text{g})}$  peak at 2343  $\text{cm}^{-1}$  shifted to 2350  $\text{cm}^{-1}$  for 10%Co-2%Ce/ $\text{ZrO}_2$ , and the peak intensities were low for 10%Co-3%Ce/ $\text{ZrO}_2$ . All peaks retained upon He flush for the catalysts with 5% Co loading revealing strong adsorption of  $\text{CO}_2$ , which was formed through CO-catalyst interaction. On the other hand, some peaks corresponding to adsorbed  $\text{CO}_2$  diminished after He flush for the catalysts having 10% Co loading, indicating  $\text{CO}_2$ -catalyst interaction weakens with the increase in Co loading.

#### 4.4.4. $\text{ZrO}_2$ - $\text{CO}_2$ Interaction

In CDRM,  $\text{CO}_2$  activation yielding surface oxygen is generally reported as the role of the supports. Therefore, understanding the  $\text{CO}_2$ -support relation in the reaction network has become the utmost importance for rational catalyst development (Kouva *et al.*, 2014). Accordingly, the details of  $\text{CO}_2$  dissociation mechanism on  $\text{ZrO}_2$  were analyzed in the current study via FTIR-DRIFT. It should be noted that the FTIR-DRIFT spectra obtained upon  $\text{CO}_2$  adsorption give information about direct  $\text{CO}_2$ - $\text{ZrO}_2$  interaction, whereas, as the spectra obtained upon He flush of the pre- $\text{CO}_2$ -adsorbed surface only shows stable adsorption, it is mostly important for stably adsorbed species and, consequently, reaction kinetics.

Figure 4.36 displays the FTIR-DRIFT spectra obtained from samples for which pre- $\text{CO}_2$  adsorption was made under the flow of 10%  $\text{CO}_2$  at different temperatures followed by He flush. In all cases, more clearly at 573 K, there were peaks corresponding to adsorbed CO (1800-2100  $\text{cm}^{-1}$ ), which is the product of  $\text{CO}_2$  dissociation reaction (Ni *et al.*, 2012). As a general trend, the similar peaks were observed in  $\text{CO}_2$  adsorption tests performed under room temperature and at 373 K, but at 573 K the adsorption profile gets more intense. In all analyses, peaks corresponding to gas phase  $\text{CO}_2$  (2378, 2360 and 2340  $\text{cm}^{-1}$ ), surface terminal and bridging OH of monoclinic  $\text{ZrO}_2$  (3770  $\text{cm}^{-1}$ ) and hydroxyl

group ( $3200\text{ cm}^{-1}$ ) were present (Bourab *et al.*, 2004; Bachiller-Baeza *et al.*, 2013; Pietrogiacomini *et al.*, 2000 and Frank *et al.*, 2007). At 573 K, a peak attributed to either gas phase or adsorbed  $\text{CO}_2$  was also noted (Garcia-Dieguez *et al.*, 2010 and Ni *et al.* 2012). Additionally, formation of bidentate formate ( $2894$  and  $2945\text{ cm}^{-1}$ ) was observed after the adsorption at 573 K (Yung *et al.*, 2008). Formation of different surface groups can be considered as a strong confirmation of  $\text{CO}_2\text{-ZrO}_2$  interaction.

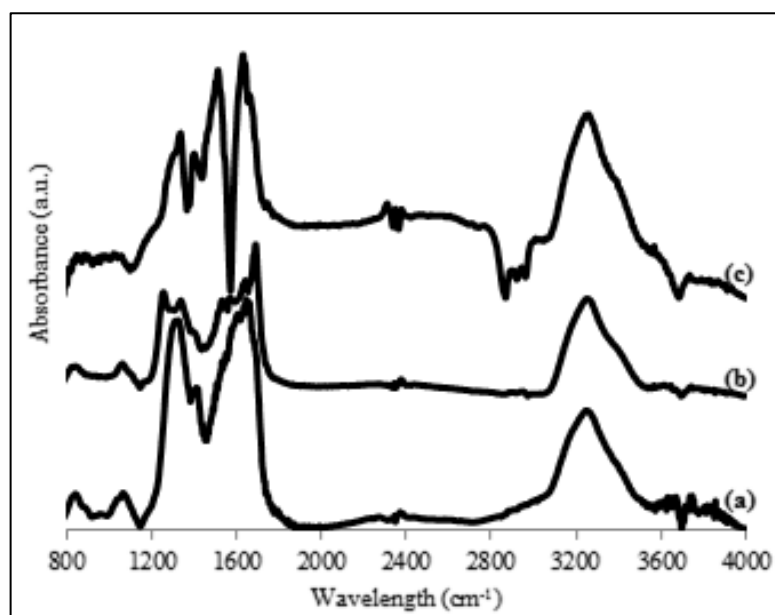


Figure 4.36. FTIR-DRIFT spectra after He flush of 10%  $\text{CO}_2$  adsorption at (a) room temperature, (b) 373 K, and (c) 573 K.

It was interesting to notice that peaks attributed to asymmetric O-C-O bands ( $1463$ ,  $1510$  and  $1631\text{ cm}^{-1}$ ) were detected more intensely at the spectra obtained at 573 K, whereas at room temperature and 373 K, symmetric O-C-O bands ( $1325$ ,  $1394$  and  $1416\text{ cm}^{-1}$ ) were dominant (Pietrogiacomini *et al.*, 2000; Khassin *et al.*, 2001). Moreover, adsorbed bicarbonate species ( $1640\text{ cm}^{-1}$ ) are seen at the spectra after He flush following adsorption at 573 K pointing out that adsorption temperature changes the structure of formed surface groups (Ni *et al.*, 2012). These can all be attributed to the temperature effect on  $\text{ZrO}_2\text{-CO}_2$  interaction.

In order to have a deeper insight on  $\text{CO}_2$  dissociation mechanism on  $\text{ZrO}_2$ , FTIR-DRIFT spectra after  $\text{CO}_2$  adsorption at different temperatures were discussed in the

wavelength range for CO band, 1800-2100  $\text{cm}^{-1}$  (Figure 4.37). At all temperatures, linear adsorption of CO was confirmed with the peak at 2077  $\text{cm}^{-1}$  (Bachiller-Baeza *et al.*, 2013). The peaks attributed to bridge-bonded CO (1991, 1966, 1943, 1920 and 1866  $\text{cm}^{-1}$ ) were, on the other hand, more pronounced at 573 K, than at other temperatures (Song and Li, 2006; Qian *et al.* 2014). Therefore, it can be said that the crystal structure of  $\text{ZrO}_2$  surface becomes more prone to interaction with  $\text{CO}_2$  as the temperature increases. Additionally, for all cases, it was observed that the intensity of CO band peaks decrease after He flush, showing that formed CO is not fully adsorbed at tested temperatures. For CDRM, this information is crucial as it can be considered as a fact that  $\text{CO}_2$  dissociation reaction is not a rate determining step for the tested temperatures.

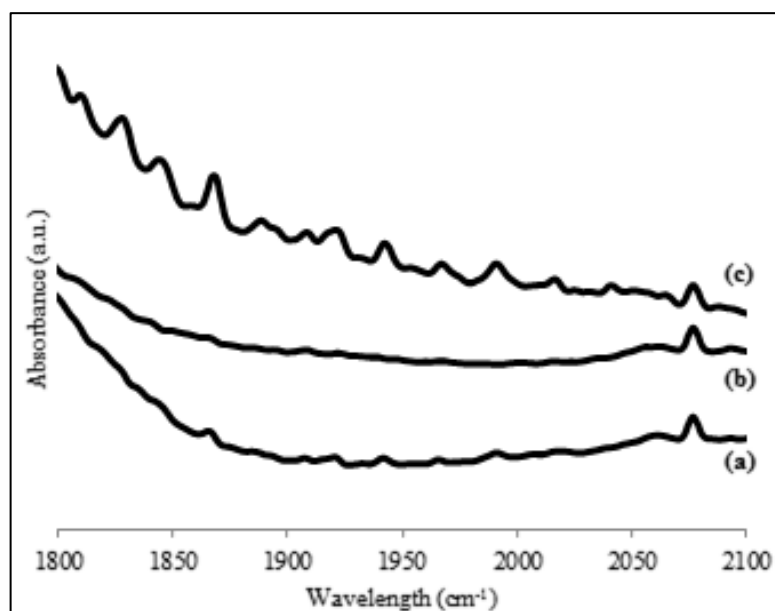


Figure 4.37. FTIR-DRIFT spectra obtained from just after 10%  $\text{CO}_2$  adsorption at (a) room temperature, (b) 373 K, and (c) 573 K.

To observe the effect of  $\text{CO}_2$  concentration on  $\text{ZrO}_2$ - $\text{CO}_2$  interaction, adsorption under 40%  $\text{CO}_2$  flow on  $\text{ZrO}_2$  was conducted at 573 K. Figure 4.38 shows the FTIR-DRIFT spectra obtained both just after  $\text{CO}_2$  adsorption and upon He flush treatment applied to pre- $\text{CO}_2$  adsorbed samples. For the case after He flush, it was important to observe that the spectra belonging to both  $\text{CO}_2$  concentrations gave the same trend. A peak at 1465  $\text{cm}^{-1}$ , corresponding to monodentate carbonate on m- $\text{ZrO}_2$ , became apparent at the test with 40%  $\text{CO}_2$  concentration; whereas different formate species peak (1390  $\text{cm}^{-1}$ ) was

detected for the test at 10% CO<sub>2</sub> concentration (Ma *et al.*, 2005; Jacobs *et al.*, 2004). Consequently, the results indicate that the formation rates of different surface groups resulting from ZrO<sub>2</sub>-CO<sub>2</sub> interaction are dependent on CO<sub>2</sub> concentration of the adsorption gas stream. The spectra at CO band range also revealed that adsorbed CO species are stronger for the test when 40% CO<sub>2</sub> was used for adsorption. It was also noted that the difference in CO band in response to change in gas phase CO<sub>2</sub> concentration was not valid for the case after He flush indicating weak/reversible adsorption. Consequently, those findings may be considered as a clue that CO<sub>2</sub> concentration changes selectivity in CDRM, as the selectivity is given in terms of H<sub>2</sub>/CO ratio, and that CO<sub>2</sub> dissociation reaction on ZrO<sub>2</sub> surface is fast.

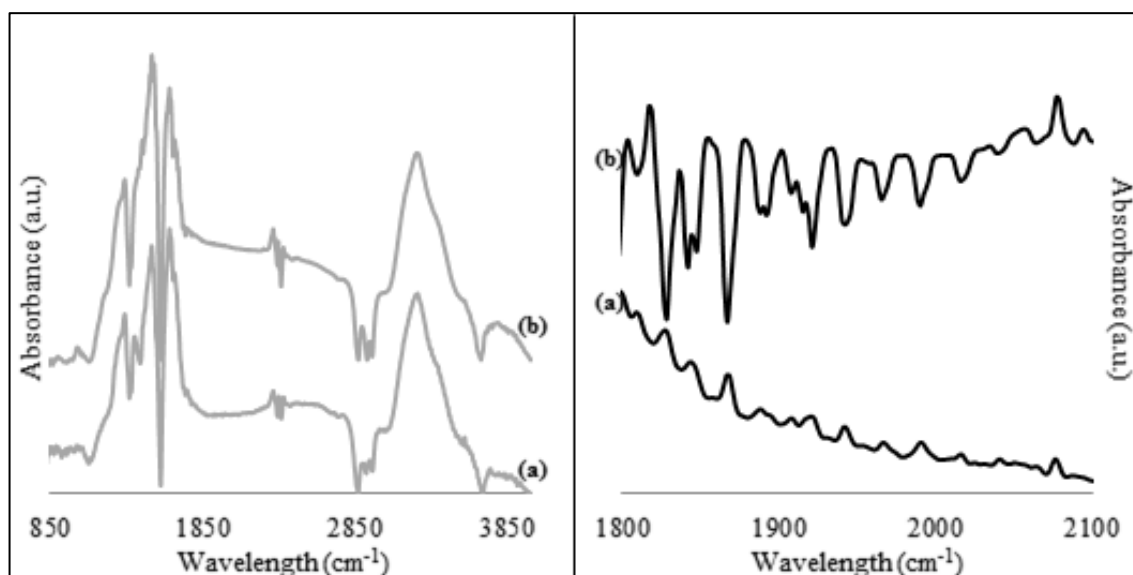


Figure 4.38. FTIR-DRIFT spectra obtained from CO<sub>2</sub> adsorption at 573 K over ZrO<sub>2</sub> just after CO<sub>2</sub> adsorption (grey spectra), and upon He flush (black spectra) under (a) 10% CO<sub>2</sub> flow, and (b) 40% CO<sub>2</sub> flow.

Conclusively, FTIR-DRIFT analyses of CO<sub>2</sub> adsorption on ZrO<sub>2</sub> samples at different temperature with different CO<sub>2</sub> concentrations confirmed ZrO<sub>2</sub>-CO<sub>2</sub> interaction, and showed that its extent is related to temperature and gas phase CO<sub>2</sub> concentration.

#### 4.4.5. CO<sub>2</sub>-Co-Ce/ZrO<sub>2</sub> System Interaction

In order to differentiate the role of support from primary metal and promoters in CO<sub>2</sub> dissociation mechanism, FTIR-DRIFT spectra obtained from 5%Co-2%Ce/ZrO<sub>2</sub> on which CO<sub>2</sub> adsorption was conducted at 573 K for 1 hour followed by He flush for 30 minutes at the same temperature was utilized. As seen in Figure 4.39, additional peaks were formed due to CO<sub>2</sub>-catalyst interaction both in OH and OCO regions. These are attributed to metal and promoter interaction with CO<sub>2</sub>, forming more OH, bridged carbonate and carboxylate groups (Pozdnyakova *et al.*, 2006). However, these peaks are not stable, since they are easily flushed with He flow.

In CO region, on the other hand, it was seen that metal and promoter addition only causes a shift in the peaks to higher wavelength values without affecting the formation of CO with different bond types. It was found out that bridge type CO species are more stable at the applied conditions.

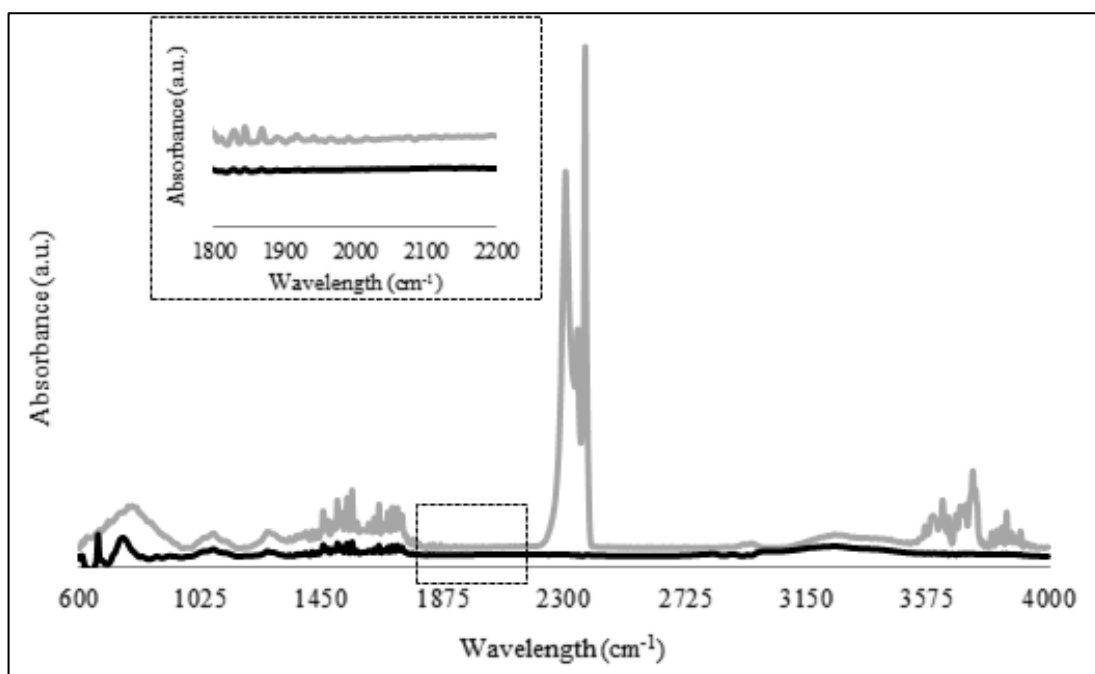


Figure 4.39. FTIR-DRIFT spectra obtained from 40% CO<sub>2</sub> adsorption at 573 K over 5%Co-2%Ce/ZrO<sub>2</sub> just after CO<sub>2</sub> adsorption of 1 hour (grey spectra), and upon He flush for 30 minutes (black spectra) (inset is the detailed view of 1800-2200 cm<sup>-1</sup> band region).

#### 4.4.6. CH<sub>4</sub>-Co-Ce/ZrO<sub>2</sub> System Interaction

CH<sub>4</sub> adsorption for 1 h TOS was also conducted over 5%Co-2%Ce/ZrO<sub>2</sub> at 573 K to analyze the interaction between CH<sub>4</sub> and the catalyst surface. In addition to the main peaks of CH<sub>4(g)</sub> at 1305 and 3016 cm<sup>-1</sup>, formate and carbonate species (Bourab *et al.*, 2004; Das and Deo, 2011) were also observed in the spectra. The peak at 1354 cm<sup>-1</sup>, for example, represents the symmetric deformation vibrations of the CH<sub>3</sub> species (Yao *et al.*, 2016). It was seen that even though the other species diminish after He flush treatment, the peaks at 1473 and 1730 cm<sup>-1</sup>, characteristic of monodentate carbonate on m-ZrO<sub>2</sub> and C=O bond, respectively, are still present at the spectra indicating the strong adsorption of the species (Ma *et al.*, 2005).

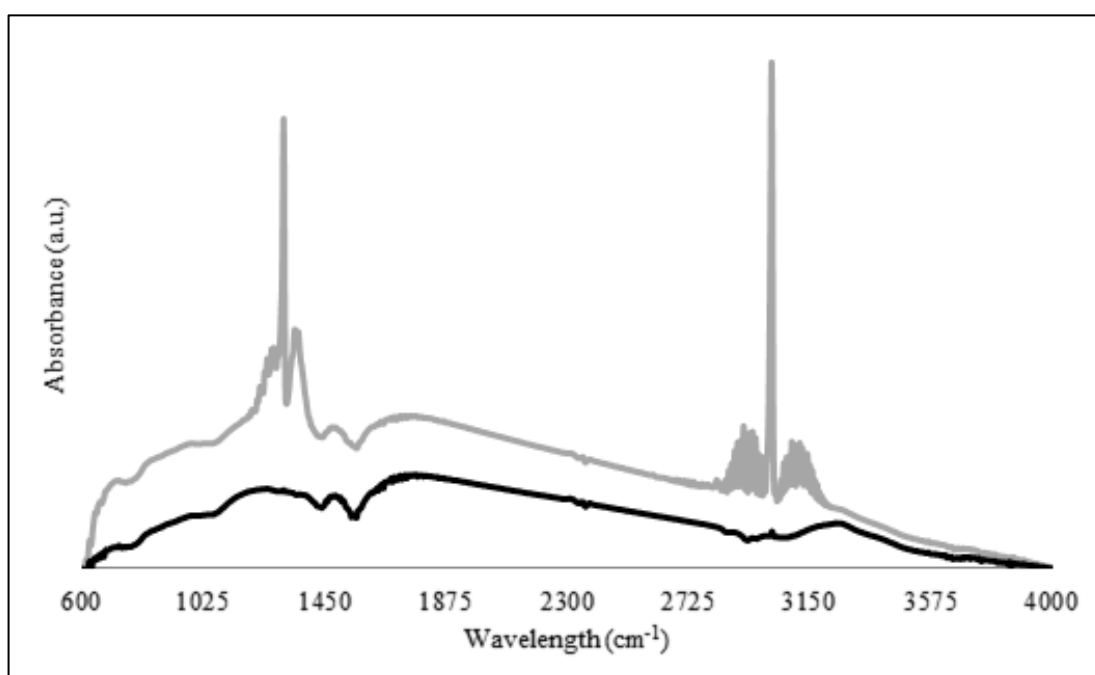


Figure 4.40. FTIR-DRIFT spectra obtained from 40% CH<sub>4</sub> adsorption at 573 K over 5%Co-2%Ce/ZrO<sub>2</sub> just after CH<sub>4</sub> adsorption for 1 hour (grey spectra), and upon He flush of 30 minutes (black spectra).

#### 4.4.7. CDRM over Co-Ce/ZrO<sub>2</sub> System

To determine reaction mechanism and have an insight about the rate of the reaction, FTIR-DRIFT analyses were performed on 5%Co-2%Ce/ZrO<sub>2</sub>, 5%Co-3%Ce/ZrO<sub>2</sub>, 10%Co-2%Ce/ZrO<sub>2</sub> and 10%Co-3%Ce/ZrO<sub>2</sub> catalysts. In the tests, first CDRM was carried out over the sample for 1 h TOS, then the sample was flushed under He flow for 30 minutes. During CDRM steps, the feed streams having different CH<sub>4</sub>/CO<sub>2</sub> ratios were used. Both reaction and flush was conducted at 573 K, and spectra just after CDRM and upon He flush were recorded to enable comparative analysis.

At the CH<sub>4</sub>/CO<sub>2</sub> feed ratio 1/1, the results obtained from all catalysts are given in Figure 4.41. It was seen that the general trend after 1 hour-on-stream reaction is common for all tested catalysts, whereas it was clearly observed that both the intensity of the peaks and the degree of the loss in their intensities after He flush change according to Co/Ce loading ratio of the samples.

The characteristic CH<sub>4(g)</sub> peak at 3016 cm<sup>-1</sup> and its harmonic peak at 1305 cm<sup>-1</sup> (Bourab *et al.*, 2004; Das and Deo, 2011) are present in the spectra upon CDRM for all catalysts and it was seen they disappear after He flush. The peaks attributed to adsorbed CO<sub>2</sub> species at 2310, 2318, 2328 and 2372 cm<sup>-1</sup> (Ni *et al.*, 2012) observed in CDRM for all tested catalyst samples also diminished upon He flush. Only the peaks at 2345 and 2354 cm<sup>-1</sup>, which were attributed to CO<sub>2(g)</sub> (Bachiller-Baeza *et al.*, 2013), remained after flushing with a slight shift at 2200-2400 cm<sup>-1</sup> band. The results indicate that reactions involving CO<sub>2</sub> in CDRM mechanism over Co-Ce/ZrO<sub>2</sub> system are probably rapid.

As it was reported that adsorption of CO<sub>2</sub> on the support yields carbonate (CO<sub>3</sub><sup>2-</sup>)/hydrocarbonate (HCO<sub>3</sub><sup>-</sup>) species that react with H atoms, produced by CH<sub>4</sub> dehydrogenation, to form formate (HCOO<sup>-</sup>) intermediates, which are then decomposed into CO and adsorbed OH groups (Son *et al.*, 2014), the effect of Co/Ce loading ratio on CDRM mechanism can be more clearly analyzed by the investigation of carbonyl, carbonate, formate and OH groups formed on the catalyst surface. Accordingly, it was interesting to notice that the peak at 2960 cm<sup>-1</sup> corresponding to bidentate formate is more pronounced at the spectra upon He flush over 5%Co-3%Ce/ZrO<sub>2</sub> and 10%Co-2%Ce/ZrO<sub>2</sub>

catalysts. The other reported peaks for bidentate formate at 2870 and 2900  $\text{cm}^{-1}$  (Yung *et al.*, 2008; Das and Deo, 2012) are common after He flush for all catalyst samples. On the other hand, bridged formate peak at 2945  $\text{cm}^{-1}$  (Pozdnyakova *et al.*, 2006) is more distinct at the spectra belonging to 10%Co-3%Ce/ZrO<sub>2</sub> catalyst. Therefore, it can be concluded that Co/Ce loading ratio affects type of the formate species formed on the catalyst surface, and the changes in the type of formate species might be the resultant of different CDRM reaction mechanisms and/or rate determining steps.

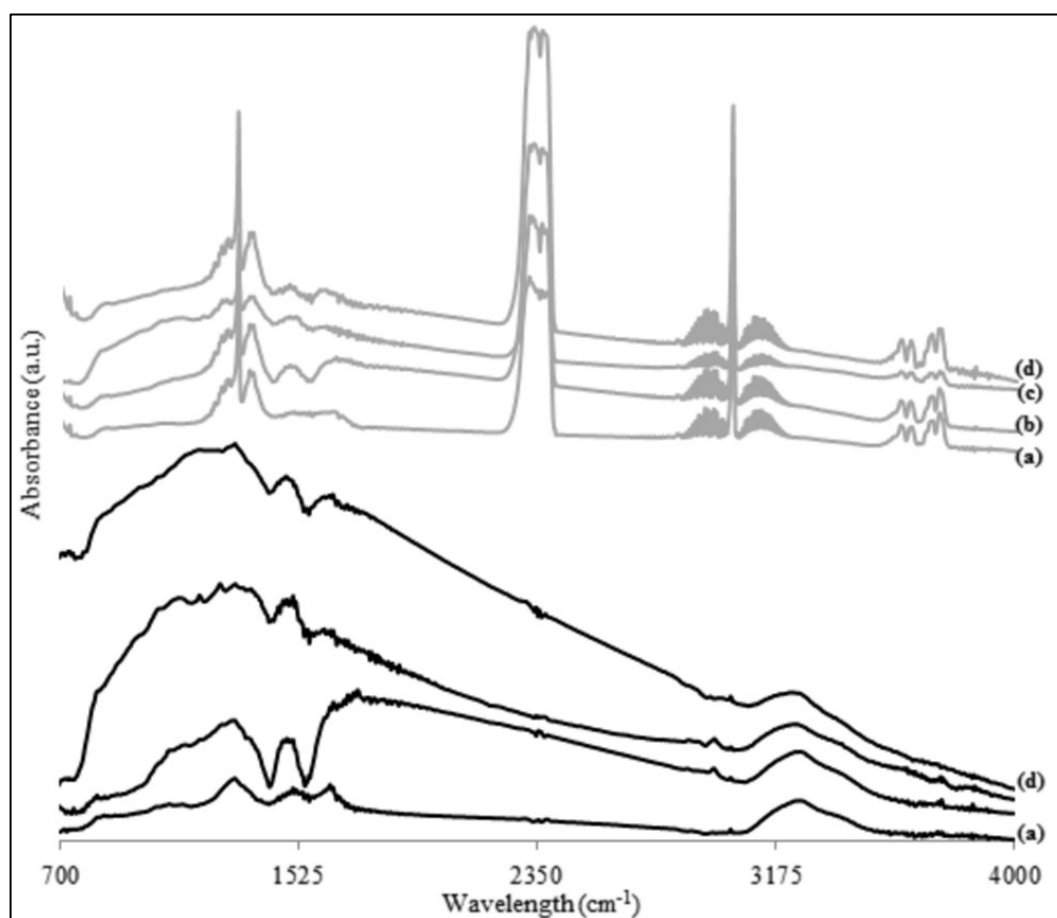


Figure 4.41. FTIR-DRIFT spectra obtained from CDRM at 573 K over (a) 5%Co-2%Ce/ZrO<sub>2</sub>, (b) 5%Co-3%Ce/ZrO<sub>2</sub>, (c) 10%Co-2%Ce/ZrO<sub>2</sub>, and (d) 10%Co-3%Ce/ZrO<sub>2</sub> just after CDRM with 1/1 feed ratio (grey spectra), and upon He flush (black spectra).

In the OCO asymmetric and symmetric stretching vibrations region, only the peaks attributed to bicarbonates at 1481 and 1611  $\text{cm}^{-1}$  (Jacobs *et al.*, 2003; Ni *et al.*, 2012; Pozdnyakova *et al.*, 2006) were observed on the catalyst surface after He flush following

CDRM indicating that bicarbonate formations are in intensive interaction with the active sites of the catalyst and are more stable. On the other hand, unidentate carbonate species yielding peaks at 1265, 1346, 1357, 1428 and 1450  $\text{cm}^{-1}$  (Grillo *et al.*, 2004) were formed after CDRM but disappeared upon the following He flush. Formation of weak bidentate carbonate species during CDRM over Co-Ce/ZrO<sub>2</sub> catalysts is confirmed with the peaks at 1222, 1244 and 1270  $\text{cm}^{-1}$  (Borchet *et al.*, 2008; Das and Deo, 2012).

The results showed that CDRM over all tested catalysts yielded peaks at 1818, 1837, 1845, 1855, 1878, 1901, 1934, 1951, 1975, 1994 and 2078  $\text{cm}^{-1}$  in 1800-2200  $\text{cm}^{-1}$  band, which was reported as the region where carbonyl groups are observed (Pietrogiacomini *et al.*, 2000). The first peaks belong to twofold, threefold and possibly fourfold bridge-bonded CO to cobalt metal sites, whereas the last peak is attributed to linearly-bonded CO (Morales *et al.*, 2007; Ni *et al.*, 2012; Dulaurent and Bianchi, 2001). After He flush, the peak at 2078  $\text{cm}^{-1}$  diminished indicating that linear adsorption of CO is weak on the tested catalysts at the given conditions and that the steps involving linearly adsorbed CO, desorption and/or utilization, should be the rapid ones in CDRM mechanism. For bridge-bonded CO, on the other hand, the intensity of the peaks decreased sharply after He flush only for 5%Co-2%Ce/ZrO<sub>2</sub> and 10%Co-3%Ce/ZrO<sub>2</sub> samples, which have the highest Ce<sup>3+</sup> concentration confirmed by XPS (See Section 4.2), highlighting that there might be relative changes in the roles of the active sites depending on oxidation state of the promoter, and specifically that there might be a link between Ce<sup>3+</sup> concentration and fast desorption and/or utilization of bridge-bonded CO.

It is interesting to mention for OH band region that on the catalysts having 10% Co loading CDRM yielded additional peaks at 3637 and 3652  $\text{cm}^{-1}$ , the latter corresponds to Ce surface geminal OH groups (Jacobs *et al.*, 2003).

The comparative analysis of the spectra obtained during CO<sub>2</sub> and CH<sub>4</sub> adsorption tests with those obtained during CDRM under the flow of CO<sub>2</sub>-CH<sub>4</sub> mixture at the reaction conditions showed that, in general, CO<sub>2</sub> adsorption characteristics are mostly support-dependent, as the peaks present at the spectra of CO<sub>2</sub>-ZrO<sub>2</sub> interaction at 573 K and those present under the flow of feed with 1/1 feed ratio are alike for the regions attributed to

CO<sub>2</sub>, CO<sub>2</sub> related OH species and carbonates. On the other hand, the similar analysis indicates that the steps involving CH<sub>4</sub> dominantly depend on Co/Ce loading ratio.

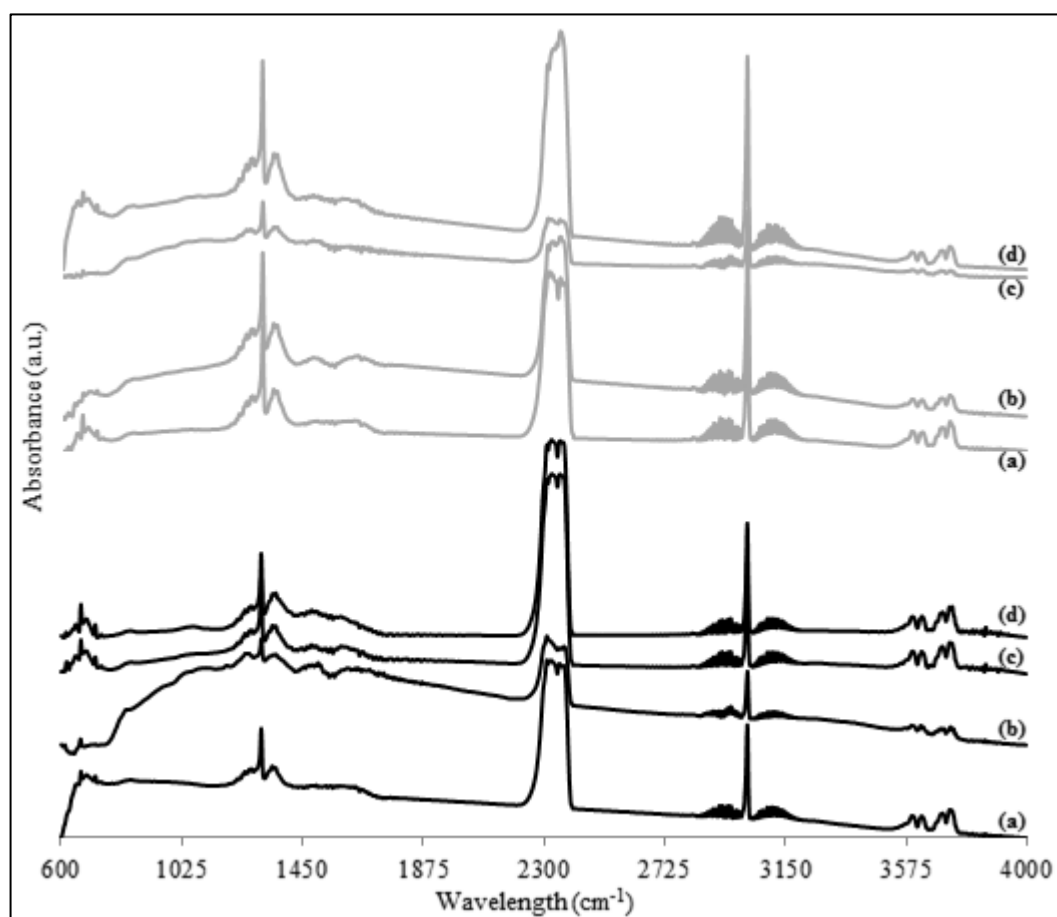


Figure 4.42. FTIR-DRIFT spectra obtained just after CDRM at 573 K over (a) 5%Co-2%Ce/ZrO<sub>2</sub>, (b) 5%Co-3%Ce/ZrO<sub>2</sub>, (c) 10%Co-2%Ce/ZrO<sub>2</sub>, and (d) 10%Co-3%Ce/ZrO<sub>2</sub> with 2/1 feed ratio (grey spectra), and 1/2 feed ratio (black spectra).

The effect of CH<sub>4</sub>/CO<sub>2</sub> feed ratio on the spectra obtained from all tested catalysts under CDRM conditions at 573 K can be seen in Figure 4.42. It was interesting to notice that adsorbed CO<sub>2</sub> at 2310 cm<sup>-1</sup> is more pronounced at the CH<sub>4</sub>/CO<sub>2</sub> feed ratio of 1/2, whereas increase of CH<sub>4</sub> in feed results in an increase in the intensity of the peak at 2375 cm<sup>-1</sup>. As the changes observed in the spectra in response to the changing feed ratios are in similar manner for all catalysts regardless of their Co/Ce loading ratio, detailed comparisons on selected bands for different feed conditions are made for the tests conducted over 5%Co-2%Ce/ZrO<sub>2</sub> catalyst (Figure 4.43) as representative examples.

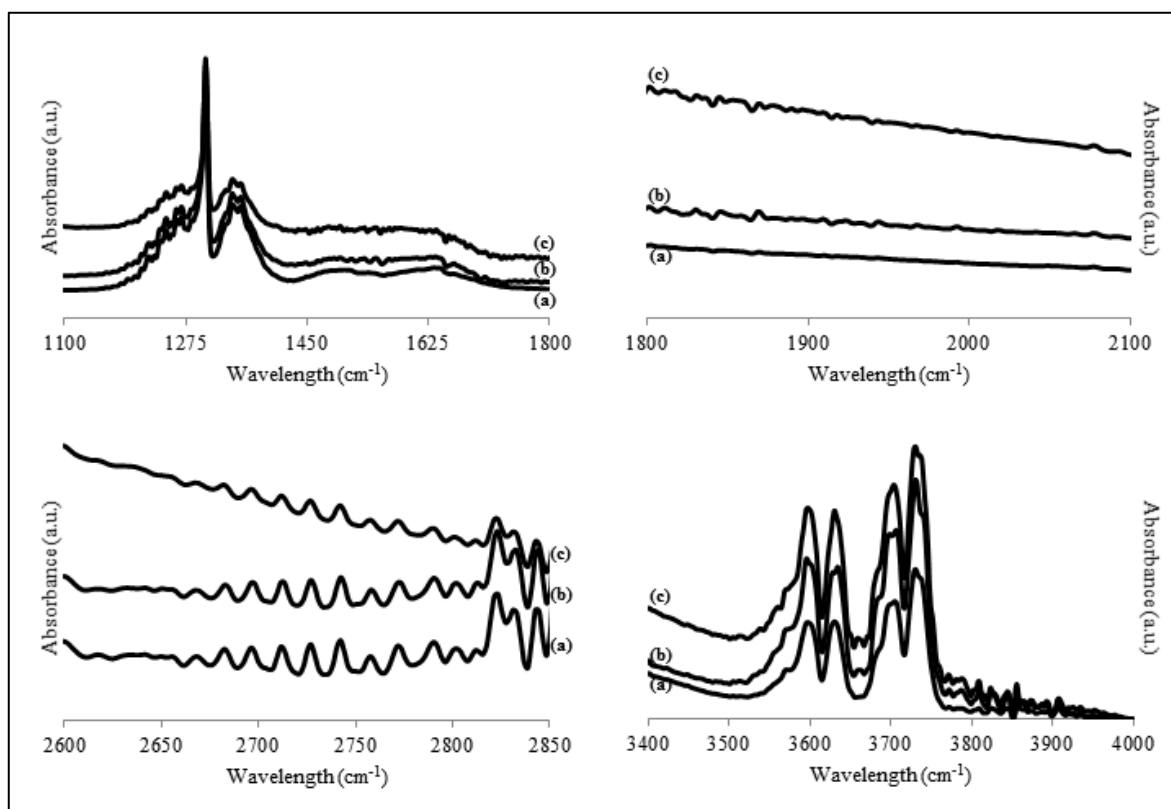


Figure 4.43. FTIR-DRIFT spectra obtained from CDRM at 573 K over 5%Co-2%Ce/ZrO<sub>2</sub> catalyst for (a) CH<sub>4</sub>/CO<sub>2</sub>=2/1, (b) CH<sub>4</sub>/CO<sub>2</sub>=1/1, and (c) CH<sub>4</sub>/CO<sub>2</sub>=1/2 at different wavelength intervals.

Based on the FTIR-DRIFT results, it can be said that bicarbonate formation is reduced for all tested catalyst samples when CH<sub>4</sub> concentration in the feed is doubled. This can be explained by the reversibility of the interaction between CO<sub>2</sub> and lattice oxygen or hydroxyl groups, since it was reported that when the CO<sub>2</sub> concentration is below a threshold value, some of the hydrogen carbonates, monodentate carbonates, or bicarbonate species are converted to CO<sub>2</sub> (Ren *et al.*, 2015). However, other carbonate types are not much affected by the CH<sub>4</sub>/CO<sub>2</sub> feed ratio, since the peak positions and intensities were essentially the same independent of the feed ratio. As expected, the peak intensities for adsorbed CO species increase as CO<sub>2</sub> in the feed increases. Additionally, it was confirmed that the production of formate species are favored in CH<sub>4</sub>-rich medium, since the peak intensities in formate region (2700-2900 cm<sup>-1</sup>) increased with increase in CH<sub>4</sub> in feed. Another important outcome is that the peak at 3665 cm<sup>-1</sup> disappears in the spectra obtained for CDRM with CH<sub>4</sub>/CO<sub>2</sub> feed ratio of 2/1, indicating consumption of surface OH groups

in the reaction with CH<sub>4</sub> (Walter *et al.*, 1994) which might be due to insufficient oxygen source (i.e. CO<sub>2</sub>) in the feed. The current results strongly confirmed the crucial importance of CH<sub>4</sub>/CO<sub>2</sub> feed ratio in CDRM selectivity.

## 5. CONCLUSION

### 5.1. Conclusions

The aim of the current work is to design and develop effective non-PGM based CDRM catalysts, to confirm the roles of each component, to determine optimum reaction conditions for the highest performance, and to reveal the details of CDRM reaction mechanism. The conclusions drawn from this study will be given in four parts. In the first part, the aim was to propose an effective Co-based non-PGM bimetallic CDRM catalyst, and to find the optimal reaction conditions to be used in the production of synthesis gas. In catalyst formulation,  $ZrO_2$ , which has ability to produce surface oxygen, was used as a support and Ce was selected as a promoter in order to increase oxygen storage capacity and regulate surface oxygen transfer. The major conclusions obtained from this part are as follows:

- The comparative analysis of Co and Ce site concentrations measured on the freshly reduced and spent samples through metal mapping and SEM-EDX indirectly confirmed that methane dehydrogenation is the primary function of Co sites.
- Combined evaluation of SEM images, Raman results and TPO profiles of spent catalyst samples clearly showed the formation of different carbon structures on the catalyst samples during CDRM, and indicated that the fraction of different carbon types depends on the reaction conditions.
- XPS Ce3d results revealed that ceria creates an additional oxygen storage capacity resulting in an enhanced surface oxygen storage/transfer function through redox cycle and higher carbon resistance.
- Co-Ce/ $ZrO_2$  catalyst has stable activity for  $CH_4/CO_2$  feed ratio of 1. Coke accumulation was mostly observed when temperature and  $CH_4/CO_2$  feed ratio were both high. Decreasing space velocity is beneficial for high and stable activities and high  $H_2/CO$  product ratio.

In the second part of the study, Co-Ce/ZrO<sub>2</sub> catalysts with different Co and Ce loadings were characterized and parametrically tested under different CDRM conditions. The following conclusions can be drawn according to the obtained data:

- HRTEM-EDX analysis showed that Co/Ce ratio does not affect the microstructural properties of the catalyst surface. It was suggested based on the mapping and EDX-Line analysis results that Co particles partially cover evenly distributed Ce particles during Co impregnation yielding nonhomogeneous dispersion of Co particles.
- Based on XPS results, the lowest degree of ceria reduction was calculated for 10%Co-2%Ce/ZrO<sub>2</sub>, which has the highest Co/Ce ratio, hinting that Co/Ce ratio plays a role in CDRM performance and/or kinetics. The highest asymmetry of the O1s spectrum was observed for this catalyst due to lattice oxygen vacancies and adsorbed oxygen. It was verified that Co species in the catalyst samples with higher Co loading are more oxidized.
- The parametric study over Co-Ce/ZrO<sub>2</sub> system indicated that cobalt is responsible for CH<sub>4</sub> dehydrogenation which is mostly favored at high temperatures; ceria has a pronounced effect on surface oxygen transfer and its activity is correlated with the oxygen concentration in the feed, and ZrO<sub>2</sub> serves for surface oxygen production via CO<sub>2</sub> dissociation stages of CDRM. The possible dominant effect of Co/Ce ratio in CDRM mechanism over the Co-Ce catalysts was also emphasized.

The third part of the study included the work to determine the CDRM kinetic behavior of 5%Co-2%Ce/ZrO<sub>2</sub> and 10%Co-2%Ce/ZrO<sub>2</sub> catalysts as a function of temperature and partial pressures of CH<sub>4</sub>, CO<sub>2</sub>, CO and H<sub>2</sub>, and to explain the effect of Co/Ce loading ratio on kinetic and mechanistic parameters through comparative analysis of power type rate expressions and possible surface reaction models obtained. The major conclusions drawn from this section are as follows:

- The CDRM kinetics over 5%Co-2%Ce/ZrO<sub>2</sub> and 10%Co-2%Ce/ZrO<sub>2</sub> catalysts can be expressed for the parameter range investigated by a simple power-law rate equation, with reaction orders of 1.63 and 1.12 for CH<sub>4</sub> and 0.29 and -0.12 for CO<sub>2</sub>, respectively.

- The detailed analysis of the activation energies of both catalysts indicated that CH<sub>4</sub> utilization is a major factor in CDRM, and it even indirectly affects CO<sub>2</sub> utilization. The effect of Co/Ce ratio on CDRM activity was also emphasized considering the dominant role of catalyst composition in forming a balance between C-formation and C-oxidation.
- Introducing H<sub>2</sub> to the feed creates an inhibitory effect on CDRM rate, as the presence of H<sub>2</sub> in the feed slows down the mechanistic steps involving CH<sub>4</sub> or its constituents.
- The comparative analysis of the optimized parameters for common surface reaction models explaining CDRM mechanism over the catalysts highlighted the relative changes in the roles of their active sites.

The final part focused on the FTIR-DRIFT studies conducted to attain more information on the surface characteristics of each catalyst, and to validate CDRM reaction mechanism. Accordingly, the following conclusions are drawn:

- ZrO<sub>2</sub>-CO<sub>2</sub> interaction was confirmed with the formation of different surface groups and adsorbed CO in the CO<sub>2</sub> adsorption tests conducted at different temperatures and CO<sub>2</sub> concentrations. It was also shown that both the structure and the formation rates of formed surface groups depend on temperature and CO<sub>2</sub> concentration of the feed stream.
- The experiments at CDRM conditions indicated that reactions involving CO<sub>2</sub> in CDRM mechanism over Co-Ce/ZrO<sub>2</sub> system are probably rapid.
- Co/Ce loading ratio affects type of the formate species formed on the catalyst surface, and the changes in the type of formate species might be the resultant of different CDRM reaction mechanisms and/or rate determining steps.
- The importance of CH<sub>4</sub>/CO<sub>2</sub> feed ratio in activity and selectivity was verified with the favored production of formate species in CH<sub>4</sub>-rich medium.

## 5.2. Recommendations

Regarding the results of this work, following studies are recommended for obtaining further useful results:

- The effect of heat treatment conditions (calcination and reduction temperature, and time) on CDRM activity and structural characteristics of the catalysts can be investigated.
- Co and Ce can be co-impregnated to zirconia support to determine the influence of impregnation strategy on CDRM activity, stability and selectivity.
- The kinetic studies can be performed over a wider range of partial pressures of both CH<sub>4</sub> and CO<sub>2</sub>.
- FTIR-DRIFT studies can be performed at CDRM operating temperatures used in performance and kinetic tests to attain more information on CDRM mechanism.

## REFERENCES

- Alberton, A. L., M. M. V. M. Souza and M. Schmal, 2007, “Carbon Formation and Its Influence on Ethanol Steam Reforming over Ni/Al<sub>2</sub>O<sub>3</sub> Catalysts”, *Catalysis Today*, Vol. 123, pp. 257–264.
- Al-Fatesh, A. S. A. and A. H. Fakeeha, 2012, “Effects of Calcination and Activation Temperature on Dry Reforming Catalysts”, *Journal of Saudi Chemical Society*, Vol. 16, pp. 55–61.
- Arkatova, L. A., 2010, “The Deposition of Coke during Carbon Dioxide Reforming of Methane over Intermetallides”, *Catalysis Today*, Vol. 157, pp. 170–176.
- Avetisov, A. K., J. R. Rostrup-Nielsen, V. L. Kuchaev, J. H. B. Hansen, A. G. Zyskin and E. N. Shapatina, 2010, “Steady-state Kinetics and Mechanism of Methane Reforming with Steam and Carbon Dioxide over Ni Catalyst”, *Journal of Molecular Catalysis A: Chemical*, Vol. 315, pp. 155–162.
- Ayodele, B. V., M. R. Khan and C. K. Cheng, 2015, “Syngas Production from CO<sub>2</sub> Reforming of Methane over Ceria Supported Cobalt Catalyst: Effects of Reactants Partial Pressure”, *Journal of Natural Gas Science and Engineering*, Vol. 27, pp. 1016–1023.
- Ayodele, B. V., M. R. Khan and C. K. Cheng, 2016, “Catalytic Performance of Ceria-supported Cobalt Catalyst for CO-rich Hydrogen Production from Dry Reforming of Methane”, *International Journal of Hydrogen Energy*, Vol. 41, pp. 198–207.
- Bachiller-Baeza, B., C. Mateos-Pedrero, M. A. Soria, A. Guerrero-Ruiz, U. Rodemerck and I. Rodríguez-Ramos, 2013, “Transient Studies of Low-temperature Dry Reforming of Methane over Ni-CaO/ZrO<sub>2</sub>-La<sub>2</sub>O<sub>3</sub>”, *Applied Catalysis B: Environmental*, Vol. 129, pp. 450–459.

- Ballarini, A. D., S. R. de Miguel, E. L. Jablonski, O. A. Scelza and A. A. Castro, 2005, "Reforming of CH<sub>4</sub> with CO<sub>2</sub> on Pt-Supported Catalysts: Effect of the Support on the Catalytic Behaviour", *Catalysis Today*, Vol. 107–108, pp. 481–486.
- Barrai, F., T. Jackson, N. Whitmore and M. J. Castaldi, 2007, "The Role of Carbon Deposition on Precious Metal Catalyst Activity during Dry Reforming of Biogas", *Catalysis Today*, Vol. 129, pp. 391–396.
- Barroso-Quiroga, M. M. and A. E. Castro-Luna, 2010, "Catalytic Activity and Effect of Modifiers on Ni-Based Catalysts for the Dry Reforming of Methane", *International Journal of Hydrogen Energy*, Vol. 35, pp. 6052–6056.
- Bartholomew, C. H., 2001, "Mechanisms of Catalyst Deactivation", *Applied Catalysis A: General*, Vol. 212, pp. 17–60.
- Bellido, J. D. A. and E. M. Assaf, 2009, "Effect of the Y<sub>2</sub>O<sub>3</sub>–ZrO<sub>2</sub> Support Composition on Nickel Catalyst Evaluated in Dry Reforming of Methane", *Applied Catalysis A: General*, Vol. 352, pp. 179–187.
- Biesinger, M. C., B. P. Payne, A. P. Grosvenord, L. W. M. Lau, A. R. Gerson and R. Smart, 2011, "Resolving Surface Chemical States in XPS Analysis of First Row Transition Metals, Oxides and Hydroxides: Cr, Mn, Fe, Co and Ni", *Applied Surface Science*, Vol. 257, pp. 2717–2730.
- Bobrova, L.N., A. S. Bobin, N.V. Mezentseva, V. A. Sadykov, J. W. Thybaut and G. B. Marin, 2016, "Kinetic Assessment of Dry Reforming of Methane On Pt + Ni Containing Composite of Fluorite-Like Structure", *Applied Catalysis B: Environmental*, Vol. 182, pp. 513–524.
- Borchert, H., B. Jürgens, T. Nowitzki, P. Behrend, Y. Borchert, V. Zielasek, S. Giorgioc, C. R. Henry and M. Bäumer, 2008, "Decomposition of Methanol by Pd, Co, and Bimetallic Co–Pd Catalysts: A Combined Study of Well-defined Systems under Ambient and UHV Conditions", *Journal of Catalysis*, Vol. 256, pp. 24–36.

- Bouarab, R., O. Akdim, A. Auroux, O. Cherifi and C. Mirodatos, 2004, "Effect of MgO Additive on Catalytic Properties of Co/SiO<sub>2</sub> in the Dry Reforming of Methane", *Applied Catalysis A: General*, Vol. 264, pp. 161–168.
- Boukha, Z., M. Kacimi, M. F. R. Pereira, J. L. Faria, J. L. Figueiredo and M. Ziyad, 2007, "Methane Dry Reforming on Ni Loaded Hydroxyapatite and Fluoroapatite", *Applied Catalysis A: General*, Vol. 317, pp. 299–309.
- Bradford, M. C. J. and M. A. Vannice, 1999, "The Role of Metal–support Interactions in CO<sub>2</sub> Reforming of CH<sub>4</sub>", *Catalysis Today*, Vol. 50, pp. 87–96.
- Budiman, A. W., S. H. Song, T. Chang and M. Choi, 2016, "Preparation of a High Performance Cobalt Catalyst for CO<sub>2</sub> Reforming of Methane", *Advanced Powder Technology*, Vol. 27, pp. 584–590.
- Cai, W., Q. Zhong, Y. Yu and S. Dai, 2016, "Correlation of Morphology with Catalytic Performance of CrO<sub>x</sub>/Ce<sub>0.2</sub>Zr<sub>0.8</sub>O<sub>2</sub> Catalysts for NO Oxidation via in-situ STEM", *Chemical Engineering Journal*, Vol. 288, pp. 238–245.
- Chai, J. W., J. S. Pan, S. J. Wang, C. H. A. Huan, G. S. Lau, Y. B. Zheng and S. Xu, 2005, "Thermal Behaviour of Ultra-thin Co over Layers on Rutile TiO<sub>2</sub>(100) Surface", *Surface Science*, Vol. 589, 32–41.
- Chen, D., R. Lodeng, A. Anundskas, O. Olsvik and Anders Holmen, 2001, "Deactivation During Carbon Dioxide Reforming of Methane over Ni Catalyst: Microkinetic Analysis", *Chemical Engineering Science*, Vol. 56, pp. 1371–1379.
- Chen, J., C. Yao, Y. Zhao and P. Jia, 2010, "Synthesis Gas Production from Dry Reforming of Methane over Ce<sub>0.75</sub>Zr<sub>0.25</sub>O<sub>2</sub>-supported Ru Catalysts", *International Journal of Hydrogen Energy*, Vol. 35, pp. 1630–1642.

- Cheng, D., X. Zhu, Y. Ben, F. He, L. Cui and C. Liu, 2006, “Carbon Dioxide Reforming of Methane over Ni/Al<sub>2</sub>O<sub>3</sub> Treated with Glow Discharge Plasma”, *Catalysis Today*, Vol. 115, pp. 205–210.
- Cheng, J. and W. Huang, 2010, “Effect of Cobalt (Nickel) Content on the Catalytic Performance of Molybdenum Carbides in Dry-methane Reforming”, *Fuel Processing Technology*, Vol. 91, pp. 185–193.
- Corthals, S., J. V. Nederkassel, J. Geboers, H. D. Winne, J. V. Noyen, B. Moens, B. Sels and P. Jacobs, 2008, “Influence of Composition of MgAl<sub>2</sub>O<sub>4</sub> Supported NiCeO<sub>2</sub>ZrO<sub>2</sub> Catalysts on Coke Formation and Catalyst Stability for Dry Reforming of Methane”, *Catalysis Today*, Vol. 138, pp. 28–32.
- Cui, Y., H. Zhang, H. Xu and W. Li, 2007, “Kinetic Study of the Catalytic Reforming of CH<sub>4</sub> with CO<sub>2</sub> to Syngas over Ni/ $\alpha$ -Al<sub>2</sub>O<sub>3</sub> Catalyst: The Effect of Temperature on the Reforming Mechanism”, *Applied Catalysis A: General*, Vol. 318, pp. 79–88.
- Damyanova, S., B. Pawelec, K. Arishtirova, M. V. M. Huerta and J. L. G. Fierro, 2009, “The Effect of CeO<sub>2</sub> on the Surface and Catalytic Properties of Pt/CeO<sub>2</sub>-ZrO<sub>2</sub> Catalysts for Methane Dry Reforming”, *Applied Catalysis B: Environmental*, Vol. 89, pp. 149–159.
- Darujati, A. R. S. and W. J. Thomson, 2006, “Kinetic Study of a Ceria-promoted Mo<sub>2</sub>C/ $\gamma$ -Al<sub>2</sub>O<sub>3</sub> Catalyst in Dry-methane Reforming”, *Chemical Engineering Science*, Vol. 61, pp. 4309–4315.
- Das, T. and G. Deo, 2011, “Synthesis, Characterization and in situ DRIFTS during the CO<sub>2</sub> Hydrogenation Reaction over Supported Cobalt Catalysts”, *Journal of Molecular Catalysis A: Chemical*, Vol. 350, pp. 75–82.
- Das, T. and G. Deo, 2012, “Effects of Metal Loading and Support for Supported Cobalt Catalyst”, *Catalysis Today*, Vol. 198, pp. 116–124.

- Daza, C. E., A. Kiennemann, S. Moreno and R. Molina, 2009, “Dry Reforming of Methane using Ni–Ce Catalysts Supported on a Modified Mineral Clay”, *Applied Catalysis A: General*, Vol. 364, pp. 65–74.
- Daza, C. E., J. Gallego, F. Mondragón, S. Moreno and R. Molina, 2010, “High Stability of Ce-promoted Ni/Mg–Al Catalysts Derived from Hydrotalcites in Dry Reforming of Methane”, *Fuel*, Vol. 89, pp. 592–603.
- Deng, W., Q. Dai, Y. Lao, B. Shi and X. Wang, 2016, “Low Temperature Catalytic Combustion of 1,2-dichlorobenzene over CeO<sub>2</sub>–TiO<sub>2</sub> Mixed Oxide Catalysts”, *Applied Catalysis B: Environmental*, Vol. 181, pp. 848–861.
- Djinovic, P., I. G. O. Crnivec, B. Erjavec and A. Pintar, 2012a, “Influence of Active Metal Loading and Oxygen Mobility on Coke-free Dry Reforming of Ni–Co Bimetallic Catalysts”, *Applied Catalysis B: Environmental*, Vol. 125, pp. 259–270.
- Djinovic, P., J. Batista and A. Pintar, 2012b, “Efficient Catalytic Abatement of Greenhouse Gases: Methane Reforming with CO<sub>2</sub> Using a Novel and Thermally Stable Rh–CeO<sub>2</sub> Catalyst”, *International Journal of Hydrogen Energy*, Vol. 37, pp. 2699–2707.
- Dominguez, M., E. Taboada, H. Idriss, E. Molins and J. Llorca, 2010, “Fast and Efficient Hydrogen Generation Catalyzed by Cobalt Talc Nanolayers Dispersed in Silica Aerogel”, *Journal of Materials Chemistry*, Vol. 20, pp. 4875–4883.
- Du, X., D. Zhang, L. Shi, R. Gao and J. Zhang, 2012, “Morphology Dependence of Catalytic Properties of Ni/CeO<sub>2</sub> Nanostructures for Carbon Dioxide Reforming of Methane”, *The Journal of Physical Chemistry*, Vol. 116, pp. 10009–10016.
- Dulaurent, O. and D. Bianchi, 2001, “Adsorption Model and Heats of Adsorption for Linear CO Species Adsorbed on ZrO<sub>2</sub> and Pt/ZrO<sub>2</sub> Using FTIR Spectroscopy”, *Applied Catalysis A: General*, Vol. 207, pp. 211–219.

- Foo, S. Y., C. K. Cheng, T. Nguyen, E. M. Kennedy, B. Z. Dlugogorski and A. A. Adesina, 2012, “Carbon Deposition and Gasification Kinetics of Used Lanthanide-promoted Co-Ni/Al<sub>2</sub>O<sub>3</sub> Catalysts from CH<sub>4</sub> Dry Reforming”, *Catalysis Communications*, Vol. 26, pp. 183–188.
- Frank, B., F. C. Jentoft, H. Soerijanto, J. Kröhnert, R. Schlögl and R. Schomäcker, 2007, “Steam Reforming of Methanol over Copper-containing Catalysts: Influence of Support Material on Microkinetics”, *Journal of Catalysis*, Vol. 246, pp. 177–192.
- Fu, G., D. Mao, S. Sun, J. Yu and Z. Yang, 2015, “Preparation, Characterization and CO Oxidation Activity of Cu-Ce-Zr Mixed Oxide Catalysts via Facile Dry Oxalate-precursor Synthesis”, *Journal of Industrial and Engineering Chemistry*, Vol. 31, pp. 283–290.
- Gallego, G. S., C. Batiot-Dupeyrat, J. Barrault, E. Florez and F. Mondragon, 2008a, “Dry Reforming of Methane Over LaNi<sub>1-y</sub>B<sub>y</sub>O<sub>3+δ</sub> (B = Mg, Co) Perovskites Used as Catalyst Precursor”, *Applied Catalysis A: General*, Vol. 334, pp. 251–258.
- Gallego, G. S., F. Mondragon, J. Tatibouet, J. Barrault and C. Batiot-Dupeyrat, 2008b, “Carbon Dioxide Reforming of Methane over La<sub>2</sub>NiO<sub>4</sub> as Catalyst Precursor-Characterization of Carbon Deposition”, *Catalysis Today*, Vol. 133–135, pp. 200–209.
- Garcia, V., M. T. Caldes, O. Joubert, G. S. Gallego, C. Batiot-Dupeyrat, Y. Piffard and J. A. Moreno, 2008, “Dry Reforming of Methane over Nickel Catalysts Supported on the Cuspidine-like Phase Nd<sub>4</sub>Ga<sub>2</sub>O<sub>9</sub>”, *Catalysis Today*, Vol. 133–135, pp. 231–238.
- García-Diéguez, M., E. Finocchio, M. A. Larrubia, L. J. Alemany and G. Busca, 2010, “Characterization of Alumina-supported Pt, Ni and PtNi Alloy Catalysts for the Dry Reforming of Methane”, *Journal of Catalysis*, Vol. 274, pp. 11–20.
- Gould, T. D., M. M. Montemore, A. M. Lubers, L. D. Ellis, A. W. Weimer, J. L. Falconer and J. W. Medlin, 2015, “Enhanced Dry Reforming of Methane on Ni and Ni-Pt

- Catalysts Synthesized by Atomic Layer Deposition”, *Applied Catalysis A: General*, Vol. 492, pp. 107–116.
- Grillo, F., M. M. Natile and A. Glisenti, 2004, “Low Temperature Oxidation of Carbon Monoxide: the Influence of Water and Oxygen on the Reactivity of a  $\text{Co}_3\text{O}_4$  Powder Surface”, *Applied Catalysis B: Environmental*, Vol. 48, pp. 267–274.
- Guczi, L., G. Stefler, O. Geszti, I. Sajo, Z. Paszti, A. Tompos and Z. Schay, 2010, “Methane Dry Reforming With  $\text{CO}_2$ : A Study on Surface Carbon Species”, *Applied Catalysis A: General*, Vol. 375, pp. 236–246.
- Hilmen, A. M., D. Schanke, K. F. Hanssen and A. Holmen, 1999, “Study of the Effect of Water on Alumina Supported Cobalt Fischer–Tropsch Catalysts”, *Applied Catalysis A: General*, Vol. 186, pp. 169–188.
- Holgado, J. P., G. Munuera, J. P. Espinos and A. R. Gonzalez-Eliphe, 2000, “XPS Study of Oxidation Processes of CeO Defective Layers”, *Applied Surface Science*, Vol. 158, pp. 164–171.
- Hou, Z., P. Chen, H. Fang, X. Zheng and T. Yashima, 2006, “Production of Synthesis Gas via Methane Reforming with  $\text{CO}_2$  on Noble Metals and Small Amount of Noble-(Rh-) Promoted Ni Catalysts”, *International Journal of Hydrogen Energy*, Vol. 31, pp. 555–561.
- Jacobs, G., P. M. Patterson, L. Williams, E. Chenu, D. Sparks, G. Thomas and Burtron H. Davis, 2004, “Water-gas Shift: in situ Spectroscopic Studies of Noble Metal Promoted Ceria Catalysts for CO Removal in Fuel Cell Reformers and Mechanistic Implications”, *Applied Catalysis A: General*, Vol. 262, pp. 177–187.
- Ji, L., S. Tang, H. C. Zeng, J. Lin and K. L. Tan, 2001, “ $\text{CO}_2$  Reforming of Methane to Synthesis Gas over Sol–gel–made  $\text{Co}/\gamma\text{-Al}_2\text{O}_3$  Catalysts from Organometallic Precursors”, *Applied Catalysis A: General*, Vol. 207, pp. 247–255.

- Jian, H., M. Renxiong, G. Zhihua, S. Chaofeng and H. Wei, 2012, “Characterization and Catalytic Activity of CeO<sub>2</sub>-Ni/Mo/SBA-15 Catalysts for Carbon Dioxide Reforming of Methane”, *Chinese Journal of Catalysis*, Vol. 33, pp. 637–644.
- Jiang, M., N. Koizumi, T. Ozaki and M. Yamada, 2001, “Adsorption Properties of Cobalt and Cobalt-manganese Catalysts Studied by in situ Diffuse Reflectance FTIR Using CO and CO+H<sub>2</sub> as Probes”, *Applied Catalysis A: General*, Vol. 209, pp. 59–70.
- José-Alonso, D. S., M. J. Illán-Gómez and M. C. Román-Martínez, 2011, “K and Sr Promoted Co Alumina Supported Catalysts for the CO<sub>2</sub> Reforming of Methane”, *Catalysis Today*, Vol. 176, pp. 187–190.
- Jozwiak, W. K., M. Nowosielska and J. Rynkowski, 2005, “Reforming of Methane with Carbon Dioxide over Supported Bimetallic Catalysts Containing Ni and Noble Metal I. Characterization and Activity of SiO<sub>2</sub> Supported Ni–Rh Catalysts”, *Applied Catalysis A: General*, Vol. 280, pp. 233–244.
- Juan-Juan, J., M. C. Roman-Martinez and M. J. Illan-Gomez, 2006, “Effect of Potassium Content in the Activity of K-promoted Ni/Al<sub>2</sub>O<sub>3</sub> Catalysts for the Dry Reforming of Methane”, *Applied Catalysis A: General*, Vol. 301, pp. 9–15.
- Juan-Juan, J., M. C. R. Martinez and M. J. Illan-Gomez, 2009, “Nickel Catalyst Activation in the Carbon Dioxide Reforming of Methane: Effect Of Pretreatments”, *Applied Catalysis A: General*, Vol. 355, pp. 27–32.
- Khassin, A. A., T. M. Yurieva, V. V. Kaichev, V. I. Bukhtiyarov, A. A. Budneva, E. A. Paukshtis and V. N. Parmon, 2001, “Metal–support Interactions in Cobalt-aluminum Co-precipitated Catalysts: XPS and CO Adsorption Studies”, *Journal of Molecular Catalysis A: Chemical*, Vol. 175, pp. 189–204.
- Konsolakis, M., M. Sgourakis and S. A. C. Carabineiro, 2015, “Surface and Redox Properties of Cobalt–Ceria Binary Oxides: On the Effect of Co Content and Pretreatment Conditions”, *Applied Surface Science*, Vol. 341, pp. 48–54.

- Kouva, S., J. Andersin, K. Honkala, J. Lehtonen, L. Leffertsac and J. Kanervo, 2014, “Water and Carbon Oxides on Monoclinic Zirconia: Experimental and Computational Insights”, *Physical Chemistry Chemical Physics*, Vol. 16, pp. 20650–20664.
- Lemonidou, A. A. and I. A. Vasalos, 2002, “Carbon Dioxide Reforming of Methane over 5 wt.% Ni/CaO-Al<sub>2</sub>O<sub>3</sub> Catalyst”, *Applied Catalysis A: General*, Vol. 228, pp. 227–235.
- Leppelt, P., B. Schumacher, V. Plzak, M. Kinne and R. J. Behm, 2006, “Kinetics and Mechanism of the Low-Temperature Water-Gas Shift Reaction on Au/CeO<sub>2</sub> Catalysts in an Idealized Reaction Atmosphere”, *Journal of Catalysis*, Vol. 244, pp. 137–152.
- Lin, S. S.-Y., D. H. Kim, M. H. Engelhard and S. Y. Ha, 2010, “Water-induced Formation of Cobalt Oxides over Supported Cobalt/Ceria–Zirconia Catalysts under Ethanol-Steam Conditions”, *Journal of Catalysis*, Vol. 273, pp. 229–235.
- Lin, S. S.-Y., H. Daimon and S. Y. Ha, 2009, “Co/CeO<sub>2</sub>-ZrO<sub>2</sub> Catalysts Prepared by Impregnation and Coprecipitation for Ethanol Steam Reforming”, *Applied Catalysis A: General*, Vol. 366, pp. 252–261.
- Liu, D. Liu, W. N. E. Cheo, Y. W. Y. Lim, A. Borgna, R. Lau and Y. Yang, 2010, “A Comparative Study on Catalyst Deactivation of Nickel and Cobalt Incorporated MCM-41 Catalysts Modified by Platinum in Methane Reforming with Carbon Dioxide”, *Catalysis Today*, Vol. 154, pp. 229–236.
- Luisetto, I., S. Tuti and E. D. Bartolomeo, 2012, “Co and Ni Supported on CeO<sub>2</sub> as Selective Bimetallic Catalyst for Dry Reforming of Methane”, *International Journal of Hydrogen Energy*, Vol. 37, pp. 1–8.
- Luna, A. E. C. and M. E. Iriarte, 2008, “Carbon Dioxide Reforming of Methane over a Metal Modified Ni-Al<sub>2</sub>O<sub>3</sub> Catalyst”, *Applied Catalysis A: General*, Vol. 343, pp. 10–15.

- Ma, Z., C. Yang, W. Wei, W. Li and Y. Sun, 2005, "Surface Properties and CO Adsorption on Zirconia Polymorphs", *Journal of Molecular Catalysis A: Chemical*, Vol. 227, pp. 119–124.
- Ma, Z., R. Xu, C. Yang, Q. N. Dong, W. Wei and Y. Sun, 2004, Infrared Study of CO and CO/H<sub>2</sub> Adsorption on Copper Catalysts Supported on Zirconia Polymorphs", *Studies in Surface Science and Catalysis*, Vol. 147, pp. 625–630.
- Mark, F. M., F. Mark and W. F. Maier, 1997, "Reaction Kinetics of the CO<sub>2</sub> Reforming of Methane", *Chemical Engineering and Technology*, Vol. 20, pp. 361–370.
- Mattos, L. V., E. Rodino, D. E. Resasco, F. B. Passos and F. B. Noronha, 2003, "Partial Oxidation and CO<sub>2</sub> Reforming of Methane on Pt/Al<sub>2</sub>O<sub>3</sub>, Pt/ZrO<sub>2</sub>, and Pt/Ce–ZrO<sub>2</sub> Catalysts", *Fuel Processing Technology*, Vol. 83, pp. 147–161.
- Melchionna M. and P. Fornasiero, 2014, "The Role of Ceria-based Nanostructured Materials in Energy Applications", *Materials Today*, Vol. 17, pp. 349–357.
- Miguel, S. R. D., I. M. J. Vilella, S. P. Maina, D. S. José-Alonso, M. C. Román-Martínez and M. J. Illán-Gómez, 2012, "Influence of Pt Addition to Ni Catalysts on the Catalytic Performance for Long Term Dry Reforming of Methane", *Applied Catalysis A: General*, Vol. 435–436, pp. 10–18.
- Mondal, K. C., V. R. Choudhary and U. A. Joshi, 2007, "CO<sub>2</sub> Reforming of Methane to Syngas over Highly Active and Stable Supported CoO<sub>x</sub> (Accompanied with MgO, ZrO<sub>2</sub> or CeO<sub>2</sub>) Catalysts", *Applied Catalysis A: General*, Vol. 316, pp.47–52.
- Moradi, G. R., M. Rahmanzadeh and S. Sharifnia, 2010, "Kinetic Investigation of CO<sub>2</sub> Reforming of CH<sub>4</sub> over La–Ni Based Perovskite", *Chemical Engineering Journal*, Vol. 162, pp. 787–791.
- Morales, F., E. de Smit, F. M. F. de Groot, T. Visser and Bert M. Weckhuysen, 2007, "Effects of Manganese Oxide Promoter on the CO and H<sub>2</sub> Adsorption Properties of

- Titania-supported Cobalt Fischer–Tropsch Catalysts”, *Journal of Catalysis*, Vol. 246, pp. 91–99.
- Moses, A. W., H. G. Garcia Flores, J. Kim and M. A. Langell, 2007, “Surface Properties of  $\text{LiCoO}_2$ ,  $\text{LiNiO}_2$  and  $\text{LiNi}_{1-x}\text{Co}_x\text{O}_2$ ”, *Applied Surface Science*, Vol. 253, pp. 4782–4791.
- Múnera, J. F., S. Irusta, L. M. Cornaglia, E. A. Lombardo, D. V. Cesar and M. Schmal, 2007, “Kinetics and Reaction Pathway of the  $\text{CO}_2$  Reforming of Methane on Rh Supported on Lanthanum-based Solid”, *Journal of Catalysis*, Vol. 245, pp. 25–34.
- Nagaoka, K., K. Takahabe and K. Aika, 2004, “Modification of  $\text{Co/TiO}_2$  for Dry Reforming of Methane at 2 MPa by Pt, Ru or Ni”, *Applied Catalysis A: General*, Vol. 268, pp. 151–158.
- Nandini A., K. K. Pant and S. C. Dhingra, 2006, “Kinetic Study of the Catalytic Carbon Dioxide Reforming of Methane to Synthesis Gas over Ni-K/ $\text{CeO}_2$ - $\text{Al}_2\text{O}_3$  Catalyst”, *Applied Catalysis A: General*, Vol. 308, pp. 119–127.
- Ni, Jun, L. Chen, J. Lin and S. Kawi, 2012, “Carbon Deposition on Borated Alumina Supported Nano-sized Ni Catalysts for Dry Reforming of  $\text{CH}_4$ ”, *Nano Energy*, Vol. 1, pp. 674–686.
- Ocsachoque, M., F. Pompeo and G. Gonzalez, 2011, “Rh–Ni/ $\text{CeO}_2$ - $\text{Al}_2\text{O}_3$  Catalysts for Methane Dry Reforming”, *Catalysis Today*, Vol. 172, pp. 226–231.
- Omae, I., 2006, “Aspects of Carbon Dioxide Utilization”, *Catalysis Today*, Vol. 115, pp. 33–52.
- Omata, K., N. Nukui, T. Hottai and M. Yamada, 2004a, “Cobalt–magnesia Catalyst by Oxalate Co-precipitation Method for Dry Reforming of Methane under Pressure”, *Catalysis Communications*, Vol. 5, pp. 771–775.

- Omata, K., N. Nukui, T. Hottai, Y. Showa and M. Yamada, 2004b, “Strontium Carbonate Supported Cobalt Catalyst for Dry Reforming of Methane under Pressure”, *Catalysis Communications*, Vol. 5, pp. 755–758.
- Olsbye, U., T. Wurzel and L. Mleczko, 1997, “Kinetic and Reaction Engineering Studies of Dry Reforming of Methane over a Ni/La/Al<sub>2</sub>O<sub>3</sub> Catalyst”, *Industrial & Engineering Chemistry Research*, Vol. 36, pp. 5180–5188.
- Ozkara-Aydinoglu, S. and A. E. Aksoylu, 2010, “Carbon Dioxide Reforming of Methane over Co-X/ZrO<sub>2</sub> Catalysts (X=La, Ce, Mn, Mg, K)”, *Catalysis Communications*, Vol. 11, pp. 1165–1170.
- Ozkara-Aydinoglu, S. and A. E. Aksoylu, 2013, “A Comparative Study on the Kinetics of Carbon Dioxide Reforming of Methane over Pt–Ni/Al<sub>2</sub>O<sub>3</sub> Catalyst: Effect of Pt/Ni Ratio”, *Chemical Engineering Journal*, Vol. 215–216, pp. 542–549.
- Ozkara-Aydinoglu, S., E. Ozensoy and A. E. Aksoylu, 2009, “The Effect of Impregnation Strategy on Methane Dry Reforming Activity of Ce Promoted Pt/ZrO<sub>2</sub>”, *International Journal of Hydrogen Energy*, Vol. 34, pp. 9711–9722.
- Pakhare, D., V. Schwartz, V. Abdelsayed, D. Haynes, D. Shekhawat, J. Poston and J. Spivey, 2014, “Kinetic and Mechanistic Study of Dry (CO<sub>2</sub>) Reforming of Methane over Rh-substituted La<sub>2</sub>Zr<sub>2</sub>O<sub>7</sub> pyrochlores”, *Journal of Catalysis*, Vol. 316, pp. 78–92.
- Paksoy, A. I., 2010, *An Experimental Study on Design and Development of Efficient Catalysts for Dry Reforming of Methane (CDRM)*, M. S. Thesis, Boğaziçi University.
- Paksoy, A. I., B. S. Caglayan, A. E. Aksoylu, 2015, “A Study on Characterization and Methane Dry Reforming Performance of Co–Ce/ZrO<sub>2</sub> Catalyst”, *Applied Catalysis B: Environmental*, Vol.168, pp. 164–174.

- Pietrogiacomì, D., S. Tuti, M. C. Campa and V. Indovina, 2000, “Cobalt Supported on ZrO<sub>2</sub>: Catalysts Characterization and Their Activity for the Reduction of NO with C<sub>3</sub>H<sub>6</sub> in the Presence of Excess O<sub>2</sub>”, *Applied Catalysis B: Environmental*, Vol. 28, pp. 43–54.
- Piumetti, M., S. Bensaid, N. Russo and D. Fino, 2016, “Investigations into Nanostructured Ceria–zirconia Catalysts for Soot Combustion”, *Applied Catalysis B: Environmental*, Vol. 180, pp. 271–282.
- Pompeo, F., D. Gazzoli and N. N. Nichio, 2009, “Stability Improvements of Ni/ $\alpha$ -Al<sub>2</sub>O<sub>3</sub> Catalysts to Obtain Hydrogen from Methane Reforming”, *International Journal of Hydrogen Energy*, Vol. 34, pp. 2260–2268.
- Pompeo, F., N. N. Nichio, M. M. V. M. Souza, D. V. Cesar, O. A. Ferretti and M. Schmal, 2007, “Study of Ni and Pt Catalysts Supported on  $\alpha$ -Al<sub>2</sub>O<sub>3</sub> and ZrO<sub>2</sub> Applied in Methane Reforming with CO<sub>2</sub>”, *Applied Catalysis A: General*, Vol. 316, pp. 175–183.
- Pozdnyakova, O., D. Teschner, A. Wootsch, J. Kröhnert, B. Steinhauer, H. Sauer, L. Toth, F. C. Jentoft, A. Knop-Gericke, Z. Paál and R. Schlögl, 2006, “Preferential CO Oxidation in Hydrogen (PROX) on Ceria-supported Catalysts, Part I: Oxidation State and Surface Species on Pt/CeO<sub>2</sub> under Reaction Conditions”, *Journal of Catalysis*, Vol. 237, pp. 1–16.
- Qian, L., W. Cai, L. Zhang, L. Ye, J. Li, M. Tang, B. Yue and H. He, 2015, “The Promotion Effect of Hydrogen Spillover on CH<sub>4</sub> Reforming with CO<sub>2</sub> over Rh/MCF Catalysts”, *Applied Catalysis B: Environmental*, Vol. 164, pp. 168–175.
- Qian, L., Z. Ma, Y. Ren, H. Shi, B. Yue, S. Feng, J. Shen and S. Xie, 2014, “Investigation of La Promotion Mechanism on Ni/SBA-15 Catalysts in CH<sub>4</sub> Reforming with CO<sub>2</sub>”, *Fuel*, Vol. 122, pp. 47–53.

- Reddy, G. K., S. Loidant, A. Takahashi, P. Delichère and B. M. Reddy, 2010, “Reforming of Methane with Carbon Dioxide over Pt/ZrO<sub>2</sub>/SiO<sub>2</sub> Catalysts – Effect of Zirconia to Silica Ratio”, *Applied Catalysis A: General*, Vol. 389, pp. 92–100.
- Ren, J., X. Qin, J. Yang, Z. Qin, H. Guo, J. Lin and Z. Li, 2015, “Methanation of Carbon Dioxide over Ni–M/ZrO<sub>2</sub> (M = Fe, Co, Cu) Catalysts: Effect of Addition of a Second Metal”, *Fuel Processing Technology*, Vol. 137, pp. 204–211.
- Renuka, L., K. S. Anantharaju, S. C. Sharma, H. P. Nagaswarupa, S. C. Prashantha, H. Nagabhushana and Y. S. Vidya, 2016, “Hollow Microspheres Mg-doped ZrO<sub>2</sub> Nanoparticles: Green Assisted Synthesis and Applications in Photocatalysis and Photoluminescence”, *Journal of Alloys and Compounds*, Vol. 672, pp. 609–622.
- Rezaei, M., S. M. Alavi, S. Sahebdehfar and Z. Yan, 2006, “Syngas Production by Methane Reforming with Carbon Dioxide on Noble Metal Catalysts”, *Journal of Natural Gas Chemistry*, Vol., pp. 327–334.
- Rezaei, M., S. M. Alavi, S. Sahebdehfar and Z. Yan, 2007, “Mesoporous Nanocrystalline Zirconia Powders: A Promising Support for Nickel Catalyst in CH<sub>4</sub> Reforming with CO<sub>2</sub>”, *Materials Letters*, Vol. 61, pp. 2628–2631.
- Rezaei, M., S. M. Alavi, S. Sahebdehfar and Z. Yan, 2009, “A Highly Stable Catalyst in Methane Reforming with Carbon Dioxide”, *Scripta Materialia*, Vol. 61, pp. 173–176.
- Roh, H., H. S. Potdar, K. Jun, J. Kim and Y. Oh, 2004, “Carbon Dioxide Reforming of Methane over Ni Incorporated into Ce–ZrO<sub>2</sub> Catalysts”, *Applied Catalysis A: General*, Vol. 276, pp. 231–239.
- Ruckenstein, E. and H. Y. Wang, 2002, “Carbon Deposition and Catalytic Deactivation during CO<sub>2</sub> Reforming of CH<sub>4</sub> over Co/γ-Al<sub>2</sub>O<sub>3</sub> Catalysts”, *Journal of Catalysis*, Vol. 205, pp. 289–293.

- San-Jose' Alonso, D., J. Juan-Juan, M. J. Illan-Gomez and M. C. Roman-Martinez, 2009, "Ni, Co and Bimetallic Ni-Co Catalysts for the Dry Reforming of Methane", *Applied Catalysis A: General*, Vol. 371, pp. 54–59.
- Sarusi, I., K. Fodor, K. Baan, A. Oszko, G. Potari and A. Erdohelyi, 2011, "CO<sub>2</sub> Reforming of CH<sub>4</sub> on Doped Rh/Al<sub>2</sub>O<sub>3</sub> Catalysts", *Catalysis Today*, Vol. 171, pp. 132–139.
- Schulz, L. A., L. C. S. Kahle, K. H. Delgado, S. A. Schunk, A. Jentys, O. Deutschmann, J. A. Lercher, 2015, "On the Coke Deposition in Dry Reforming of Methane at Elevated Pressures", *Applied Catalysis A: General*, Vol. 504, pp. 599–607.
- Solymosi, F., P. Tolmascov and T. S. Zakar, 2005, "Dry Reforming of Propane over Supported Re Catalyst", *Journal of Catalysis*, Vol. 233, pp. 51–59.
- Son, I. H., S. J. Lee and H. Roh, 2014, "Hydrogen Production from Carbon Dioxide Reforming of Methane over Highly Active and Stable MgO Promoted Co-Ni/ $\gamma$ -Al<sub>2</sub>O<sub>3</sub> Catalyst", *International Journal of Hydrogen Energy*, Vol. 39, pp. 3762–3770.
- Sousa, F. F., H. S. A. de Sousa, A. C. Oliveira, M. C. C. Junior, A. P. Ayala, E. B. Barros, B. C. Viana, J. M. Filho and A. C. Oliveira, 2012, "Nanostructured Ni-containing Spinel Oxides for the Dry Reforming of Methane: Effect of the Presence of Cobalt and Nickel on the Deactivation Behaviour of Catalysts", *International Journal of Hydrogen Energy*, Vol. 37, pp. 3201–3212.
- Souza, G., N. R. Marcilio and O. W. Perez-Lopez, 2014, "Dry Reforming of Methane at Moderate Temperatures over Modified Co-Al Co-precipitated Catalysts", *Materials Research*, Vol. 17, pp. 1047–1055.
- Souza, M. M. V. M., D. A. G. Aranda and M. Schmal, 2001, "Reforming of Methane with Carbon Dioxide over Pt/ZrO<sub>2</sub>/Al<sub>2</sub>O<sub>3</sub> Catalysts", *Journal of Catalysis*, Vol. 204, pp. 498–511.

- Sutthiumporn, K. and S. Kawi, 2011, “Promotional Effect of Alkaline Earth over Ni-La<sub>2</sub>O<sub>3</sub> Catalyst for CO<sub>2</sub> Reforming of CH<sub>4</sub>: Role of Surface Oxygen Species on H<sub>2</sub> Production and Carbon Suppression”, *International Journal of Hydrogen Energy*, Vol. 36, pp. 14435–14446.
- Takanabe, K., K. Nagaoka, K. Nariai and K. Aika, 2005, “Titania-supported Cobalt and Nickel Bimetallic Catalysts for Carbon Dioxide Reforming of Methane”, *Journal of Catalysis*, Vol. 232, pp. 268–275.
- Tankov, I., K. Arishtirova, J. M. C. Bueno and S. Damyanova, 2014, “Surface and Structural Features of Pt/PrO<sub>2</sub>–Al<sub>2</sub>O<sub>3</sub> Catalysts for Dry Methane Reforming”, *Applied Catalysis A: General*, Vol. 474, pp. 135–148.
- Tao, K., Y. Zhang, S. Terao and N. Tsubaki, 2010, “Development of Platinum-based Bimodal Pore Catalyst for CO<sub>2</sub> Reforming of CH<sub>4</sub>”, *Catalysis Today*, Vol. 153, pp. 150–155.
- Varga, E., Z. Ferencz, A. Oszko, A. Erdohelyi and J. Kiss, 2015, “Oxidation States of Active Catalytic Centers in Ethanol Steam Reforming Reaction on Ceria Based Rh Promoted Co Catalysts: An XPS Study”, *Journal of Molecular Catalysis A: Chemical*, Vol. 397, pp. 127–133.
- Verykios, X. E., 2003a, “Catalytic Dry Reforming of Natural Gas for the Production of Chemicals and Hydrogen”, *International Journal of Hydrogen Energy*, Vol. 28, pp. 1045–1063.
- Verykios, X. E., 2003b, “Mechanistic Aspects of the Reaction of CO<sub>2</sub> Reforming of Methane over Rh/Al<sub>2</sub>O<sub>3</sub> Catalyst”, *Applied Catalysis A: General*, Vol. 255, pp. 101–111.
- Vicente, J., J. Erena, C. Montero, M. J. Azkoiti, J. Bilbao and A. G. Gayubo, 2014, “Reaction Pathway for Ethanol Steam Reforming on a Ni/SiO<sub>2</sub> Catalyst Including

- Coke Formation”, *International Journal of Hydrogen Energy*, Vol. 39, pp. 18820–18834.
- Walter, K., O. V. Buyevskaya, D. Wolf and M. Baerns, 1994, “Rhodium-catalyzed Partial Oxidation of Methane to CO and H<sub>2</sub>. In situ DRIFTS Studies on Surface Intermediates”, *Catalysis Letters*, Vol. 29, pp. 261–270.
- Wang, N., W. Chu, L. Huang and T. Zhang, 2010, “Effects of Ce/Zr Ratio on the Structure and Performances of Co-Ce<sub>1-x</sub>Zr<sub>x</sub>O<sub>2</sub> Catalysts for Carbon Dioxide Reforming of Methane”, *Journal of Natural Gas Chemistry*, Vol. 19, pp. 117–122.
- Wang, N., W. Chu, T. Zhang and X. Zhao, 2011, “Manganese Promoting Effects on the Co-Ce-Zr-O<sub>x</sub> Nano Catalysts for Methane Dry Reforming with Carbon Dioxide to Hydrogen and Carbon Monoxide”, *Chemical Engineering Journal*, Vol. 170, pp. 457–463.
- Wang, S. and G. Q. Lu, 1998, “Role Of CeO<sub>2</sub> in Ni/CeO<sub>2</sub>-Al<sub>2</sub>O<sub>3</sub> Catalysts for Carbon Dioxide Reforming of Methane”, *Applied Catalysis B: Environmental*, Vol. 19, pp. 267–277.
- Wang, S. and G. Q. Lu, 1999, “Comprehensive Study on Carbon Dioxide Reforming of Methane over Ni/γ-Al<sub>2</sub>O<sub>3</sub> Catalysts”, *Industrial and Engineering Chemistry Research*, Vol. 38, pp. 2615–2625.
- Watanabe, R., Y. Hondo, K. Mukawa, C. Fukuhara, E. Kikuchi and Y. Sekine, 2013, “Stable and Selective Perovskite Catalyst for Dehydrogenation of Propane Working with Redox Mechanism”, *Journal of Molecular Catalysis A: Chemical*, Vol. 377, pp. 74–84.
- Weidler, N., S. Paulus, J. Schuch, J. Klett, S. Hoch, P. Stenner, A. Maljusch, J. Brötz, C. Wittich, B. Kaiser and W. Jaegermann, 2016, “CoO<sub>x</sub> Thin Film Deposited by CVD as Efficient Water Oxidation Catalyst: Change of Oxidation State in XPS and Its

- Correlation to Electrochemical Activity”, *Physical Chemistry Chemical Physics*, Vol. 18, pp. 10708–10718.
- Westermann, A., B. Azambre and A. Koch, 2012, “Effect of Ag, Pd and Co Promoters on the Selective Catalytic Reduction (SCR) of NO<sub>x</sub> by Ethanol over Sulfated Ceria-zirconia Catalysts”, *Catalysis Today*, Vol. 191, pp. 65–74.
- Wragg, D. S., A. Gronvold, P. Norby and H. Fjellvag, 2013, “Combined XRD and Raman Studies of Coke Types Found in SAPO-34 after Methanol and Propene Conversion”, *Microporous and Mesoporous Materials*, Vol. 173, pp. 166–174.
- Xu, J., W. Zhou, Z. Li, J. Wang and J. Ma, 2009, “Biogas Reforming for Hydrogen Production over Nickel and Cobalt Bimetallic Catalysts”, *International Journal of Hydrogen Energy*, Vol. 34, pp. 6646–6654.
- Yang, J., H. Liu, W. N. Martens and R. L. Frost, 2010, “Synthesis and Characterization of Cobalt Hydroxide, Cobalt Oxyhydroxide, and Cobalt Oxide Nanodiscs”, *The Journal of Physical Chemistry C*, Vol. 114, pp. 111–119.
- Yao, L., J. Shi, H. Xu, W. Shen and C. Hu, 2016, “Low-temperature CO<sub>2</sub> Reforming of Methane on Zr-promoted Ni/SiO<sub>2</sub> Catalyst”, *Fuel Processing Technology*, Vol. 144, pp. 1–7.
- Yassi, C., 2014, *An Experimental Study on Cobalt Based Catalytic Dry Reforming of Methane Catalysts*, M. S. Thesis, Boğaziçi University.
- Yung, M. M., Z. Zhao, M. P. Woods and U. S. Ozkan, 2008, “Preferential Oxidation of Carbon Monoxide on CoO<sub>x</sub>/ZrO<sub>2</sub>”, *Journal of Molecular Catalysis A: Chemical*, Vol. 279, pp. 1–9.
- Zhang, Z. L. and X. E. Verykios, 1994, “Carbon Dioxide Reforming of Methane to Synthesis Gas over Supported Ni Catalysts”, *Catalysis Today*, Vol. 21, pp. 589–595.